Supplementary Information

Host-guest binding of tetracationic cyclophanes for photodynamic agents that inhibits posttreatment phototoxicity and maintains antitumour efficacy

Jian-Da Sun,[a] Yamin Liu,[a] Zijian Zhao,[a] Shang-Bo Yu,[b] Qiao-Yan Qi,[b] Wei Zhou,[a] Hui Wang,[a] Ke Hu,[a] Dan-Wei Zhang*[a] and Zhan-Ting Li*[a,b]

[a] Department of Chemistry, Shanghai Key Laboratory of Molecular Catalysis and Innovative Materials, Fudan University, 2205 Songhu Road, Shanghai 200438, China.

[b] Key Laboratory of Synthetic and Self-Assembly Chemistry for Organic Functional Molecules, Shanghai Institute of Organic Chemistry, Chinese Academy of Sciences, 345 Lingling Lu, Shanghai 200032, China

E-mails: zhangdw@fudan.edu.cn, ztli@fudan.edu.cn

General methods and materials. ^{1}H NMR spectra were recorded with an AVANCE III HD 400 MHz spectrometer (Bruker) in the indicated solvents at 25 °C. Chemical shifts were referenced to the residual solvent peaks. Fluorescent measurements were performed on a VARIAN CARY Eclipse Fluorescence Spectrophotometer. Dynamic light scattering (DLS) experiments were conducted on a Malvern Zetasizer Nano ZS90 using a monochromatic coherent He–Ne laser (633 nm) as the light source and a detector that detected the scattered light at an angle of 90°. The crystal was measured using Bruker D8 Venture-Metaljet diffractometer equipped with a PHOTON II area detector and HELIOS multilayer optics monochrommated Cu-K and Mo-K alpha radiation (lambda = 1.54184 and 0.71073 Å) and the crystal structure was solved by direct method and refined by full-matrix least-squares methods based on F2 using SHELXL-2014 software. All the reagents and solvents were commercially available and used as received unless otherwise specified purification. Fetal bovine serum (FBS), 1640 Medium, McCoy's 5A (Modified) Medium and DMEM Medium were purchased from Thermo Fisher Scientific.

Statement of Ethical Approval: Scientific research with human platelet poor plasma and human whole blood was approved by Shanghai Municipal Commission of Health and Family Planning. Animal experiments were performed in agreement with the guidelines of the Animal Care and Use Committee of Fudan University (2020-Department of Chemistry-JS-003).

Measurement of $^1O_2$ quantum-yield. 1,3-Diphenylisobenzofuran acid (DPBF, 5 mM) in DMSO was added into 2 mL of NaH_2PO_4 buffer (PBS, 20 mM, pH 7.4, [DPBF] = 25 μM). The aqueous solution of PDA or **NpBox** was added separately and the absorbance at 427 nm was monitored every 10 s with the irradiation of 655 nm laser (0.1 W cm^{-2}) for Chlorin e6 or 635 nm laser (0.1 W cm^{-2}) for Photofrin and HiPorfin. The relative $^1O_2$ quantum yield of the mixture (PDA + **NpBox**) was calculated by divided by $^1O_2$ quantum yield of PDA itself.

Transient state absorption measurements. Nanosecond transient absorption spectra were acquired on a TSP-2000 (Unisoku) laser flash photolysis system. Briefly, A Q-switched frequency-doubled pulsed Nd:YAG laser (Quantel Q-Smart 450, 10 Hz) equipped with an OPO (MagicPRISM VIS, OPOtek) was used as the excitation source to output 680 nm laser pulses (5-8 nm full width at half-maximum, 3 mJ/cm^2 per pulse). A 75 W Xenon arc lamp was served as the probe beam that focused onto the solution sample in a 10 mm cuvette. The probe beam was aligned orthogonally to the excitation laser pulse and was passed into an f/4 monochromator (Acton, Princeton Instrument) that coupled an R2949 photomultiplier tube (Hamamatsu) to achieve signal detection (400 nm-540 nm). For kinetics of probe wavelengths from 550 nm to 1000 nm, signal detection was achieved by a preamplified S3399 silicon photodiode (Hamamatsu). Transient absorption kinetic data at each wavelength were acquired on a computer interfaced digital oscilloscope (LeCroy 4024, 12 bit, 200 MHz) with typical 50-100 laser pulse averages. For transient photoluminescence data acquisition, the white light probe beam was blocked and the sample was only exposed to pulsed laser excitations.

The signal detection was achieved in the same way as described above. The samples were bubbled with N_2 for 15 min before nsTA measurements. All the measurements were carried out at room temperature.

Density functional theory (DFT) calculations. The calculations were performed with spin restriction using DMol3 code in Materials Studio 7.0 software (Accelrys Inc). The exchange – correlation energy was calculated within the generalized gradient approximation (GGA) using PBE functional. As the PBE energy functional cannot describe the van der Waals dispersion interactions, a Grimme custom method for DFT-D correction was employed for the calculation of molecular adsorption. The valence electron functions were expanded into a set of numerical atomic orbitals by a double numerical basis with polarization functions (DNP), all-electron core treatment. The convergence criteria of energy, displacement and gradient were set as 1×10^{-5} Ha, 5×10^{-3} Å and 2×10^{-3} Ha/Å, respectively. The effect of the bulk solvent was investigated using the conductor-like screening model (COSMO) as implemented in Dmol3. This is a dielectric continuum solvation model in which the mutual polarization of the solute and solvent is represented by screening charges on the surface of the solute cavity. These charges are derived under the simplified boundary condition that the electrostatic potential vanishes for a conductor ($\varepsilon = 0$), and the charges are scaled to account for the finite dielectric permittivity of a real solvent. In this case, bulk water solvent is represented by a dielectric permittivity $\varepsilon = 78.54$.

Cell culture. L02 cells were incubated in 1640 medium, which contained 20% FBS and 1% penicillin streptomycin, at 37 °C in a humidified atmosphere containing CO_2 (5%). H9C2 cells were incubated in DMEM, containing 10% FBS and 1% penicillin streptomycin, at 37 °C in a humidified atmosphere containing CO_2 (5%).

In vitro cytotoxicity assay of 2,6-NpBox. The cytotoxicity of **2,6-NpBox** against H9C2 or L02 cells was evaluated by the Cell Counting Kit-8 (CCK-8) assay. In brief, cells were seeded in 96-well plates at an appropriate density of 1×10^4 cells per well and then incubated for 24 h. After adherence, the cells were treated with the **2,6-NpBox** with different concentrations ranging from 0 to 100 μg/mL. After 24 hours of incubation, the medium was replaced with fresh medium containing CCK-8. Then, after incubating for 1 hours, the absorbance was measured at 450 nm using a microplate reader (Bio-Tek, Synergy H1, USA). The relative cell viability was calculated as: cell viability = (OD450 (samples)/OD450 (control)) × 100%, where OD450 (control) was obtained in the absence of **2,6-NpBox**, and OD450 (samples) was obtained in the presence of **2,6-NpBox**. Each value was averaged from six independent experiments.

Hemolytic activity. Sprague Dawley rat erythrocyte or human O-type erythrocyte in normal saline (140 μL, 5% (v/v)) was mixed with normal saline (490 μL) in centrifuge tubes (2 mL). Then, the solutions of **2,6-NpBox** of increasing concentrations in normal saline (70 μL) were added to the centrifuge tubes to obtain final concentrations ranging from 0 μg/mL to 100 μL/mL. The mixtures were incubated at 37 °C for 1 hour and then centrifuged at 4 °C for 10 min with rotating speed of 3000 rpm. The supernatants were transferred into sterile 96-well plates and the release of hemoglobin monitored at 545

nm using a microtiter plate reader. Normal saline in the place of **2,6-NpBox** served as negative control (0% hemolytic activity). Positive control (100% hemolytic activity) was achieved by mixing the erythrocyte with deionized water. Hemolytic activity was calculated by:

% of hemolytic activity = [(OD sample − OD negative control)/(OD positive control − OD negative control)] × 100

Maximum tolerated dose (MTD) assessment. Balb/c mice with 8–9 weeks of age were used for MTD study. After one-week acclimatization, the mice were divided into 4 groups (n = 6, 3 males and 3 females) according to the injection concentrations of **2,6-NpBox** (5, 10, 15, 20 mg/kg). After receiving a caudal vein injection of the **2,6-NpBox** solutions in 5% glucose (0.1 mL) and the mice of the control group were administrated with 5% glucose. The mice were observed every 24 h, which lasted for 14 days. The weight and lethality of the mice was recorded one time per 2 days and mice found to be moribund at the time of observation were enthanized by cervical dislocation.

Tumor Model. Animals were obtained from Shanghai Leigen Biotech Co., Ltd. The B16F10 tumor model was generated by subcutaneous inoculation on the on the right front back of mice (1×10^5 B16F10 cells in PBS, 100 μL). The method for tumor volume (V) calculation was by the following equation: $V = L_{length} \times W_{width}^2/2$.

Evaluation of PDT Efficacy and Skin Photosensitivity. The time schedule of this experiment is shown in Figure S61. The B16F10 cells were subcutaneously inoculated on the right front back of all healthy female nude BALB/c mice with 7~8 weeks of age after one-week acclimatization. When the tumors were about 20 mm^3 in size, they were randomly divided into nine groups (n = 5 for group 4 and group 5, n=8 for other groups). At day 0, mice of group 1 were intravenously injected with PBS (200 μL), mice of groups 2~5 were intravenously injected with Photofrin (4.0 mg kg^{-1}, 200 μL). After being kept in dark for 24 h, mice of groups 2~5 were exposed to 635 nm laser (145 mW/cm^2, 7 min) for oncotherapy. Then, mice of group 3, 4 and 5 were intravenously injected with **2,6-NpBox** (4.0 mg kg^{-1} for group 3, 5 and 2.0 mg kg^{-1} for group 4 , 200 μL) within 30 min. After 24h (day 2), mice of group 5 were exposed to solar simulator (100 mW/cm^2) for 30 min. At day 3, all other mice were exposed to solar simulator (100 mW/cm^2) for 30 min. Besides, three mice of group 2 and 3 were sacrificed to collect main organs (heart, liver, spleen, lung and kidney) and skin tissues from the back (1.5 cm × 1.5 cm) to weigh and homogenize in lysis buffer. The fluorescence intensity of the supernatant was determined to quantify the amount of Photofrin. At day 4, the skin images of mice in group 5 were taken (48h after sunlight). At day 5, skin images of mice in group 4 were taken (48h after sunlight), and skin images of mice in group 1 ~ 3 were taken once every 2 days from day 5 to day 13. At day 13, the remaining mice in each gourp were sacrificed, their tumor tissue and main organs (heart, liver, spleen, lung, and kidney) were excised for histological analysis. H&E staining of skin were further performed for the evaluation of light-induced skin damage. The tumor volume of each mouse was recorded daily and body weight was recorded every two days.

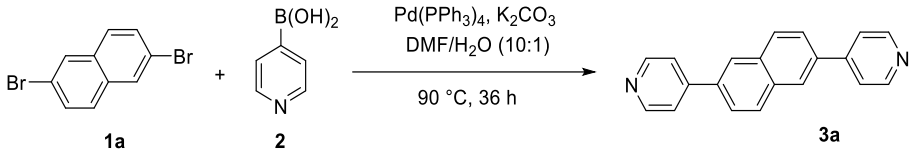

Compound 3a. 2,6-Dibromonaphthalene **1a** (2.5 g, 8.7 mmol), pyridine-4-boronic acid **2** (2.5 g, 20.3 mmol), and Na_2CO_3 (2.5 g, 20.6 mmol) were added to a 10:1 mixture of DMF/H_2O (165 mL), which had been degassed with N_2 for 15 min. Then, $Pd(PPh_3)_4$ (1.0 g, 0.87 mmol) was added to the reaction mixture and the solution heated to 90 ºC under N_2 for 36 h. Then, the reaction mixture was cooled to room temperature and the palladium catalyst filtered off using Celite. The organic phase was concentrated under vacuum and then dissolved in CH_2Cl_2 followed by extraction with H_2O three times. The organic layer was made acidic (pH 2–3) by adding dropwise concentrated HCl, which caused the desired product to precipitate from solution. The precipitate was collected by filtration and then dissolved in H_2O. Finally, aq. NaOH (10 M) was added dropwise to the water layer until the pH was ~7–8, which resulted in precipitation of pure product compound **3a** (2.2 g, 89%) as a white solid. ^{1}H NMR (400 MHz, $CDCl_3$): ^{1}H NMR (400 MHz, $CDCl_3$) δ 8.73 (d, J = 5.1 Hz, 4H), 8.17 (s, 2H), 8.06 (d, J = 8.4 Hz, 2H), 7.83 (d, J = 9.9 Hz, 2H), 7.67 (d, J = 6.3 Hz, 4H).

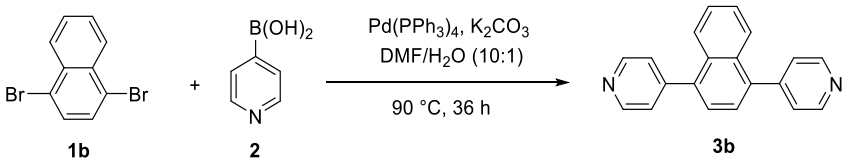

Compound 3b was prepared according to the above procedure described for **3a** from **1b** (2.5 g, 8.7 mmol) and **2** (1.6 g, 65%) as a white solid. ^{1}H NMR (400 MHz, DMSO-d_6) δ 8.75 (d, J = 6.0 Hz, 4H), 7.86 (d, J = 8.4 Hz, 2H), 7.67–7.59 (m, 2H), 7.56 (d, J = 6.1 Hz, 6H).

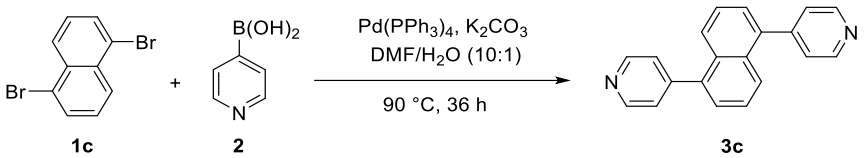

Compound 3c was prepared according to the above procedure described for **3a** from **1c** (2.5 g, 8.7 mmol) and **2** (1.7 g, 69%) as a white solid. ^{1}H NMR (400 MHz, DMSO-d_6) δ 8.76 (d, J = 6.0 Hz, 4H), 7.87 (dd, J_1 = 6.5 Hz, J_2 = 3.3 Hz, 2H), 7.68–7.54 (m, 8H).

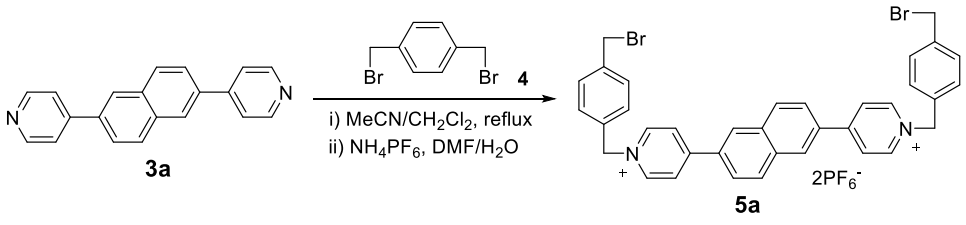

Compound 5a. α,α'-Dibromo-*p*-xylene **4** (4.6 g, 17.4 mmol) was added to CH_2Cl_2 (30 mL) in a 250 mL round-bottomed three-neck flask and the resulting mixture was refluxed while stirring until all of the solid material dissolved. The temperature of the oil bath was then raised to 90 ºC, and a suspension of compound **3a** (0.40 g, 1.4 mmol) in MeCN (60 mL) was added in five aliquots in 1 h. After refluxing for 48 h, the reaction mixture was cooled to room temperature. The yellow precipitate formed was collected by filtration and washed with CH_2Cl_2. The solid was then dissolved in DMF of minimum volume. Saturated solution of ammonium hexafluorophosphate in water was added dropwise. Then the precipitate formed was filtered, washed with water (10 mL × 3) and dried to afford compound **4·2PF$_6$** as a yellow solid (1.2 g, 90%). ^{1}H NMR (400 MHz, CD_3CN) δ 8.80 (d, *J* = 6.8 Hz, 4H), 8.60 (d, *J* = 1.9 Hz, 2H), 8.41 (d, *J* = 6.9 Hz, 4H), 8.29 (d, *J* = 8.7 Hz, 2H), 8.08 (dd, *J* = 8.6, 1.8 Hz, 2H), 7.68–7.39 (m, 8H), 5.73 (s, 4H), 4.61 (s, 4H); ^{13}C NMR (101 MHz, DMSO-d_6) δ 154.51, 144.94, 144.01, 134.06, 133.07, 132.83, 130.66, 129.12, 128.76, 127.18, 125.69, 125.40, 62.43, 39.60. MS calcd for $C_{36}H_{30}Br_2N_2PF_6$ $[M\text{-}PF_6]^+$: 795.0395; found: 795.0397.

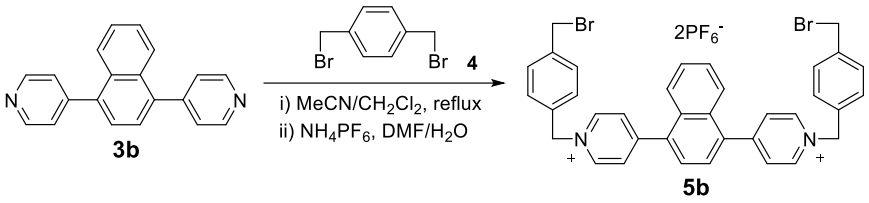

Compound 5b was prepared according to the procedure described for **5a** from the reaction of **3b** and **4** as a yellowish solid (1.1 g, 83%). ^{1}H NMR (400 MHz, DMSO-d_6) δ 9.37 (d, *J* = 6.8 Hz, , 4H), 8.41 (d, *J* = 6.7 Hz, 4H), 7.98 (dd, *J* = 6.5, 3.3 Hz, 2H), 7.86 (s, 2H), 7.74 (dd, *J* = 6.5, 3.3 Hz, 2H), 7.65 (d, *J* = 8.2 Hz, 4H), 7.58 (d, *J* = 8.3 Hz, 4H), 5.96 (s, 4H), 4.75 (s, 4H); ^{13}C NMR (101 MHz, DMSO-d_6) δ 155.81, 144.90, 139.42, 136.32, 134.28, 130.16, 129.90, 129.45, 129.32, 128.43, 127.75, 125.46, 62.52, 33.67. MS calcd for $C_{36}H_{30}Br_2N_2PF_6$ $[M\text{-}PF_6]^+$: 795.0395; found: 795.0400.

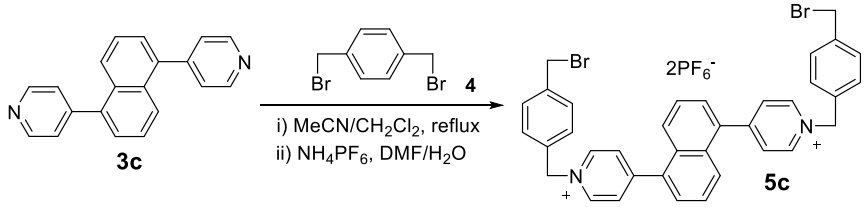

Compound 5c was prepared according to the procedure described for **5a** from the reaction of **3c** and **4** as a yellowish solid (1.2 g, 90%). ^{1}H NMR (400 MHz, DMSO-d_6) δ 9.34 (d, *J* = 6.4 Hz, 4H), 8.39 (d, *J* = 6.8 Hz, 4H), 8.07 (dd, *J* = 7.6, 1.9 Hz, 2H), 7.85–7.74 (m, 4H), 7.65 (d, *J* = 8.1 Hz, 4H), 7.58 (d, *J* = 8.2 Hz, 4H), 5.91 (s, 4H), 4.75 (s, 4H); ^{13}C NMR (101 MHz, DMSO-d_6) δ 155.45, 144.87, 139.42, 134.70, 134.35, 130.18, 129.84, 129.47, 129.39, 129.19, 127.38, 127.28, 62.46, 33.71; MS calcd for $C_{36}H_{30}Br_2N_2PF_6$ $[M\text{-}PF_6]^+$: 795.0395; found: 795.0406.

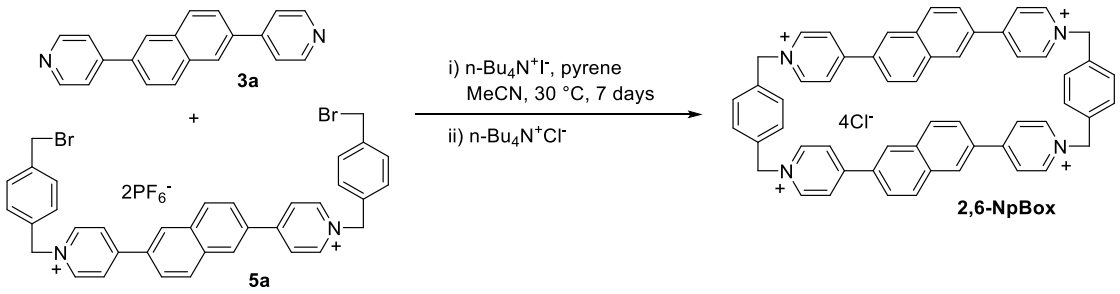

2,6-NpBox. Compound **3a** (57.2 mg, 0.20 mmol), **5b** (200 mg, 0.21 mmol), compound, TBAI (15 mg, 0.041 mmol) and the template pyrene (212 mg, 1.05 mmol) were added to dry MeCN (200 mL). The mixture was stirred at 30 ℃ for 7 days. To the the reaction mixture was added saturated $(t\text{-}Bu)_4NCl$ in CH_3CN (3 mL). The yellow precipitate formed was filtrated and then subjected to column chromatography on silica gel ($CH_3OH/H_2O/NH_4Cl$ (saturated solution), 6:3:1). The crude product obtained was further recrystallized in water and MeCN to yield **2,6-NpBox** (51.1 mg, 26%) as an orange solid. ^{1}H NMR (400 MHz, D_2O) δ 8.96 (d, J = 6.4 Hz, 8H), 8.37 (s, 4H), 8.27 (d, J = 9.5 Hz, 8H), 8.06 (d, J = 9.3 Hz, 4H), 7.87 (d, J = 7.7 Hz, 4H), 7.71 (s, 8H), 5.83 (s, 8H). ^{13}C NMR (101 MHz, DMSO-d_6) δ 154.13, 144.39, 136.49, 133.84, 132.41, 130.36, 129.99, 129.13, 125.44, 125.30, 61.20. MS calcd for $C_{56}H_{44}N_4$ $[M]^{4+}$: 193.0886; found: 193.0904.

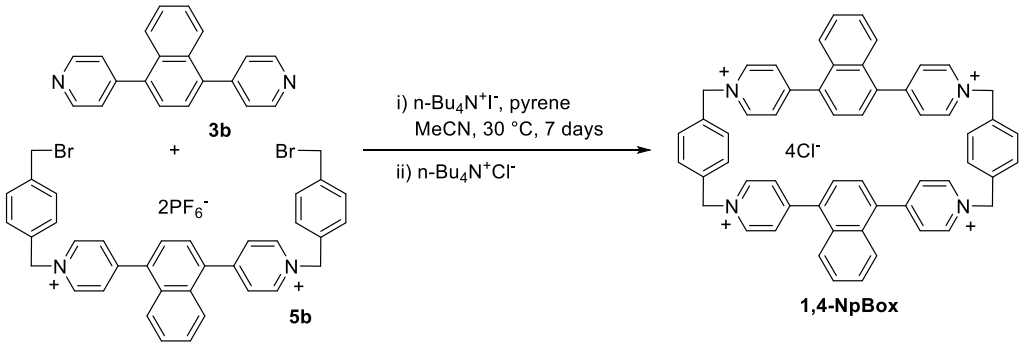

1,4-NpBox was prepared according to the procedure described for **2,6-BpBox** from the reaction of **3b** and **5b** as a yellow solid (27%). ^{1}H NMR (400 MHz, D_2O) δ 8.96 (d, J = 6.4 Hz, 8H), 8.37 (s, 4H), 8.27 (d, J = 9.5 Hz, 8H), 8.06 (d, J = 9.3 Hz, 4H), 7.87 (d, J = 7.7 Hz, 4H), 7.71 (s, 8H), 5.83 (s, 8H); ^{13}C NMR (101 MHz, DMSO-d_6) δ 154.13, 144.39, 136.49, 133.84, 132.41, 130.36, 129.99, 129.13, 125.44, 125.30, 61.20. MS calcd for $C_{56}H_{44}Cl_2N_4Cl_2^{2+}$ $[M\text{-}2Cl]^{2+}$: 421.1466; found: 421.1458.

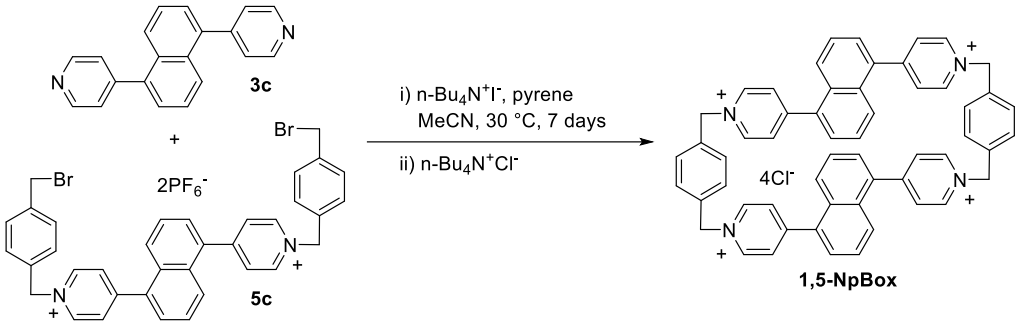

1,5-NpBox was prepared according to the procedure described for **2,6-BpBox** from the reaction of **3c** and **5c** as a yellow solid (32%). ^{1}H NMR (400 MHz, D_2O) δ 9.08 (d, J = 6.3 Hz, 8H), 8.12 (d, J = 4.6 Hz, 8H), 7.83 (s, 8H), 7.80 (d, J = 8.9 Hz, 4H), 7.48–7.42 (m, 8H), 5.94 (s, 8H); ^{13}C NMR (101 MHz, DMSO-d_6) δ 156.16, 144.25, 136.63, 134.42, 130.27, 129.55, 129.40, 129.21, 127.23, 126.83, 62.21. MS calcd for $C_{56}H_{44}Cl_2N_4Cl_2^{2+}$ $[M\text{-}2Cl]^{2+}$: 421.1466; found: 421.1463.

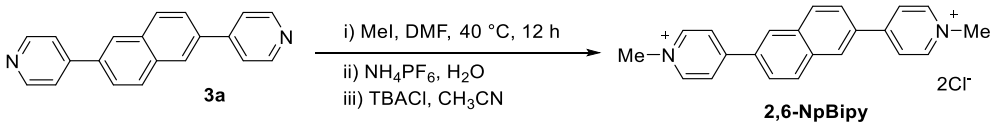

2,6-NpBipy. A mixture of compounds **3a** (0.10 g, 0.35 mmol) and MeI (0.5 g, 3.5 mmol) in DMF (10 mL) was stirred at 40 °C for 12 h and then cooled to room temperature. Et_2O (50 mL) was added and the precipitate formed was filtrated. The solid was dissolved in water of minimum volume and a saturated solution of ammonium hexafluorophosphate in water was added dropwise. The precipitate formed was filtered, washed with water (10 mL × 3) and dried. The solid was then dissolved in MeCN of minimum volume. A saturated solution of tetrabutylammonium chloride in MeCN was added dropwise until no precipitation occurred. The precipitate formed was filtered, washed with MeCN (10 mL × 3) and dried to afford **2,6-NpBipy** as white solid (98 mg, 72%). ^{1}H NMR (400 MHz, DMSO-d_6) δ 9.10 (d, J = 6.6 Hz, 4H), 8.89 (s, 2H), 8.68 (d, J = 6.8 Hz, 4H), 8.35 (d, J = 8.7 Hz, 2H), 8.29 (d, J = 10.4 Hz, 2H), 4.38 (s, 6H). ^{13}C NMR (101 MHz, D_2O) δ 155.65, 145.05, 133.41, 131.06, 130.24, 128.65, 125.37, 125.18, 45.32. MS calcd for $C_{22}H_{20}N_2$ $[M]^{2+}$: 156.0808; found: 156.0806.

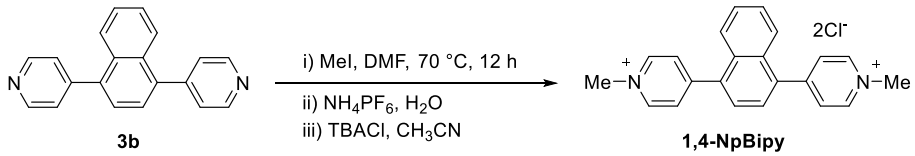

1,4-NpBox was prepared according to the procedure described for **2,6-BpBipy** from the reaction of **3b** and MeI as a white solid (84.4 mg, 62%). ^{1}H NMR (400 MHz, D_2O) δ 8.95 (d, J = 6.6 Hz, 4H), 8.29 (d, J = 6.6 Hz, 4H), 8.00 (dd, J_1 = 6.5 Hz, J_2 = 3.3 Hz, 2H), 7.82 (s, 2H), 7.74 (dd, J = 6.5, 3.2 Hz, 2H), 4.52 (s, 6H). ^{13}C NMR (101 MHz, D_2O) δ 156.70, 145.03, 136.35, 130.10, 128.93, 128.36, 127.49, 125.16, 47.51. MS calcd for $C_{22}H_{20}N_2$ $[M]^{2+}$: 156.0808; found: 156.0808.

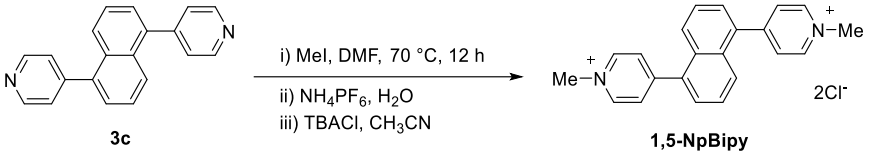

1,5-NpBipy was prepared according to the procedure described for **2,6-BpBipy** from the reaction of **3c** and MeI as a white solid (89.9mg, 66%). ^{1}H NMR (400 MHz, D_2O) δ 8.93 (d, J = 6.5 Hz, 4H), 8.28 (d, J = 6.3 Hz, 4H), 8.08 (dd, J_1 = 6.3 Hz, J_2 = 3.2 Hz, 2H), 7.81–7.75 (m, 4H), 4.51 (s, 6H). ^{13}C NMR (101 MHz, D_2O) δ 157.10, 144.93, 134.56, 130.00, 128.97, 127.13, 127.05, 47.30. MS calcd for $C_{22}H_{20}N_2$ $[M]^{2+}$: 156.0808; found: 156.0818.

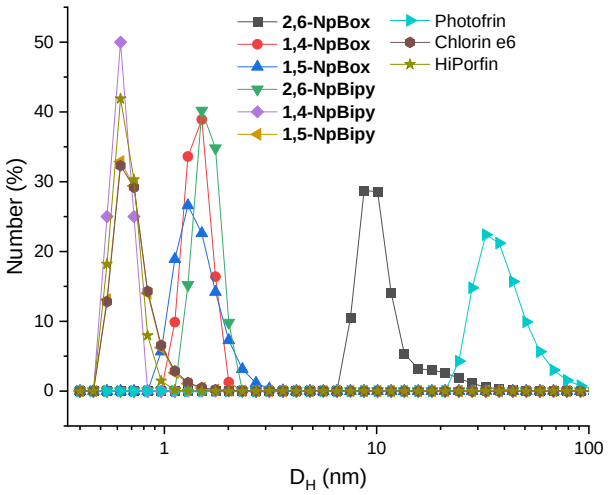

Fig. S1 DLS of Photofrin ([porphyrin] = 0.1 mM), Chlorin e6 (0.1 mM), HiPorfin (0.1 mM), **2,6-NpBox** (0.1 mM), **1,4-NpBox** (0.1 mM), **1,5-NpBox** (0.1 mM), **2,6-NpBipy** (0.2 mM), **1,4-NpBipy** (0.2 mM) and **1,5-NpBipy** (0.2 mM) in water at 25 °C.

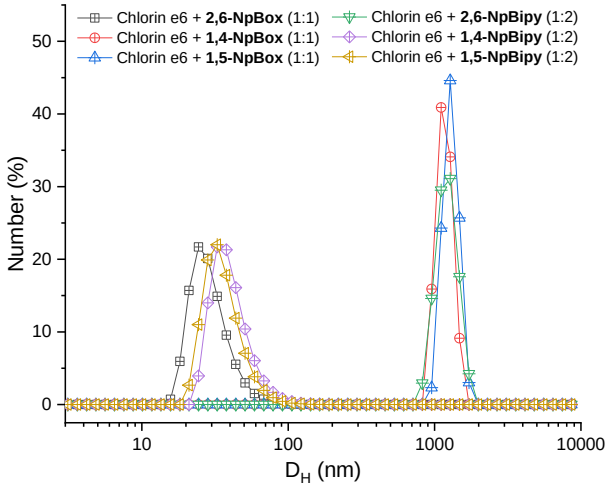

Fig. S2 DLS of the mixtures of Chlorin e6 (0.1 mM) with **2,6-NpBox** (0.1 mM), **1,4-NpBox** (0.1 mM), **1,5-NpBox** (0.1 mM), **2,6-NpBipy** (0.2 mM), **1,4-NpBipy** (0.2 mM) and **1,5-NpBipy** (0.2 mM) in water at 25 °C.

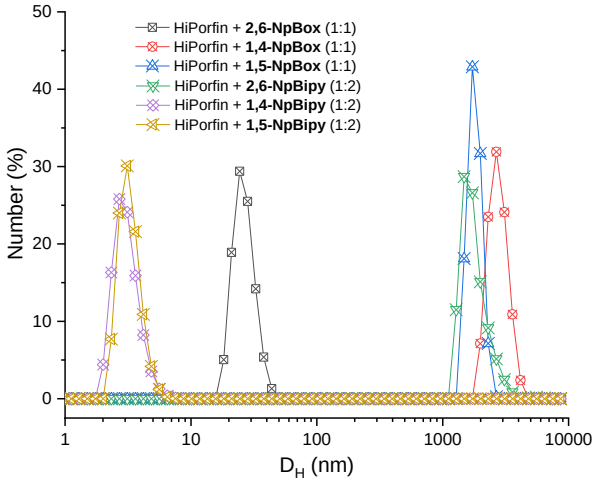

Fig. S3 DLS of the mixtures of HiPorfin (0.1 mM) with **2,6-NpBox** (0.1 mM), **1,4-NpBox** (0.1 mM), **1,5-NpBox** (0.1 mM), **2,6-NpBipy** (0.2 mM), **1,4-NpBipy** (0.2 mM) and **1,5-NpBipy** (0.2 mM) in water at 25 °C.

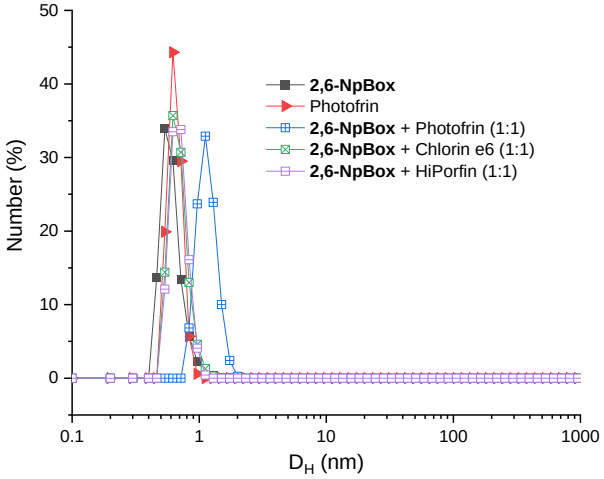

Fig. S4 DLS of the mixtures of **2,6-NpBox** (0.1 mM), Photofrin ([porphyrin] = 0.1 mM) and the mixtures of **2,6-NpBox** ([porphyrin] = 0.1 mM) with Photofrin (0.1 mM), Chlorin e6 (0.1 mM) and HiPorfin (0.1 mM) in water and DMSO (20%, v/v) at 25 °C.

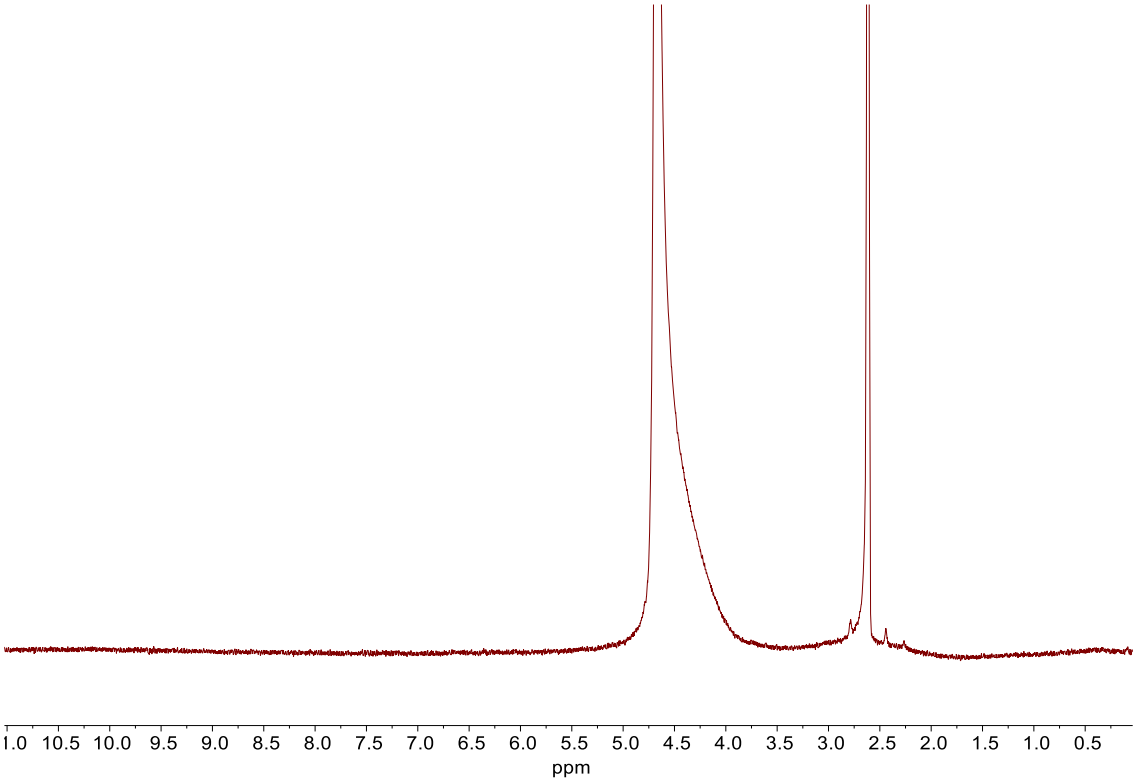

Fig. S5 ^{1}H NMR spectrum (400 MHz) of Photofrin ([porphyrin] = 0.3 mM) in D_2O and DMSO-d_6 (20%, v/v) at 25 °C.

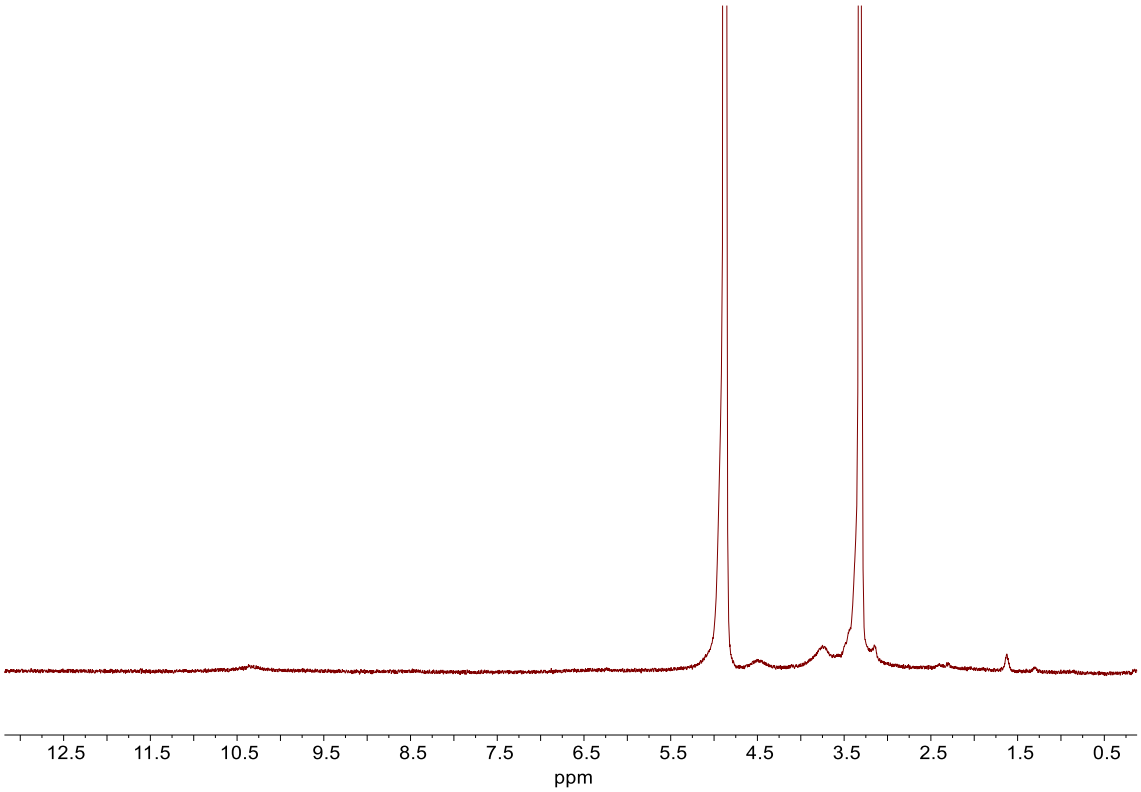

Fig. S6 ^{1}H NMR spectrum (400 MHz) of Photofrin ([porphyrin] = 0.3 mM) in CD_3OD at 25 °C.

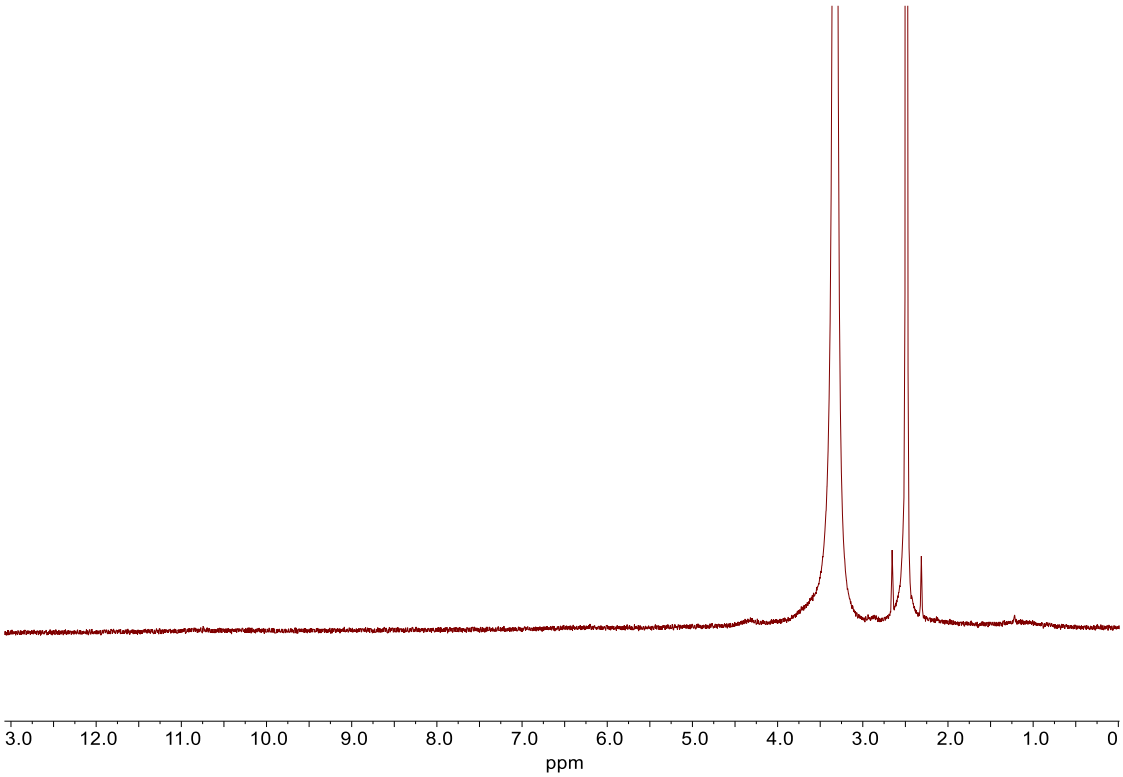

Fig. S7 ^{1}H NMR spectrum (400 MHz) of Photofrin ([porphyrin] = 0.3 mM) in DMSO-d_6 at 25 °C.

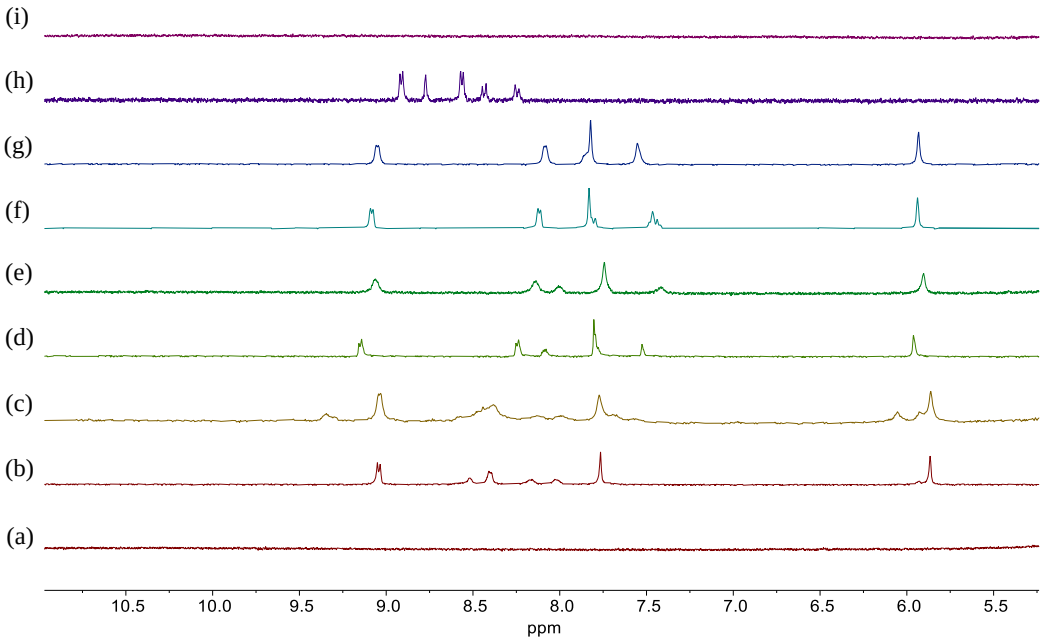

Fig. S8 ^{1}H NMR spectra (400 MHz, DMSO-d_6/D_2O 1:4) recorded at 25 °C for (a) Photofrin (0.2 mM), (b) [**2,6-NpBox**] (0.2 mM), (c) [**2,6-NpBox**]/[Photofrin] = 1, (d) [**1,4-NpBox**] (0.2 mM), (e) [**1,4-NpBox**]/[Photofrin] = 1, (f) [**1,5-NpBox**] (0.2 mM), (g) [**1,5-NpBox**]/[Photofrin] = 1, (h) [**2,6-NpBipy**] (0.4 mM) and (i) [**2,6-NpBipy**]/[Photofrin] = 2.

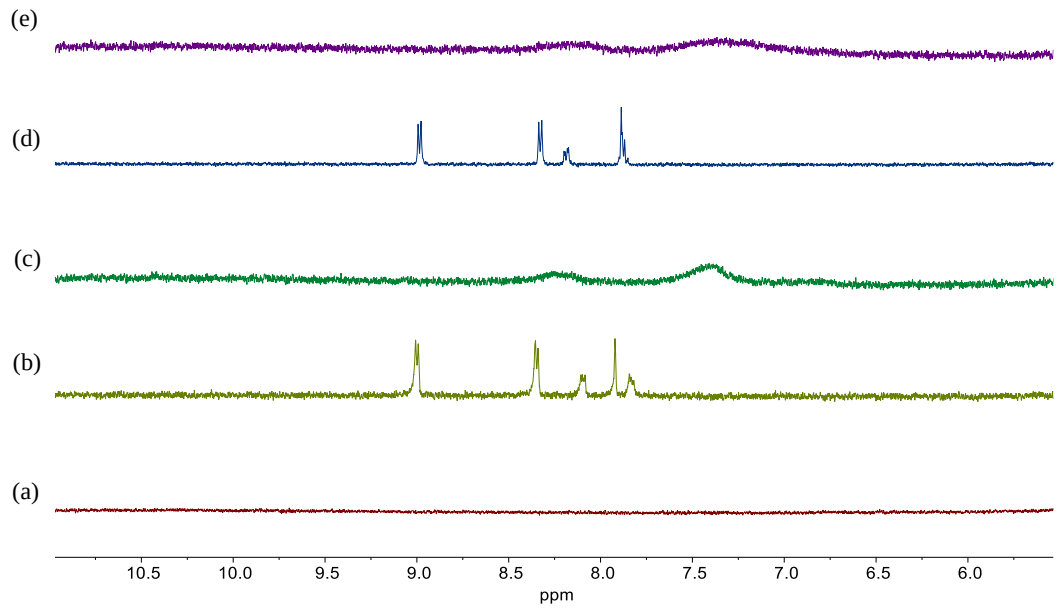

Fig. S9 ^{1}H NMR spectra (400 MHz, DMSO-d_6/D_2O 1:4) recorded at 25 °C for (a) Photofrin (0.2 mM), (b) [**1,4-NpBipy**] (0.4 mM), (c) [**1,4-NpBipy**]/[Photofrin] = 2, (d) [**1,5-NpBipy**] (0.4 mM) and (e) [**1,5-NpBipy**]/[Photofrin] = 2.

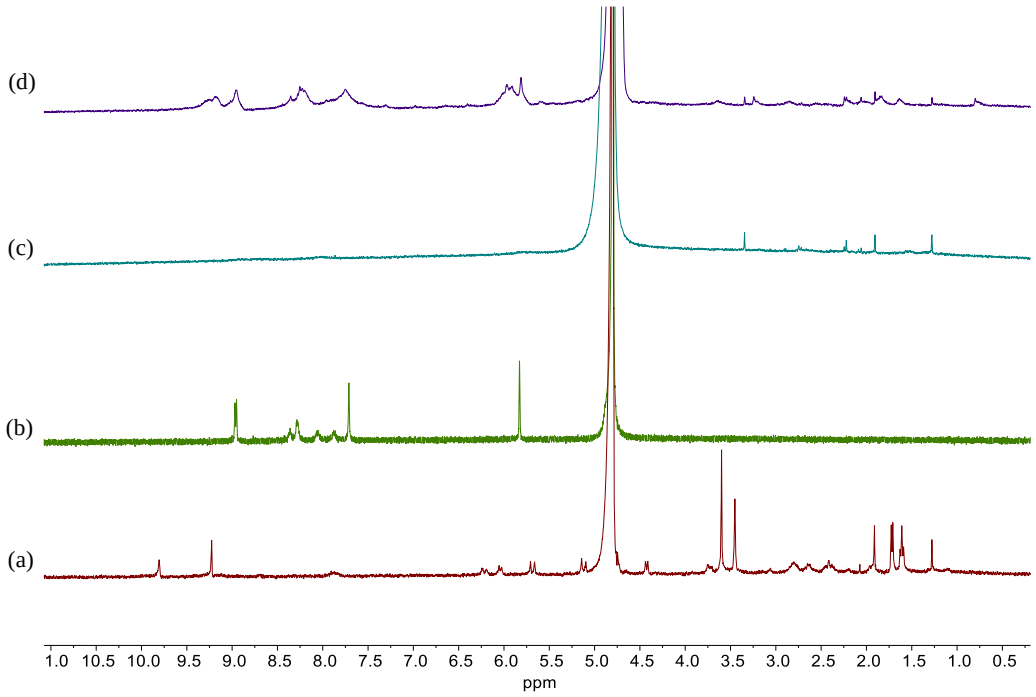

Fig. S10 ^{1}H NMR spectra (400 MHz, D_2O) recorded at 25 °C for (a) Chlorin e6 (0.2 mM), (b) **2,6-NpBox** (0.2 mM), (c) [**2,6-NpBox**]/[Chlorin e6] = 0.5 ([Chlorin e6] = 0.2 mM) and (d) [**2,6-NpBox**]/[Chlorin e6] = 1 ([Chlorin e6] = 0.2 mM).

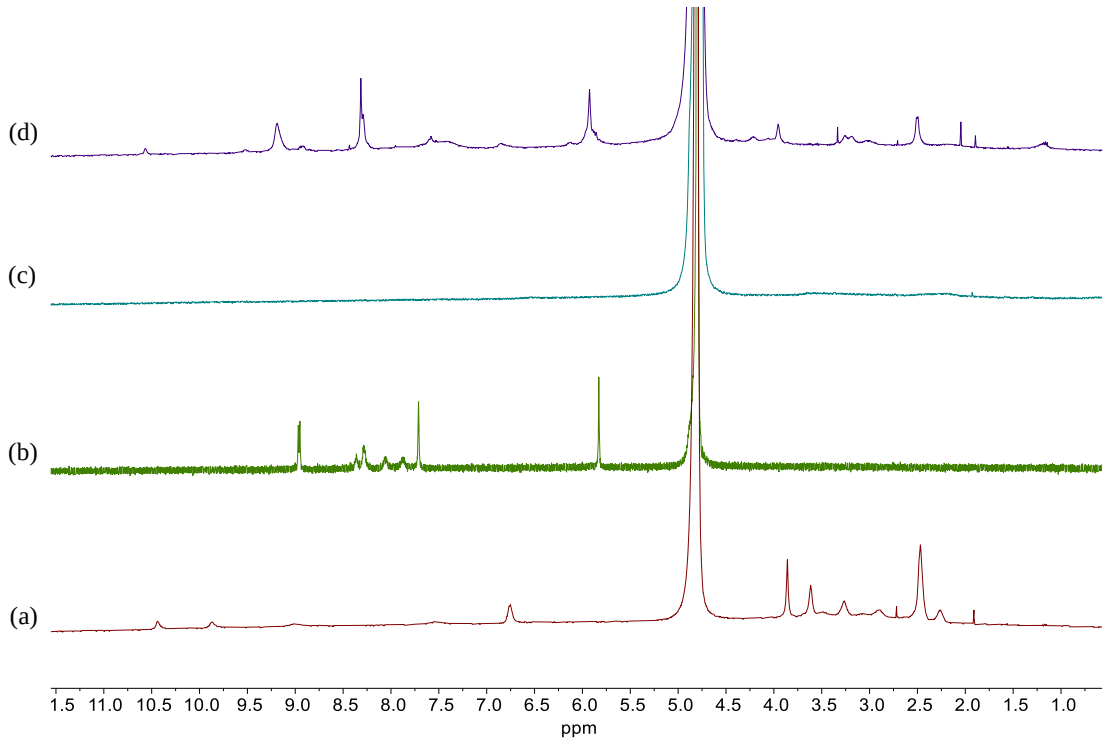

Fig. S11 ^{1}H NMR spectra (400 MHz, D_2O) recorded at 25 °C for (a) HiPorfin (0.2 mM), (b) **2,6-NpBox** (0.2 mM), (c) [**2,6-NpBox**]/[HiPorfin] = 0.5 ([HiPorfin] = 0.2 mM), (d) [**2,6-NpBox**]/[HiPorfin] = 1 ([HiPorfin] = 0.2 mM).

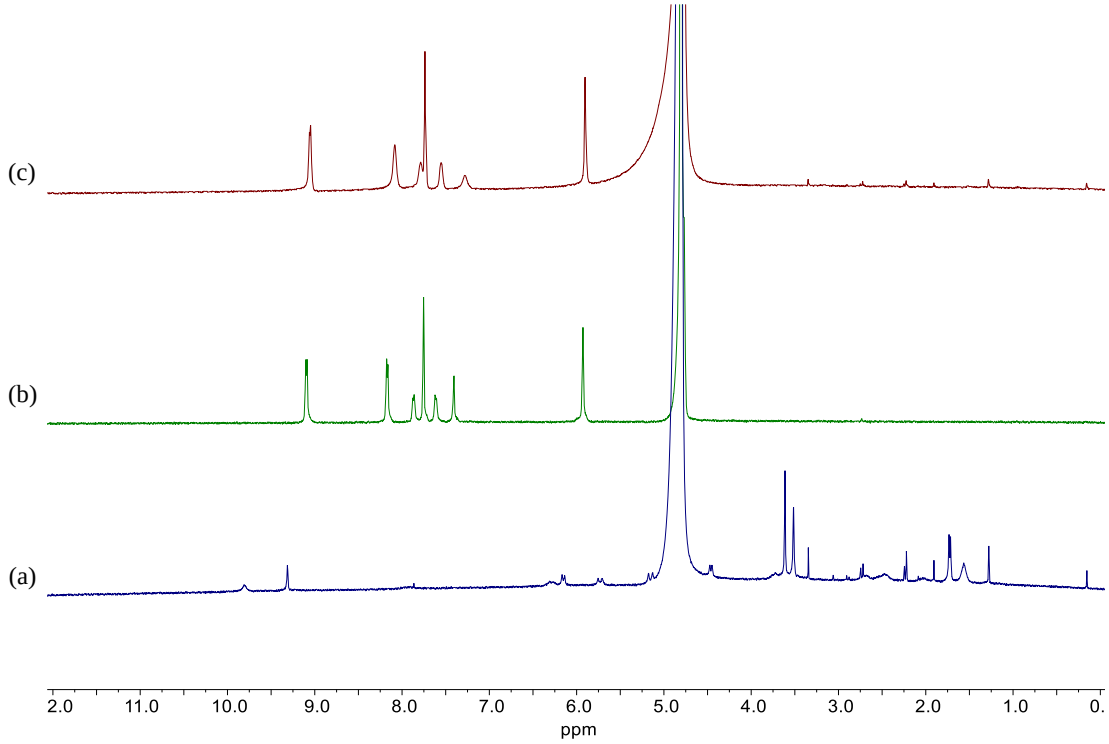

Fig. S12 ^{1}H NMR spectra (400 MHz, D_2O) recorded at 25 °C for (a) Chlorin e6 (0.2 mM), (b) **1,4-NpBox** (0.2 mM), and (c) the 1:1 mixture of Chlorin e6 and **1,4-NpBox** (0.2 mM).

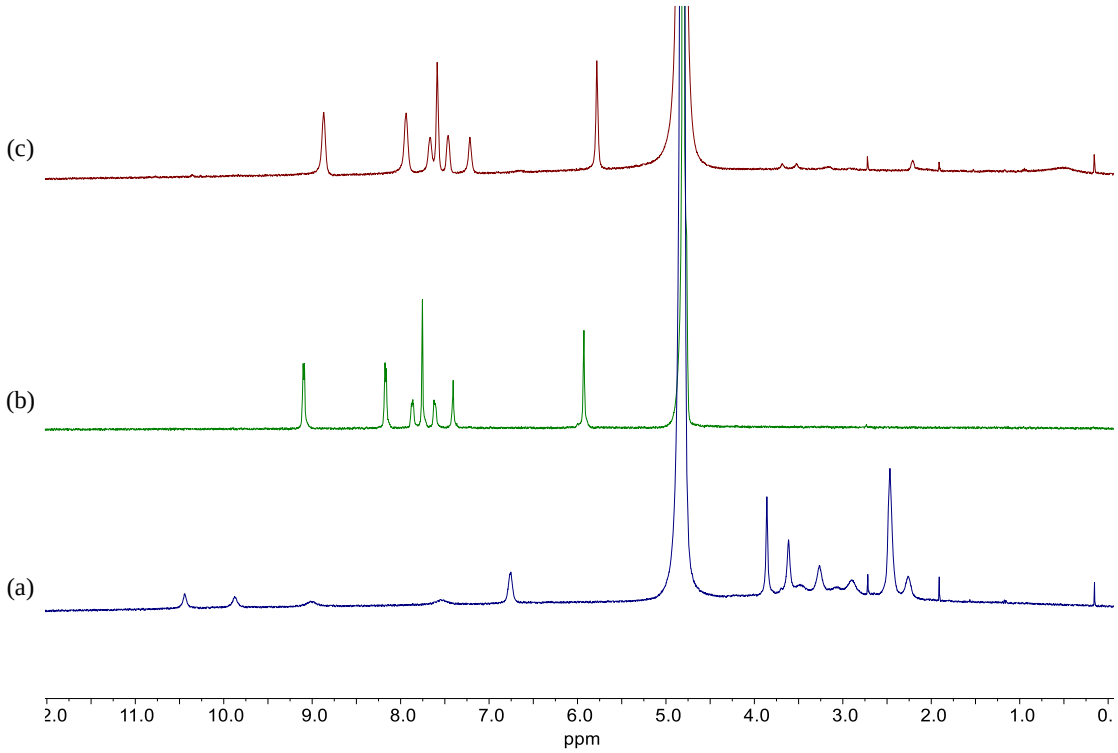

Fig. S13 ^{1}H NMR spectra (400 MHz, D_2O) recorded at 25 °C for (a) HiPorfin (0.2 mM), (b) **1,4-NpBox** (0.2 mM), and (c) the 1:1 mixture of HiPorfin and **1,4-NpBox** (0.2 mM).

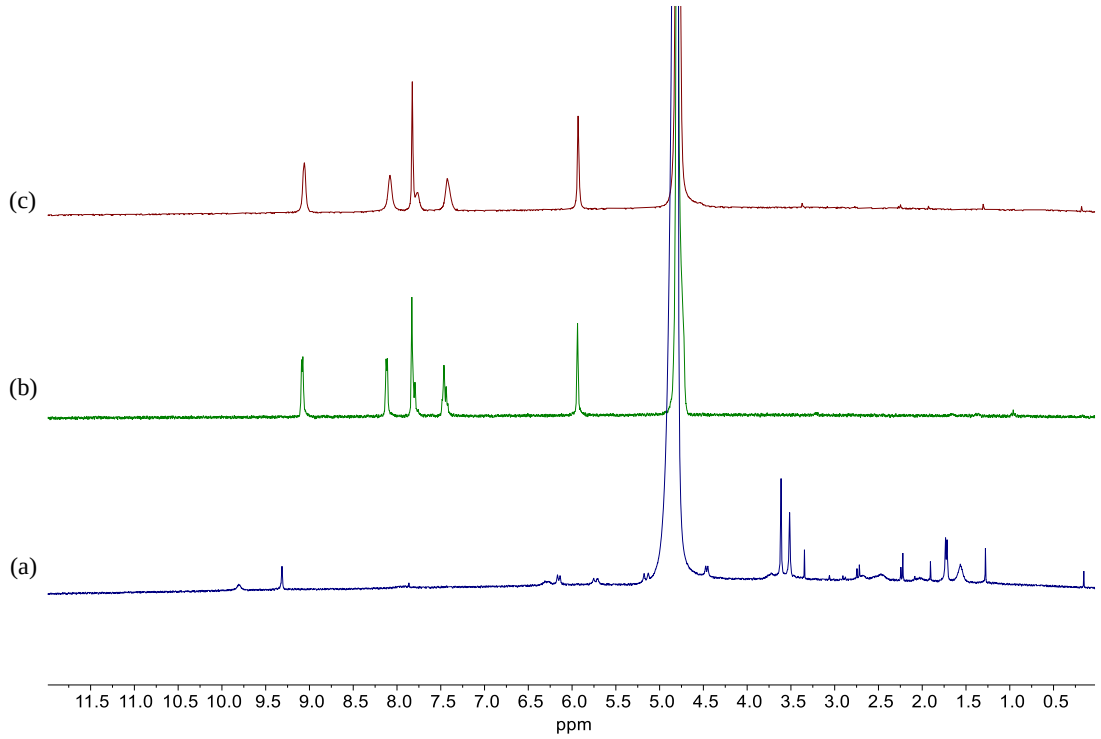

Fig. S14 ^{1}H NMR spectra (400 MHz, D_2O) recorded at 25 °C for (a) Chlorin e6 (0.2 mM), (b) **1,5-NpBox** (0.2 mM), and (c) the 1:1 mixture of Chlorin e6 and **1,5-NpBox** (0.2 mM).

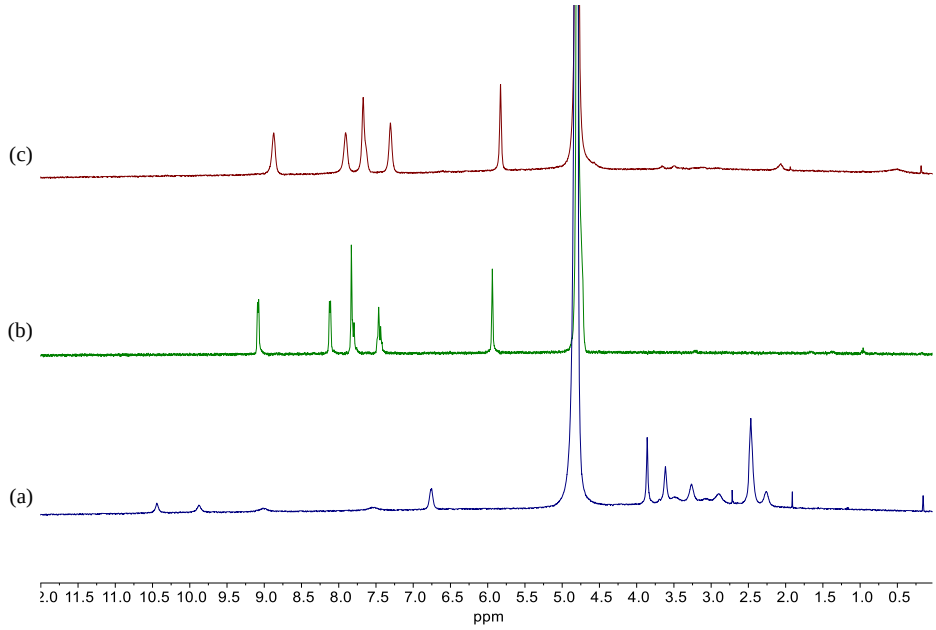

Fig. S15 ^{1}H NMR spectra (400 MHz, D_2O) recorded at 25 °C for (a) HiPorfin (0.2 mM), (b) **1,5-NpBox** (0.2 mM) and (c) the 1:1 mixture of HiPorfin and **1,5-NpBox** (0.2 mM).

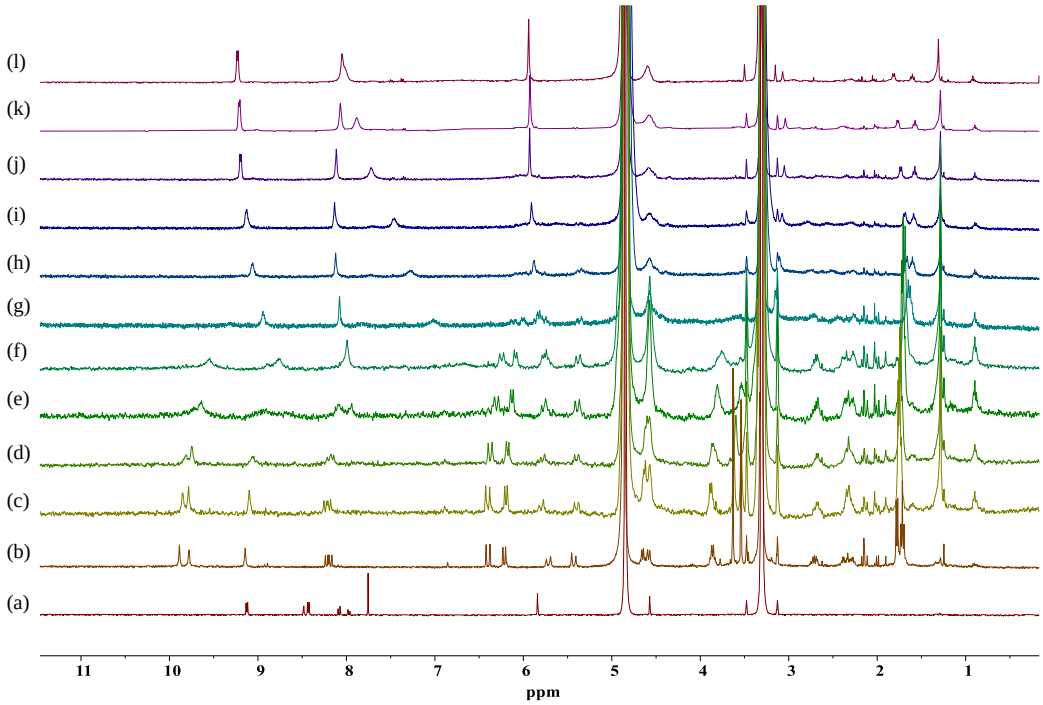

Fig. S16 ^{1}H NMR spectra (400 MHz, CD_3OD) recorded at 25 °C for (a) **2,6-NpBox** (0.2 mM), (b) Chlorin e6 (0.2 mM), (c) [**2,6-NpBox**]/[Chlorin e6] = 0.05, (d) [**2,6-NpBox**]/[Chlorin e6]= 0.1, (e) [**2,6-NpBox**]/[Chlorin e6] = 0.2, (f) [**2,6-NpBox**]/[Chlorin e6] = 0.3, (g) [**2,6-NpBox**]/[Chlorin e6] = 0.4, (h) [**2,6-NpBox**]/[Chlorin e6] = 0.6, (i) [**2,6-NpBox**]/[Chlorin e6] = 0.8, (j) [**2,6-NpBox**]/[Chlorin e6] = 1 , (k) [**2,6-NpBox**]/[Chlorin e6] = 1.2 , (l) [**2,6-NpBox**]/[Chlorin e6] = 1.4.

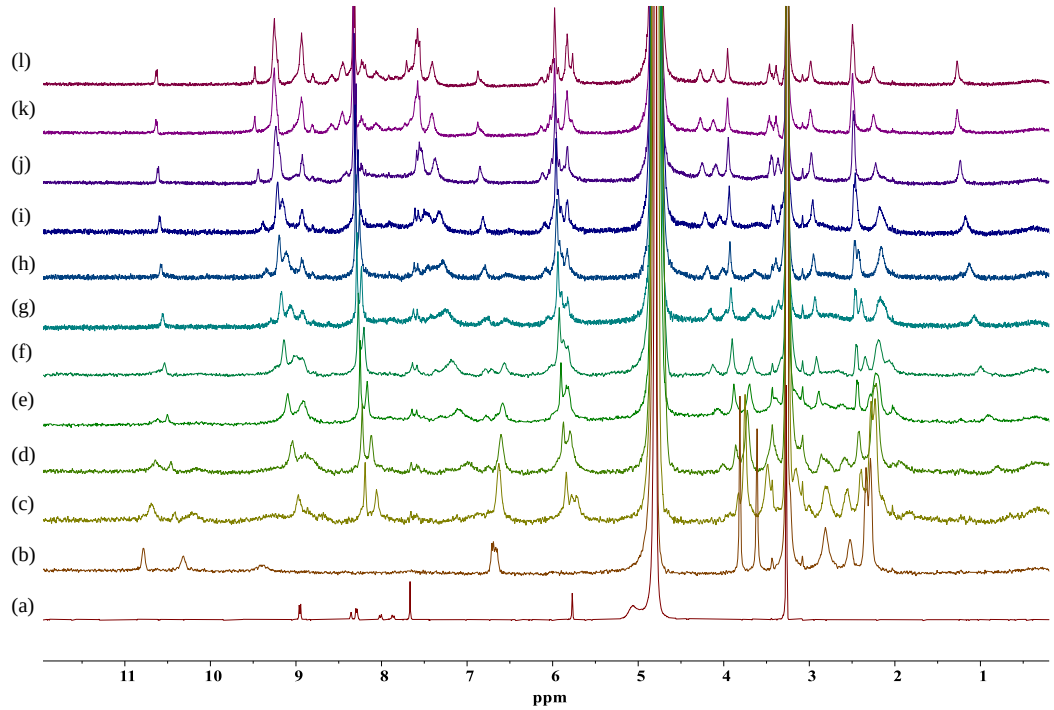

Fig. S17 ^{1}H NMR spectra (400 MHz, CD_3OD/D_2O 1:4 v/v) at 25 °C recorded for (a) **2,6-NpBox** (0.2 mM), (b) HiPorfin (0.2 mM), (c) [**2,6-NpBox**]/[HiPorfin] = 0.05, (d) [**2,6-NpBox**]/[HiPorfin] = 0.1, (e) [**2,6-NpBox**]/[HiPorfin] = 0.2, (f) [**2,6-NpBox**]/[HiPorfin] = 0.3, (g) [**2,6-NpBox**]/[HiPorfin] = 0.4, (h) [**2,6-NpBox**]/[HiPorfin] = 0.6, (i) [**2,6-NpBox**]/[HiPorfin] = 0.8, (j) [**2,6-NpBox**]/[HiPorfin] = 1, (k) [**2,6-NpBox**]/[HiPorfin] = 1.2 , (l) [**2,6-NpBox**]/[HiPorfin] = 1.4.

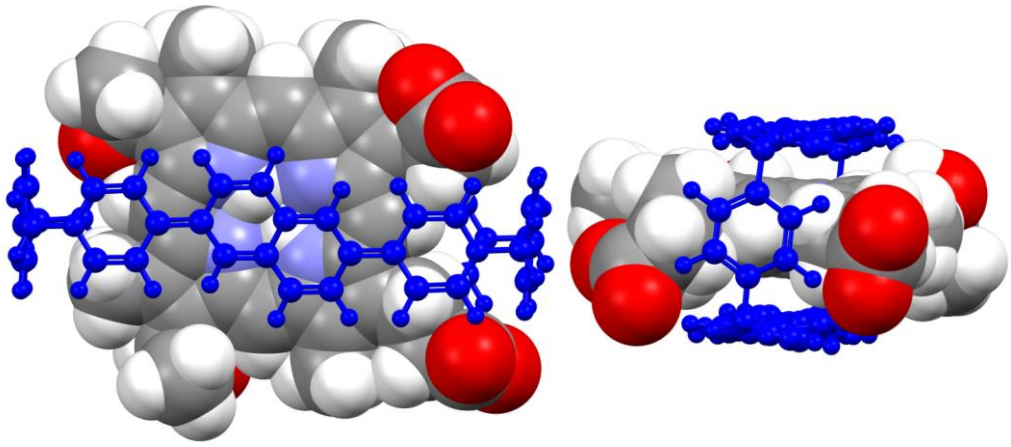

Fig. S18 Low-energy complex HiPorfin⊂**2,6-NpBox** with the carboxylate groups of HiPorfin being located on the two sides of **2,6-NpBox** (overlook and eyelevel look).

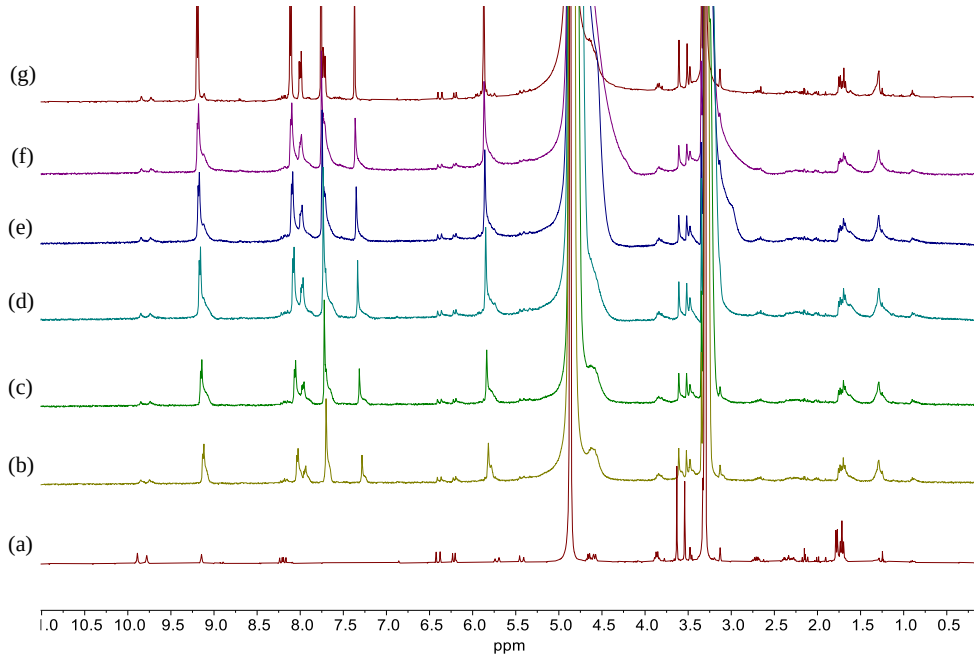

Fig. S19 ^{1}H NMR spectra recorded (400 MHz, CD_3OD) recorded at 25 °C for (a) Chlorin e6, (b) [**1,4-NpBox**]/[Chlorin e6] = 0.4, (c) [**1,4-NpBox**]/[Chlorin e6] = 0.8, (d) [**1,4-NpBox**]/[Chlorin e6] = 1.2 (e) [**1,4-NpBox**]/[Chlorin e6] = 1.6, (f) [**1,4-NpBox**]/[Chlorin e6] = 2, (g) [**1,4-NpBox**]/[Chlorin e6] = 2.4 ([Chlorin e6] = 0.2 mM).

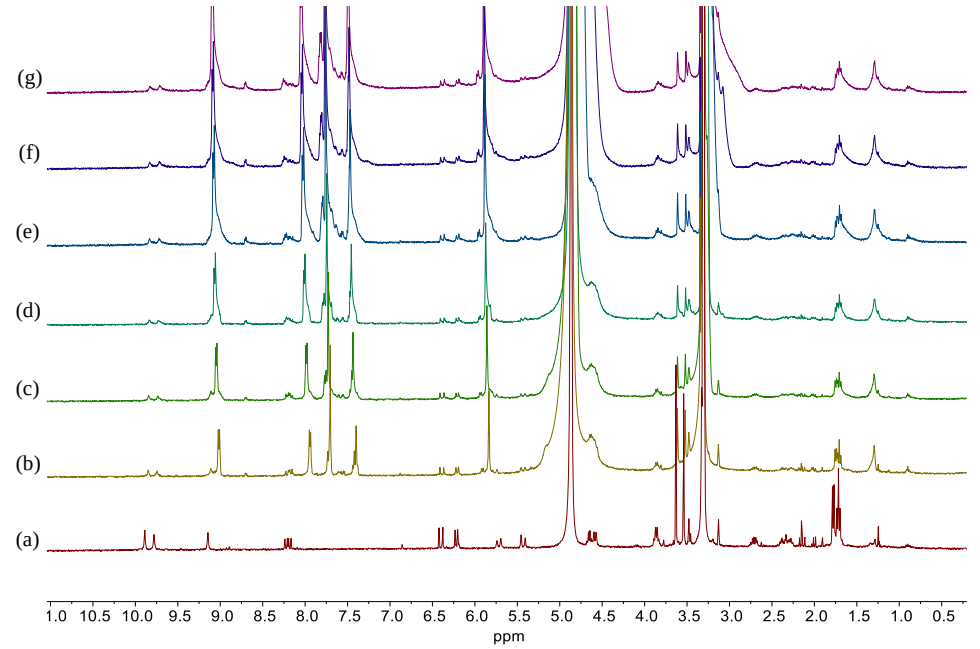

Fig. S20 ^{1}H NMR spectra recorded (400 MHz, CD_3OD) recorded at 25 °C for: (a) Chlorin e6, (b) [**1,5-NpBox**]/[Chlorin e6] = 0.4, (c) [**1,5-NpBox**]/[Chlorin e6] = 0.8, (d) [**1,5-NpBox**]/[Chlorin e6] = 1.2 (e) [**1,5-NpBox**]/[Chlorin e6] = 1.6, (f) [**1,5-NpBox**]/[Chlorin e6] = 2, (g) [**1,5-NpBox**]/[Chlorin e6] = 2.4 ([Chlorin e6] = 0.2 mM).

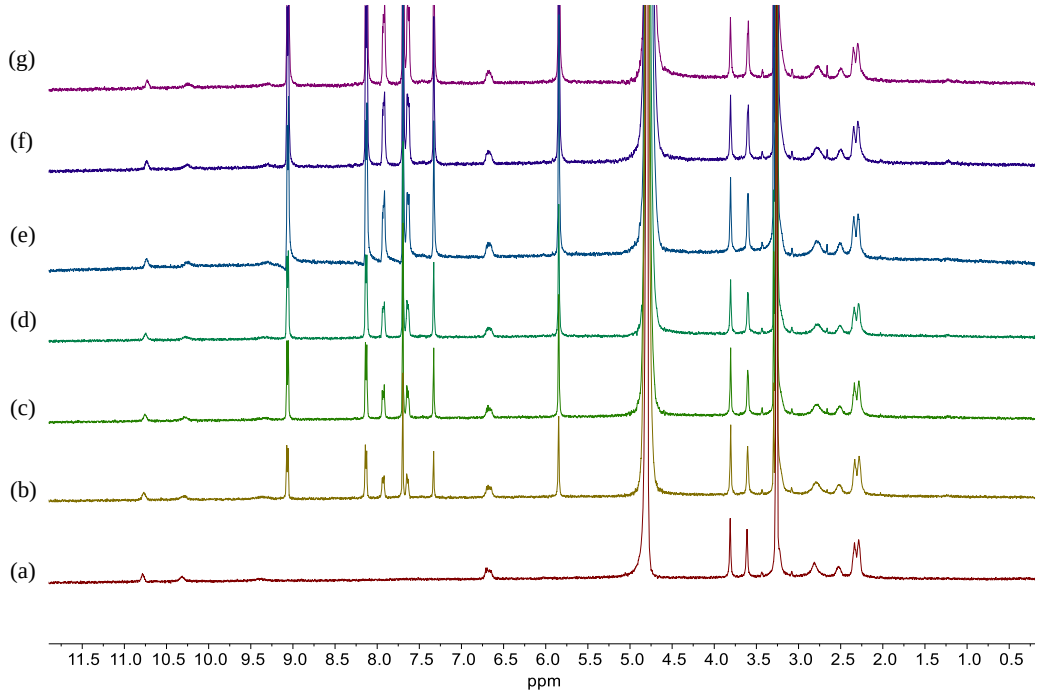

Fig. S21 ^{1}H NMR spectra recorded (400 MHz, CD_3OD/D_2O 1:4 v/v) recorded at 25 °C for (a) HiPorfin, (b) [**1,4-NpBox**]/[HiPorfin] = 0.4, (c) [**1,4-NpBox**]/[HiPorfin] = 0.8, (d) [**1,4-NpBox**]/[HiPorfin] = 1.2 (e) [**1,4-NpBox**]/[HiPorfin] = 1.6, (f) [**1,4-NpBox**]/[HiPorfin] = 2, (g) [**1,4-NpBox**]/[HiPorfin] = 2.4 ([HiPorfin] = 0.2 mM).

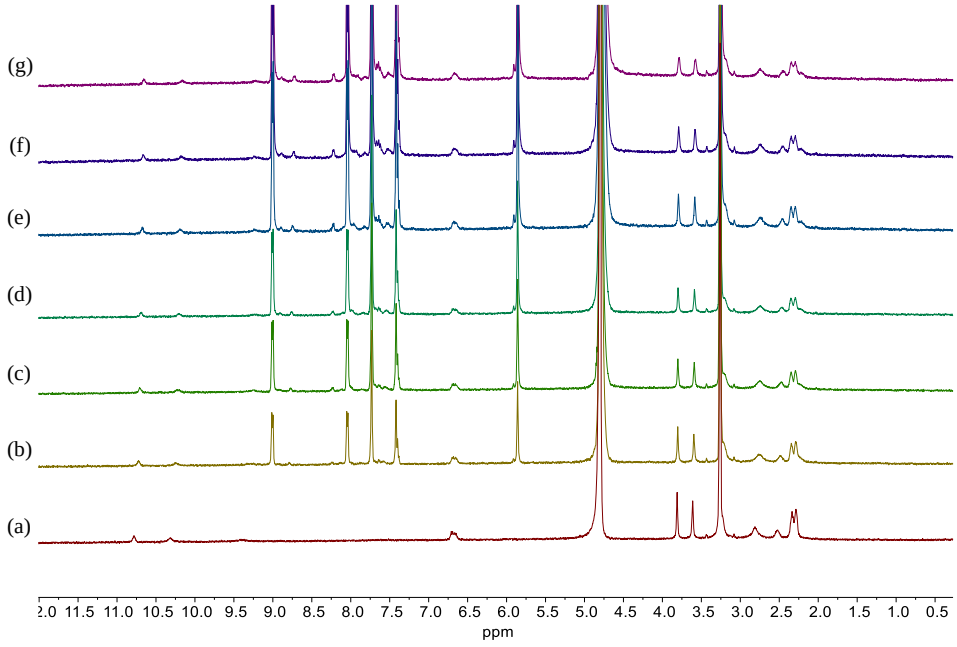

Fig. S22 ^{1}H NMR spectra recorded (400 MHz, CD_3OD/D_2O 1:4 v/v) recorded at 25 °C for: (a) HiPorfin, (b) [**1,5-NpBox**]/[HiPorfin] = 0.4, (c) [**1,5-NpBox**]/[HiPorfin] = 0.8, (d) [**1,5-NpBox**]/[HiPorfin] = 1.2 (e) [**1,5-NpBox**]/[HiPorfin] = 1.6, (f) [**1,5-NpBox**]/[HiPorfin] = 2, (g) [**1,5-NpBox**]/[HiPorfin] = 2.4 ([HiPorfin] = 0.2 mM).

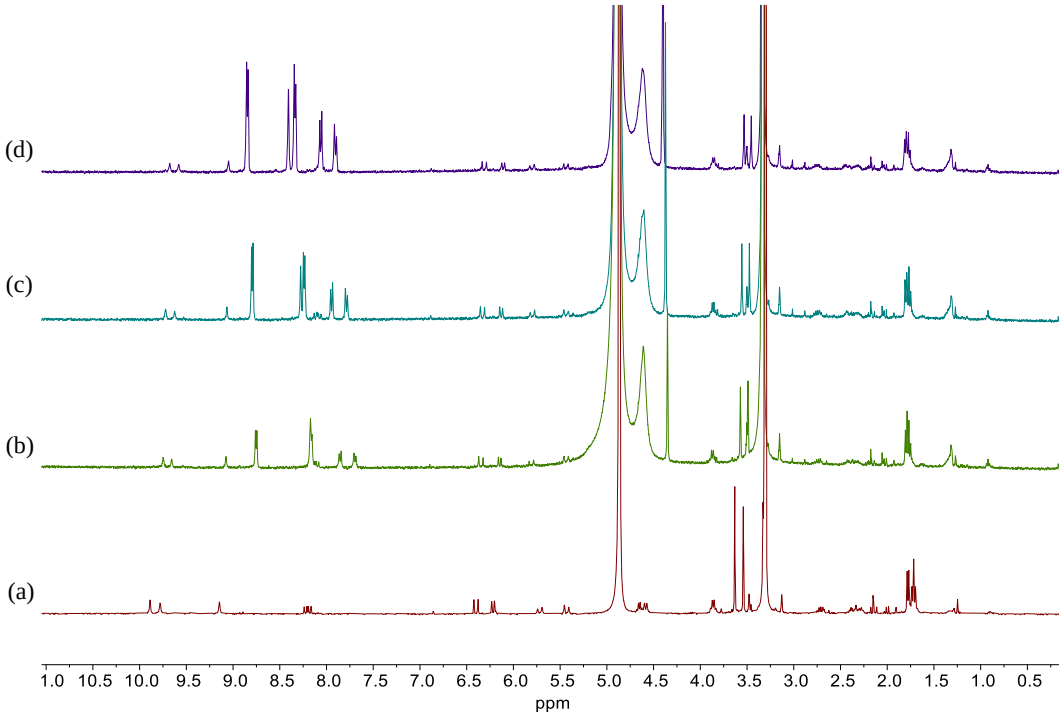

Fig. S23 ^{1}H NMR spectra recorded (400 MHz, CD_3OD) recorded at 25 °C for (a) Chlorin e6, (b) [**2,6-NpBipy**]/[Chlorin e6] = 1, (c) [**2,6-NpBipy**]/[Chlorin e6] = 2, (d) [**2,6-NpBipy**]/[Chlorin e6] = 4 ([Chlorin e6] = 0.2 mM).

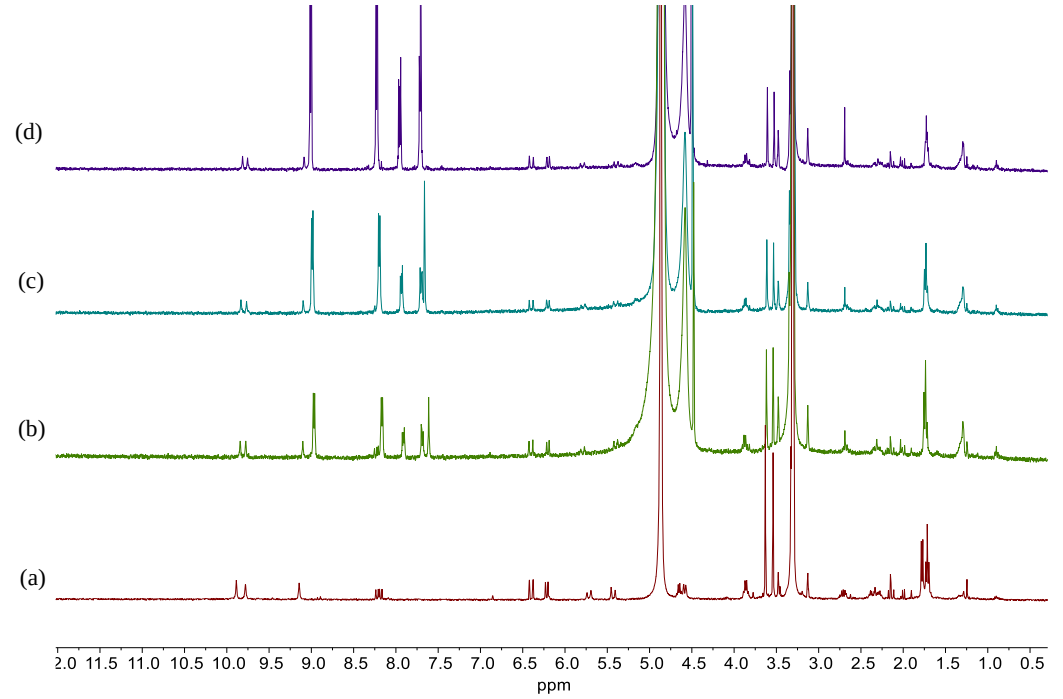

Fig. S24 ^{1}H NMR spectra recorded (400 MHz, CD_3OD) recorded at 25 °C for (a) Chlorin e6, (b) [**1,4-NpBipy**]/[Chlorin e6] = 1, (c) [**1,4-NpBipy**]/[Chlorin e6] = 2, (d) [**1,4-NpBipy**]/[Chlorin e6] = 4 ([Chlorin e6] = 0.2 mM).

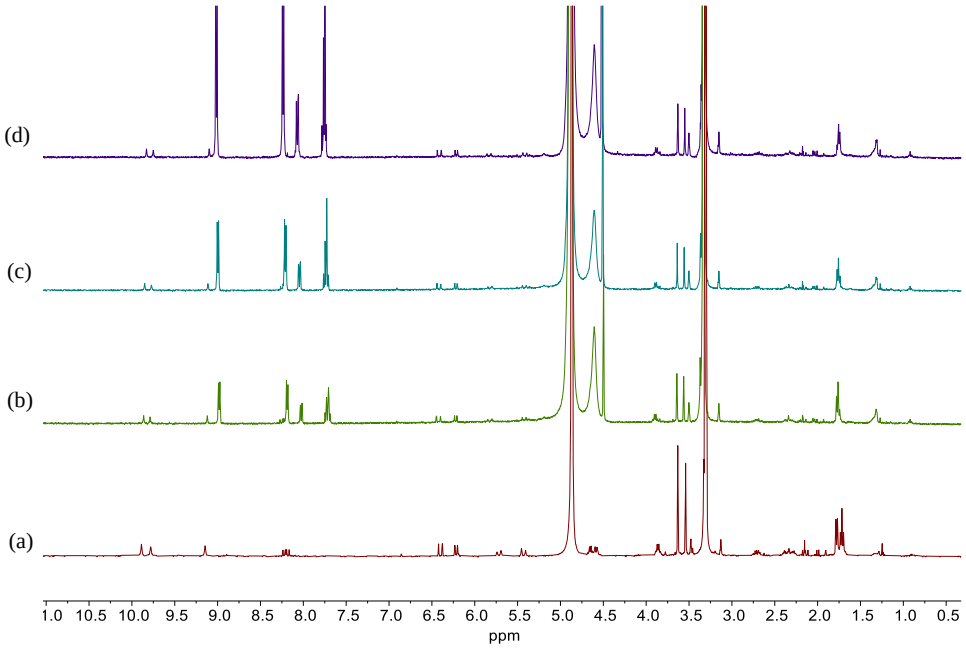

Fig. S25 ^{1}H NMR spectra recorded (400 MHz, CD_3OD) recorded at 25 °C for (a) Chlorin e6, (b) [**1,5-NpBipy**]/[Chlorin e6] = 1, (c) [**1,5-NpBipy**]/[Chlorin e6] = 2, (d) [**1,5-NpBipy**]/[Chlorin e6] = 4 ([Chlorin e6] = 0.2 mM).

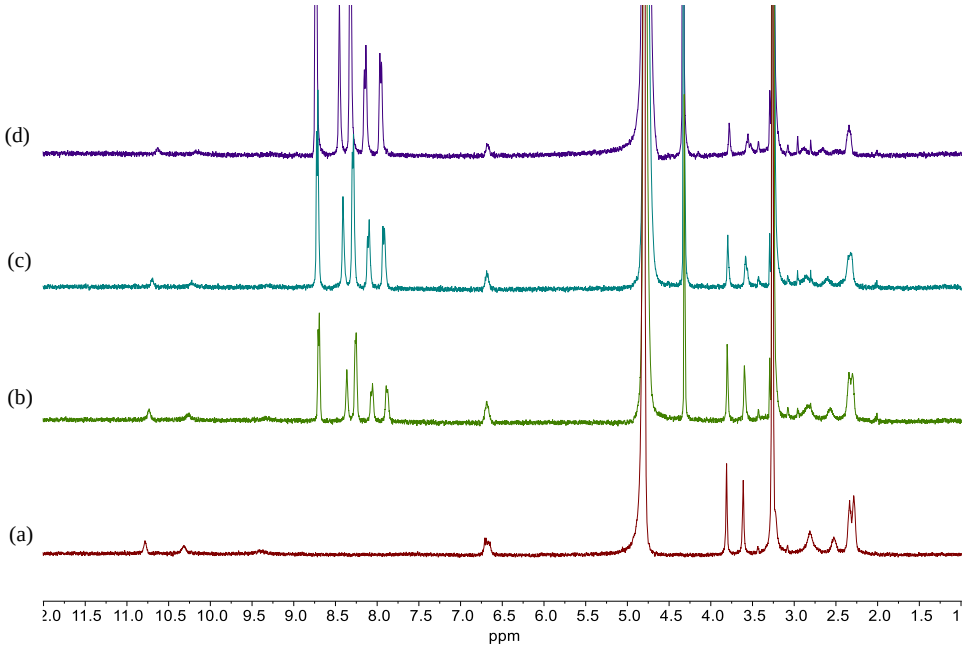

Fig. S26 ^{1}H NMR spectra recorded (400 MHz, CD_3OD/D_2O 1:4 v/v) recorded at 25 °C for (a) HiPorfin, (b) [**2,6-NpBipy**]/[HiPorfin] = 1, (c) [**2,6-NpBipy**]/[HiPorfin] = 2, (d) [**2,6-NpBipy**]/[HiPorfin] = 4 ([HiPorfin] = 0.2 mM).

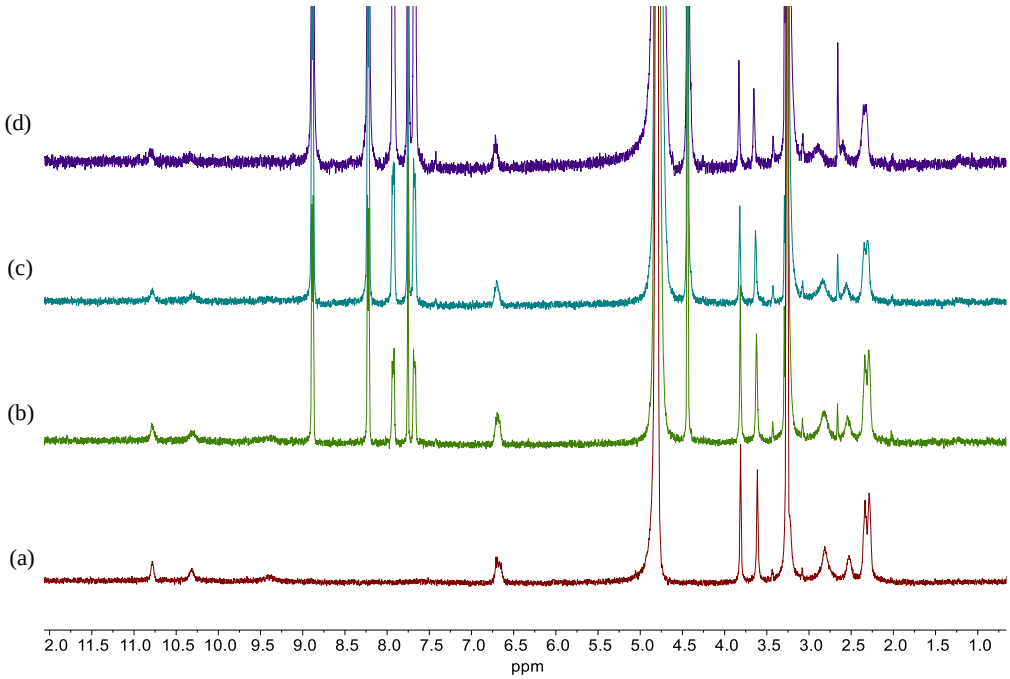

Fig. S27 ^{1}H NMR spectra recorded (400 MHz, CD_3OD/D_2O 1:4 v/v) recorded at 25 °C for (a) HiPorfin, (b) [**1,4-NpBipy**]/[HiPorfin] = 1, (c) [**1,4-NpBipy**]/[HiPorfin] = 2, (d) [**1,4-NpBipy**]/[HiPorfin] = 4 ([HiPorfin] = 0.2 mM).

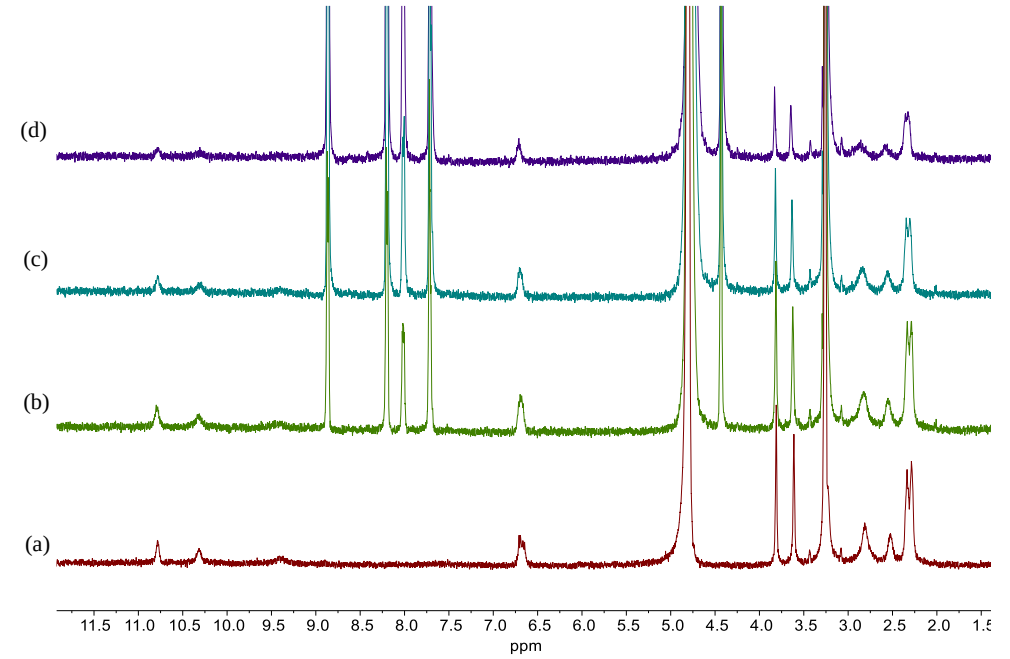

Fig. S28 ^{1}H NMR spectra recorded (400 MHz, CD_3OD/D_2O 1:4 v/v) recorded at 25 °C for (a) HiPorfin, (b) [**1,5-NpBipy**]/[HiPorfin] = 1, (c) [**1,5-NpBipy**]/[HiPorfin] = 2, (d) [**1,5-NpBipy**]/[HiPorfin] = 4 ([HiPorfin] = 0.2 mM).

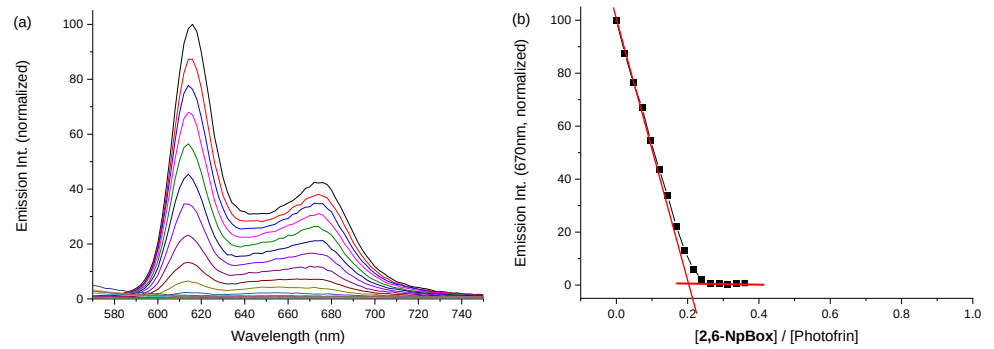

Fig. S29 (a) Fluorescence intensity of Photofrin (10 μM) with the addition of **2,6-NpBox** in 20 mM NaH_2PO_4 buffer (pH = 7.4). (b) Emission Int. (670 nm) vs [**2,6-NpBox**]/[Photofrin].

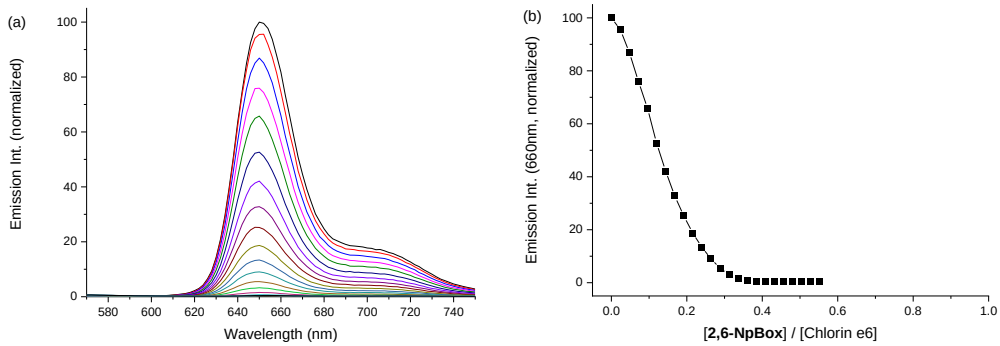

Fig. S30 (a) Fluorescence intensity of Chlorin e6 (5.0 μM) with the addition of **2,6-NpBox** in 20 mM NaH_2PO_4 buffer (pH = 7.4). (b) Emission Int. (660 nm) vs [**2,6-NpBox**]/[Chlorin e6].

\

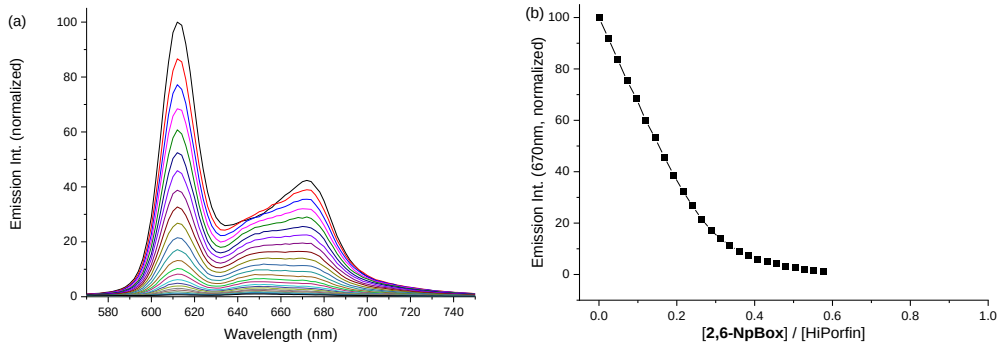

Fig. S31 (a) Fluorescence intensity of HiPorfin (5.0 μM) with the addition of **2,6-NpBox** in 20 mM NaH_2PO_4 buffer (pH = 7.4). (b) Emission Int. (670 nm) vs [**2,6-NpBox**]/[HiPorfin].

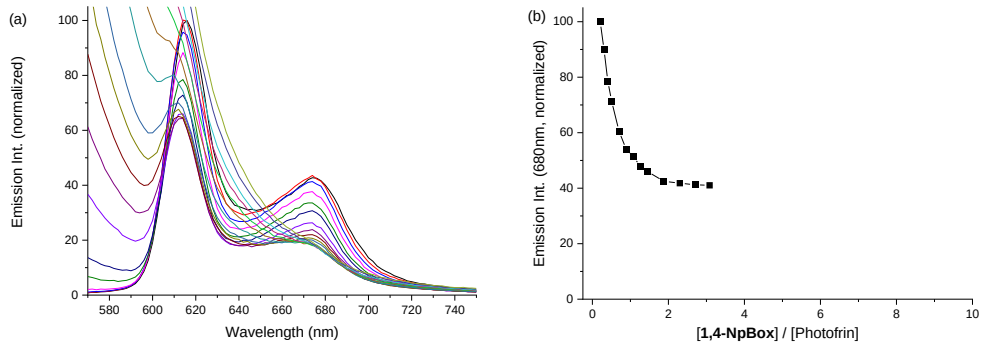

Fig. S32 (a) Fluorescence intensity of Photofrin (10 μM) with the addition of **1,4-NpBox** in 20 mM NaH_2PO_4 buffer (pH = 7.4). (b) Emission Int. (670 nm) vs [**1,4-NpBox**]/[Photofrin].

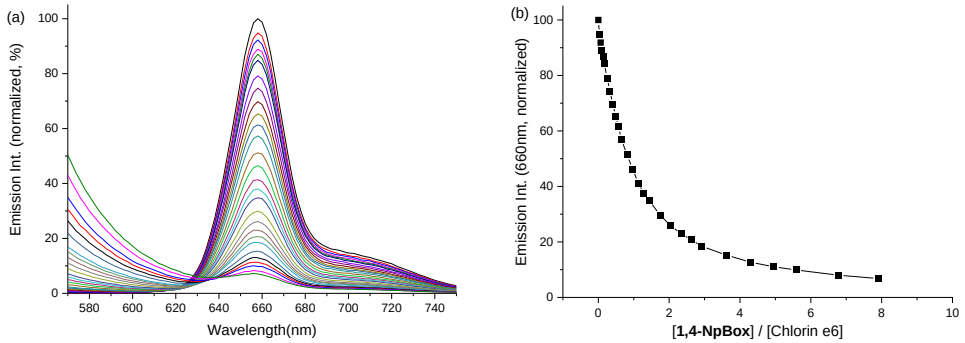

Fig. S33 (a) Fluorescence intensity of Chlorin e6 (5.0 μM) with the addition of **1,4-NpBox** in 20 mM NaH_2PO_4 buffer (pH = 7.4). (b) Emission Int. (660 nm) vs [**1,4-NpBox**]/[Chlorin e6].

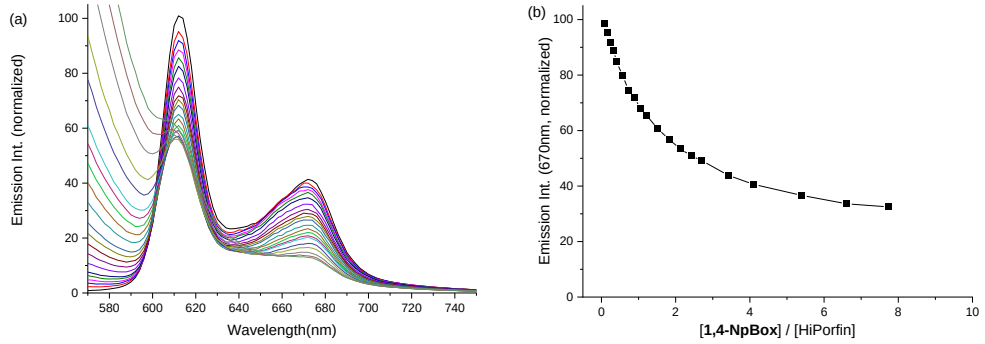

Fig. S34 (a) Fluorescence intensity of HiPorfin (5.0 μM) with the addition of **1,4-NpBox** in 20 mM NaH_2PO_4 buffer (pH = 7.4). (b) Emission Int. (670 nm) vs [**1,4-NpBox**]/[HiPorfin].

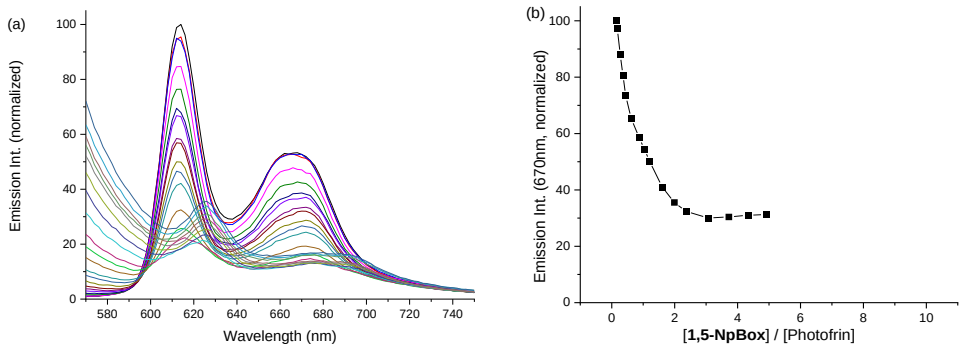

Fig. S35 (a) Fluorescence intensity of Photofrin (10 μM) with the addition of **1,5-NpBox** in 20 mM NaH_2PO_4 buffer (pH = 7.4). (b) Emission Int. (670 nm) vs [**1,5-NpBox**]/[Photofrin].

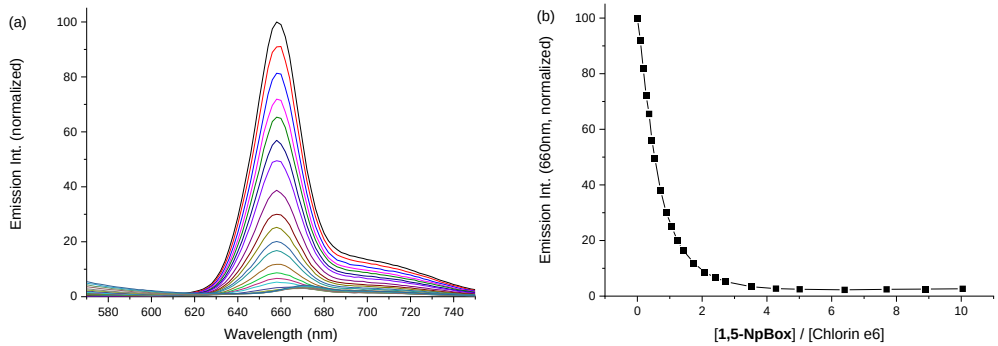

Fig. S36 (a) Fluorescence intensity of Chlorin e6 (5.0 μM) with the addition of **1,5-NpBox** in 20 mM NaH_2PO_4 buffer (pH = 7.4). (b) Emission Int. (660 nm) vs [**1,5-NpBox**]/[Chlorin e6].

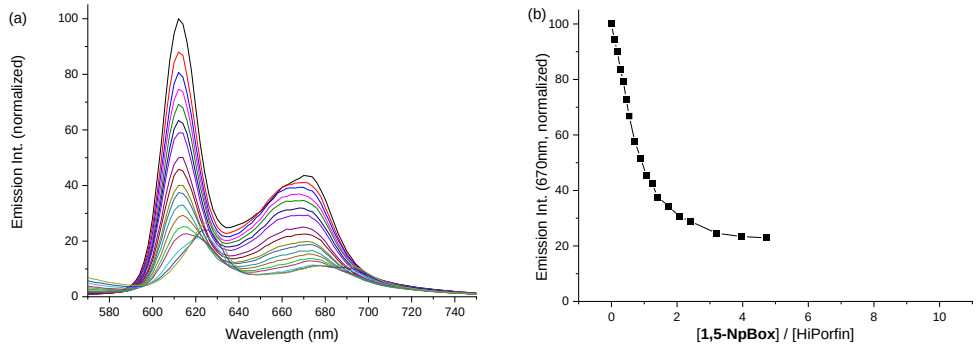

Fig. S37 (a) Fluorescence intensity of HiPorfin (5.0 μM) with the addition of **1,5-NpBox** in 20 mM NaH_2PO_4 buffer (pH = 7.4). (b) Emission Int. (670 nm) vs [**1,5-NpBox**]/[HiPorfin].

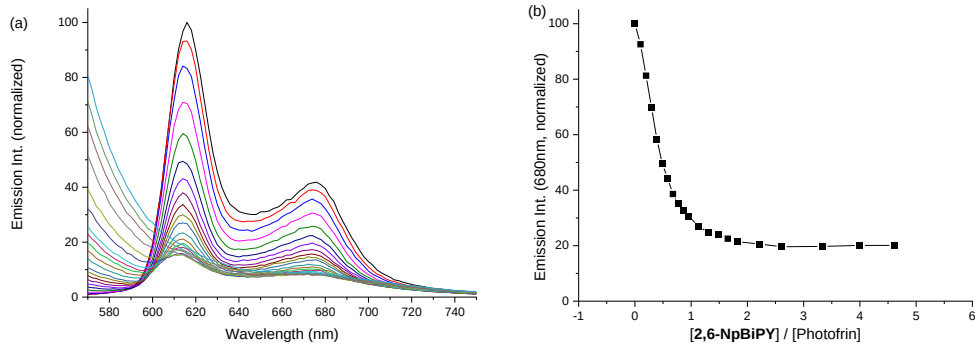

Fig. S38 (a) Fluorescence intensity of Photofrin (10 μM) with the addition of **2,6-NpBipy** in 20 mM NaH_2PO_4 buffer (pH = 7.4). (b) Emission Int. (670 nm) vs [**2,6-NpBipy**]/[Photofrin].

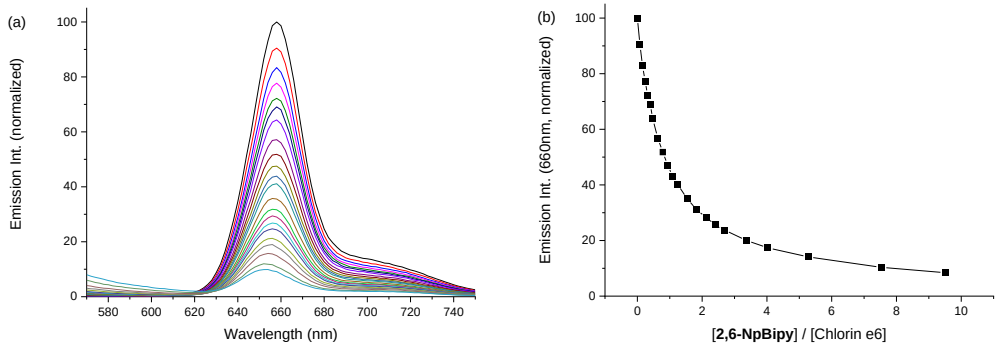

Fig. S39 (a) Fluorescence intensity of Chlorin e6 (5.0 μM) with the addition of **2,6-NpBipy** in 20 mM NaH_2PO_4 buffer (pH = 7.4). (b) Emission Int. (660 nm) vs [**2,6-NpBipy**]/[Chlorin e6].

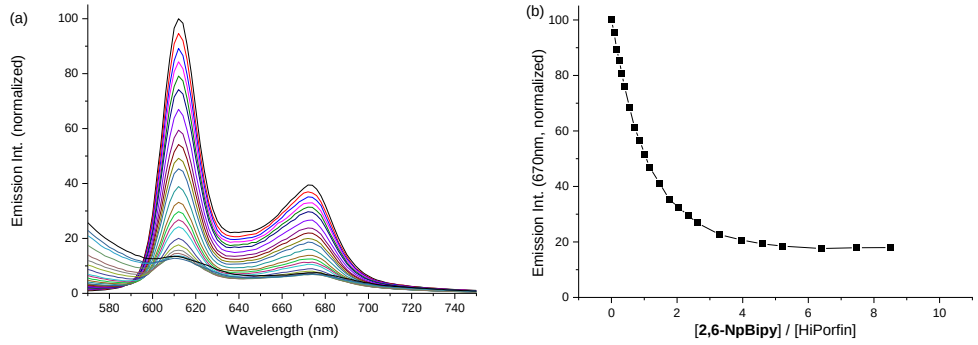

Fig. S40 (a) Fluorescence intensity of HiPorfin (5.0 μM) with the addition of **2,6-NpBipy** in 20 mM NaH_2PO_4 buffer (pH = 7.4). (b) Emission Int. (670 nm) vs [**2,6-NpBipy**]/[HiPorfin].

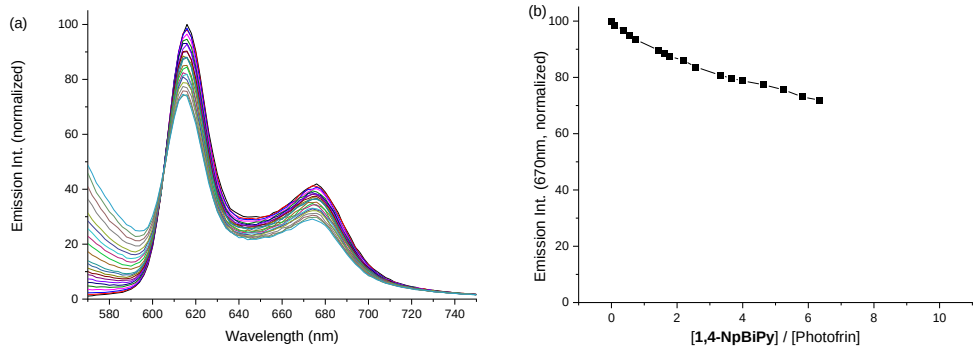

Fig. S41 (a) Fluorescence intensity of Photofrin (10 μM) with the addition of **1,4-NpBipy** in 20 mM NaH_2PO_4 buffer (pH = 7.4). (b) Emission Int. (670 nm) vs [**1,4-NpBipy**]/[Photofrin].

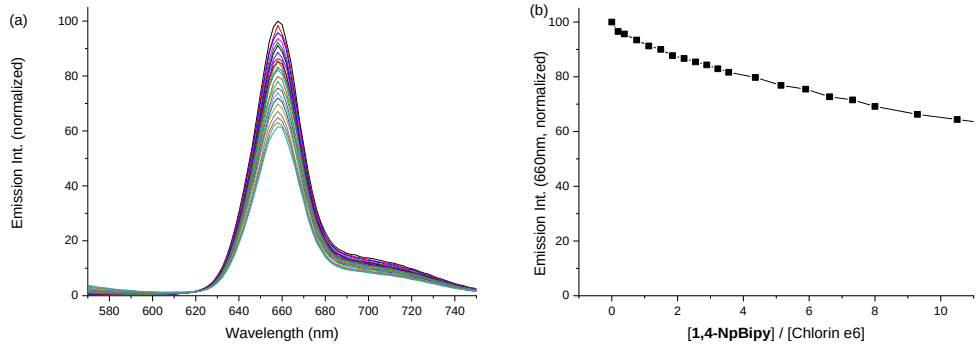

Fig. S42 (a) Fluorescence intensity of Chlorin e6 (5.0 μM) with the addition of **1,4-NpBipy** in 20 mM NaH_2PO_4 buffer (pH = 7.4). (b) Emission Int. (660 nm) vs [**1,4-NpBipy**]/[Chlorin e6].

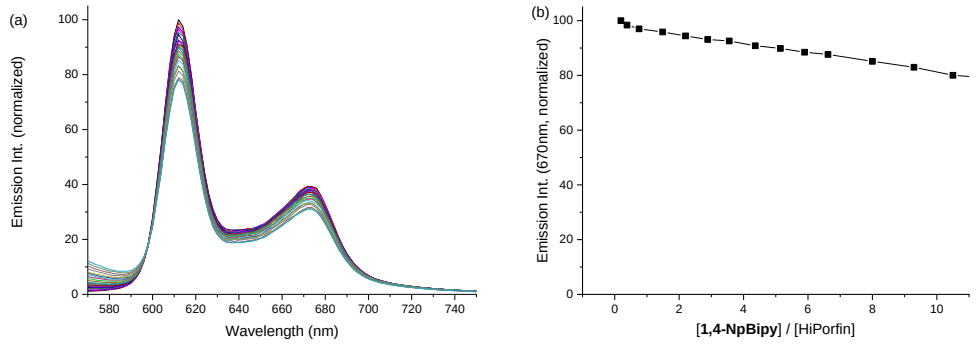

Fig. S43 (a) Fluorescence intensity of HiPorfin (5.0 μM) with the addition of **1,4-NpBipy** in 20 mM NaH_2PO_4 buffer (pH = 7.4). (b) Emission Int. (670 nm) vs [**1,4-NpBipy**]/[HiPorfin].

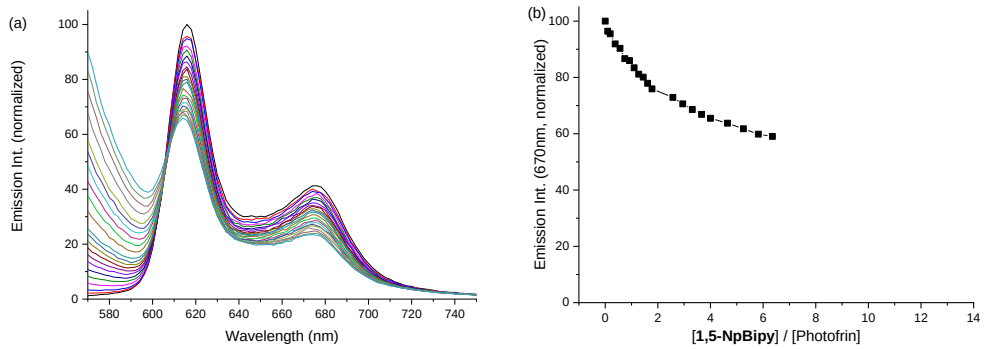

Fig. S44 (a) Fluorescence intensity of Photofrin (10 μM) with the addition of **1,5-NpBipy** in 20 mM NaH_2PO_4 buffer (pH = 7.4). (b) Emission Int. (670 nm) vs [**1,5-NpBipy**]/[Photofrin].

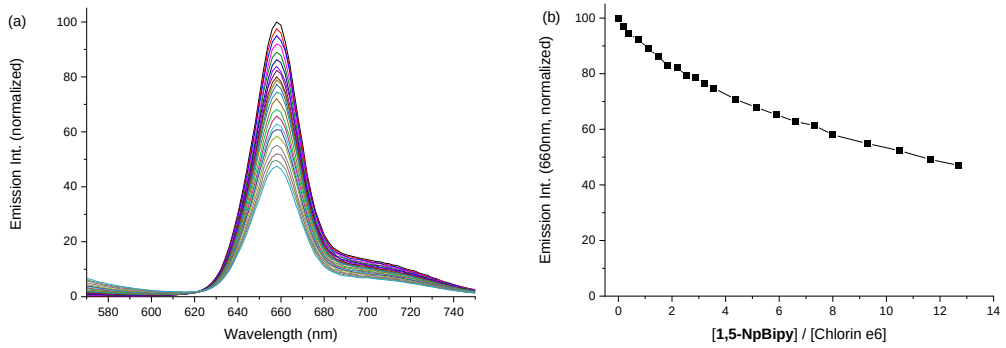

Fig. S45 (a) Fluorescence intensity of Chlorin e6 (5.0 μM) with the addition of **1,5-NpBipy** in 20 mM NaH_2PO_4 buffer (pH = 7.4). (b) Emission Int. (660 nm) vs [**1,5-NpBipy**]/[Chlorin e6].

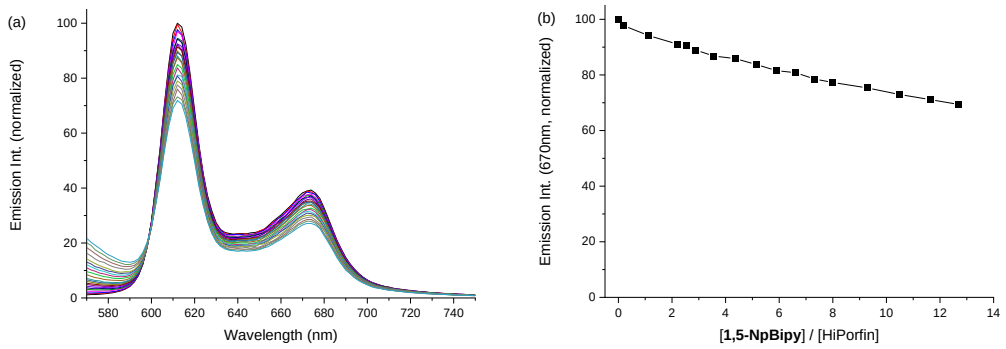

Fig. S46 (a) Fluorescence intensity of HiPorfin (5.0 μM) with the addition of **1,5-NpBipy** in 20 mM NaH_2PO_4 buffer (pH = 7.4). (b) Emission Int. (670 nm) vs [**1,5-NpBipy**]/[HiPorfin].

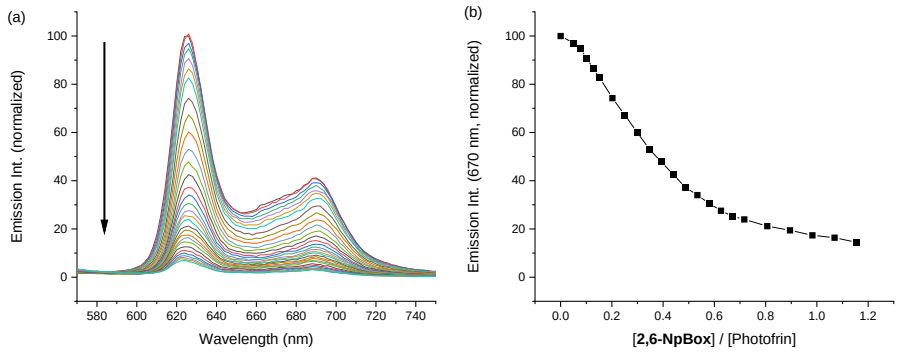

Fig. S47 (a) Fluorescence intensity of Photofrin (10 μM) with the addition of **2,6-NpBox** in bovine plasma. (b) Emission intensity (670 nm) vs [**2,6-NpBox**]/[Photofrin].

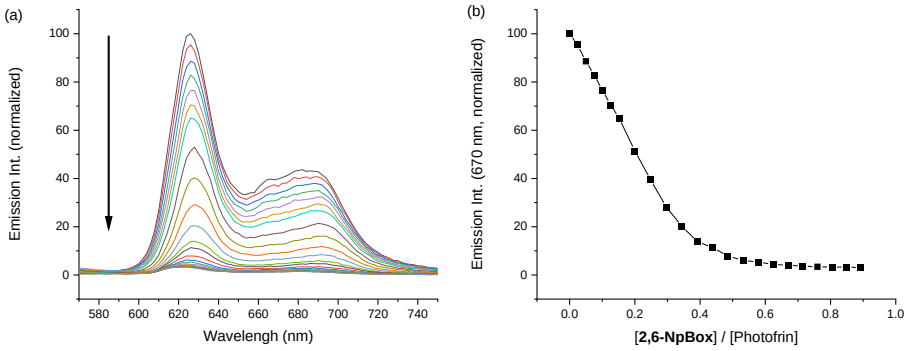

Fig. S48 (a) Fluorescence intensity of Photofrin (10 μM) with the addition of **2,6-NpBox** in the solution of 10% fetal bovine serum (FBS) in phosphate-buffered soline (PBS). (b) Emission intensity (670 nm) vs [**2,6-NpBox**]/[Photofrin].

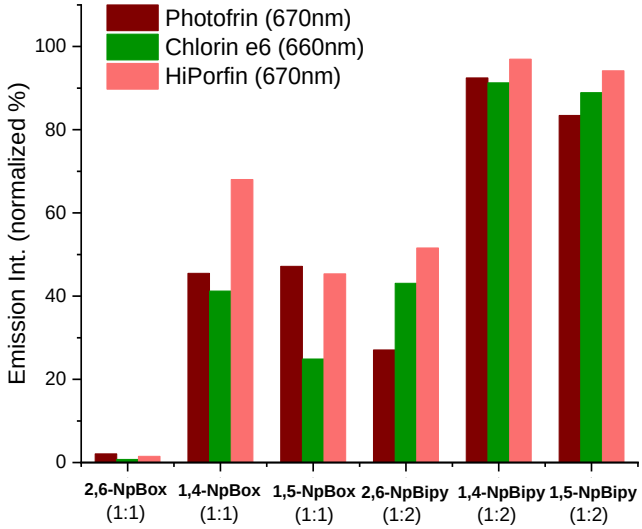

Fig. S49 The normalized fluorescence emission intensity of Photofrin ([porphyrin] = 10.0 μM, 670 nm), Chlorin e6 (5.0 μM, 660 nm) and HiPorfin (5.0 μM, 670 nm) with the addition of **NpBipys** (2:1, 20.0 μM for Photofrin,10.0 μM for Chlorin e6 or HiPorfin) or **NpBoxs** (1:1, 10.0 μM for Photofrin, 5.0 μM for Chlorin e6 or HiPorfin) in 20 mM NaH_2PO_4 buffer (pH = 7.4).

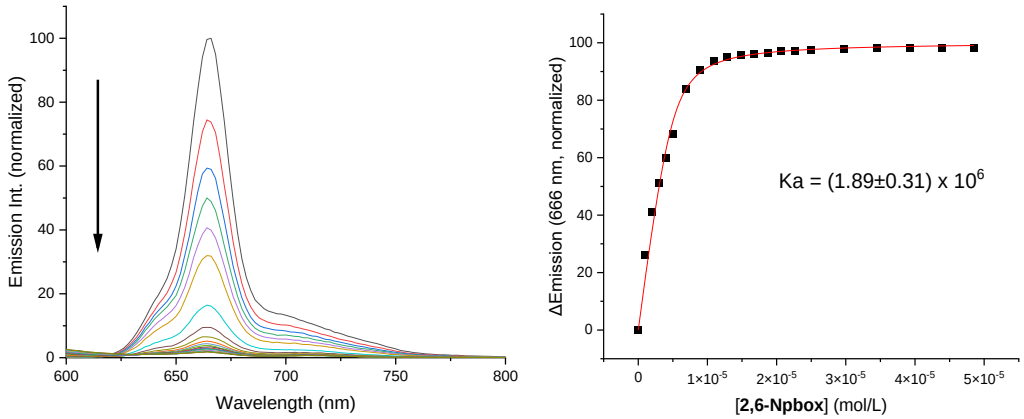

Fig. S50 Titration of **2,6-NpBox** into a solution of Chlorin e6 (5 μM, CH_3OH) monitored by fluorescence (λ_{ex} = 420 nm), and its corresponding nonlinear fitting curve for the determination of binding constant K_a.

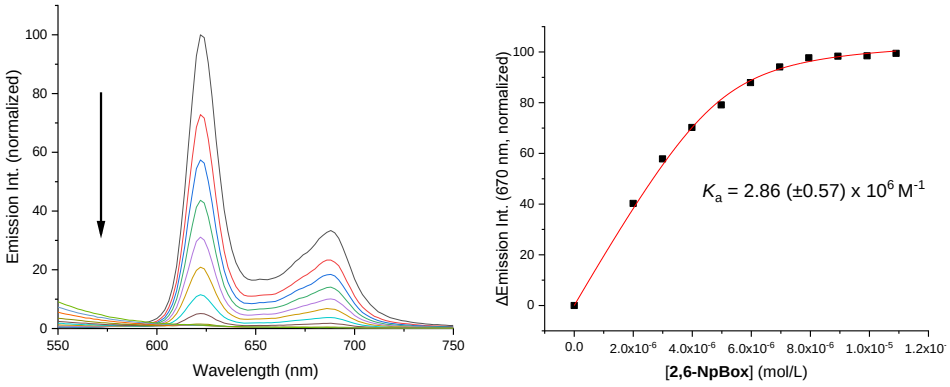

Fig. S51 Titration of **2,6-NpBox** into a solution of HiPorfin (5 μM, CH_3OH) monitored by fluorescence (λ_{ex} = 430 nm), and its corresponding nonlinear fitting curve for the determination of binding constant K_a.

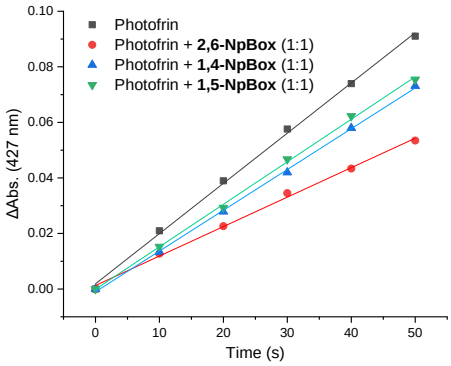

Fig. S52 Singlet oxygen generation of Photofrin (2.0 μM, black curve), Photofrin + **2,6-NpBox** (both 2.0 μM, red curve), Photofrin + **1,4-NpBox** (both 2.0 μM, blue curve), Photofrin + **1,5-NpBox** (both 2.0 μM, green curve) by the DPBF quenching method ([DPBF] = 25 μM) in 20 mM NaH_2PO_4 buffer (pH = 7.4).. UV-vis absorbance intensity at 427 nm of DPBF was recorded after irradiation.

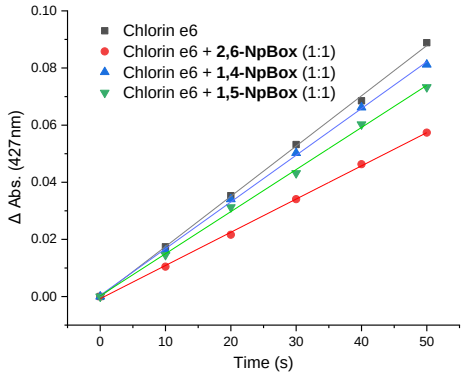

Fig. S53 Singlet oxygen generation test of Chlorin e6 (2.0 μM, black curve), Chlorin e6 + **2,6-NpBox** (both 2.0 μM, red curve), Chlorin e6 + **1,4-NpBox** (both 2.0 μM, blue curve), Chlorin e6 + **1,5-NpBox** (both 2.0 μM, green curve) by the DPBF quenching method ([DPBF] = 25 μM) in 20 mM NaH_2PO_4 buffer (pH = 7.4). UV-vis absorbance intensity at 427 nm of DPBF was recorded after irradiation.

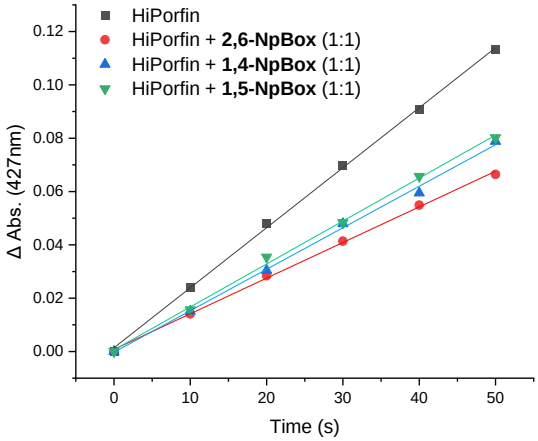

Fig. S54 Singlet oxygen generation test of HiPorfin (2.0 μM, black curve), HiPorfin + **2,6-NpBox** (both 2.0 μM, red curve), HiPorfin + **1,4-NpBox** (both 2.0 μM, blue curve), HiPorfin + **1,5-NpBox** (both 2.0 μM, green curve) by the DPBF quenching method ([DPBF] = 25 μM) in 20 mM NaH_2PO_4 buffer (pH = 7.4). UV-vis absorbance intensity at 427 nm of DPBF was recorded after irradiation.

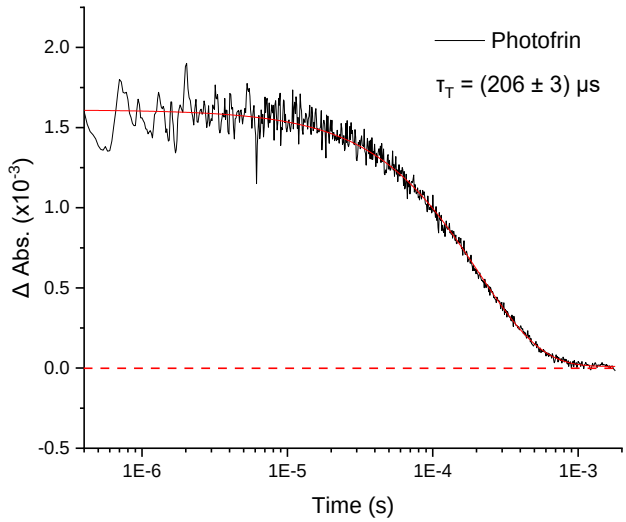

Fig. S55 Nanosecond TA spectra of Photofrin in 20 mM NaH_2PO_4 buffer (pH = 7.4) excitd at λ_{ex} = 420 nm and single exponential fit to ns TA data at 430 nm (time from 5 × 10^{-7} s to 2 × 10^{-3} s) to get the decay of the triplet state.

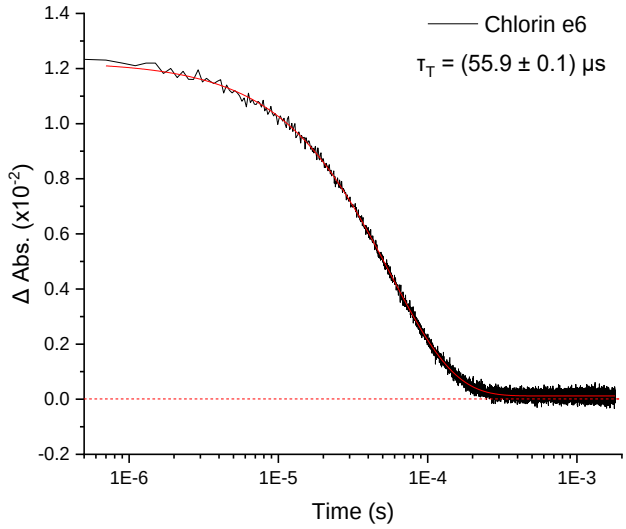

Fig. S56 Nanosecond TA spectra of Chlorin e6 in 20 mM NaH_2PO_4 buffer (pH = 7.4) excited at λ_{ex} = 420 nm and single exponential fit to ns TA data at 430 nm (time from 5 × 10^{-7} s to 2 × 10^{-3} s) to get the decay of the triplet state.

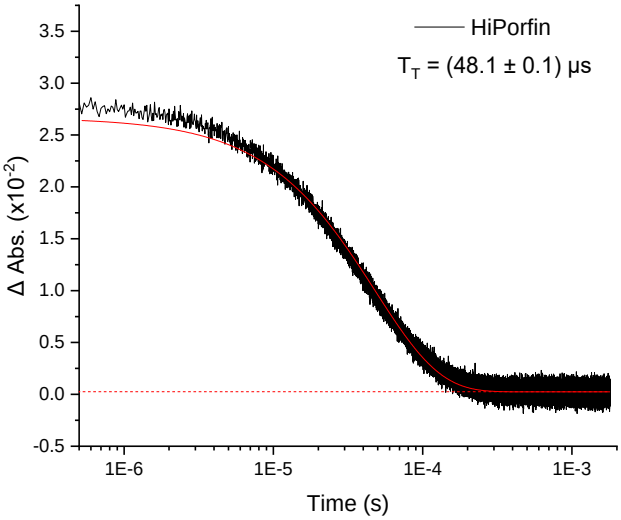

Fig. S57 Nanosecond TA spectra of HiPorfin in 20 mM NaH_2PO_4 buffer (pH = 7.4) excitd at λ_{ex} = 420 nm and single exponential fit to ns TA data at 430 nm (time from 5 × 10^{-7} s to 2 v 10^{-3} s) to get the decay of the triplet state.

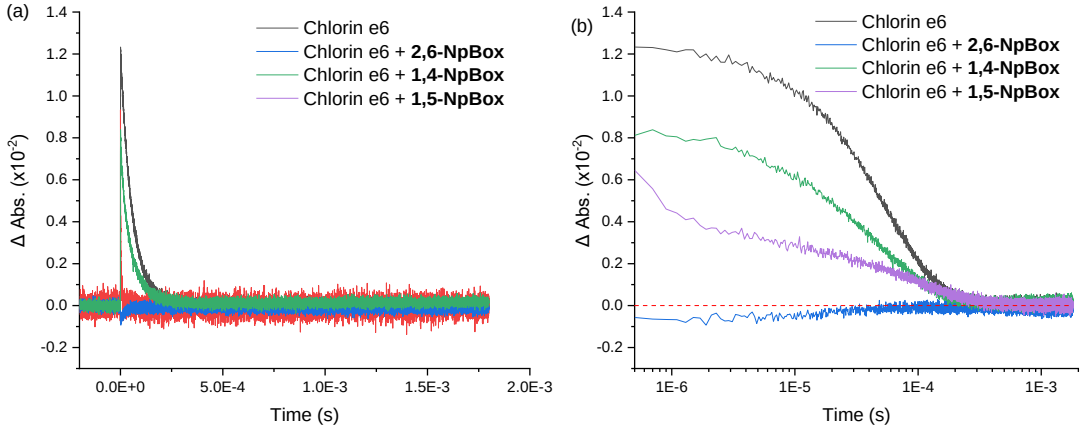

Fig. S58 Nanosecond TA spectra of Chlorin e6 in 20 mM NaH_2PO_4 buffer (pH = 7.4) excited at λ_{ex} = 420 nm and detected the ns TA data at 430 nm. (a) ns-TA spectra from 2 × 10^{-4} s to 2 × 10^{-3} s with setting horizontal type as linear ([Chlorin e6] = 7.5 µM, and (b) turn horizontal type of (a) into log10 and time from 5 × 10^{-7} s to 2 × 10^{-3} s (λ_{ex} = 420 nm and detected at 430 nm).

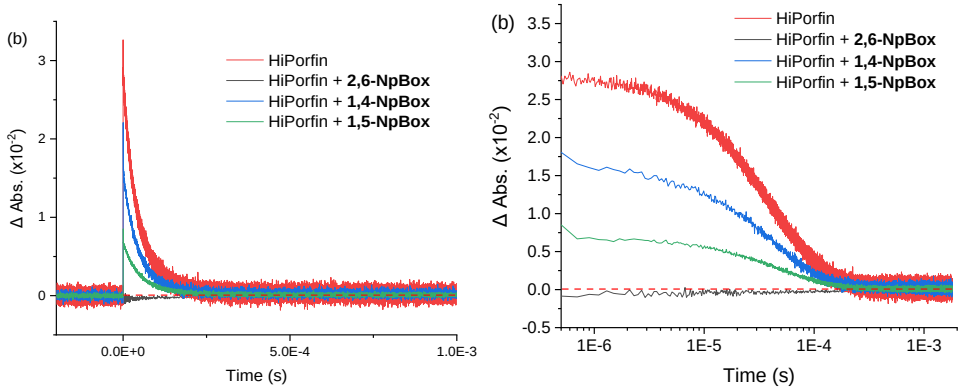

Fig. S59 Nanosecond TA spectra of HiPorfin in 20 mM NaH_2PO_4 buffer (pH = 7.4) excitd at λ_{ex} = 420 nm and detected the ns TA data at 430 nm. (a) ns-TA spectra from 2 × 10^{-4} s to 2 × 10^{-3} s with setting horizontal type as linear ([HiPorfin] = 30 μM, and (b) turn horizontal type of (a) into log10 and time from 5 × 10^{-7} s to 2 × 10^{-3} s (λ_{ex} = 420 nm and detected at 430 nm).

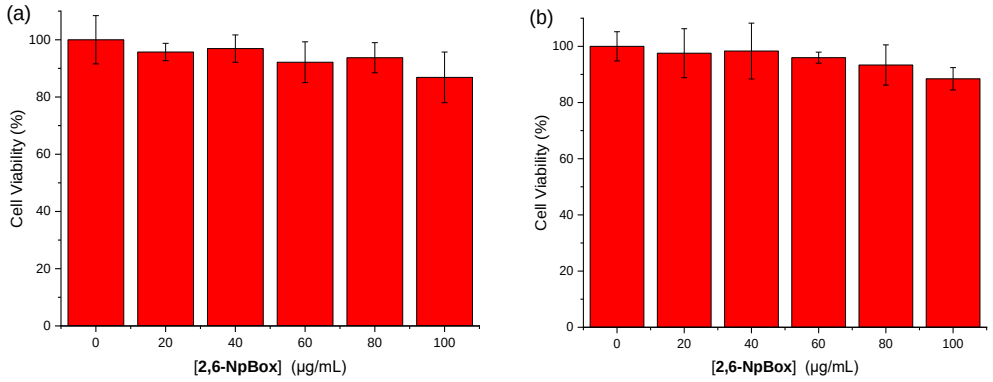

Fig. S60 Viability of (a) H9C2 and (b) L02 cells treated with **2,6-NpBox** (Incubation time: 24 h, n = 6).

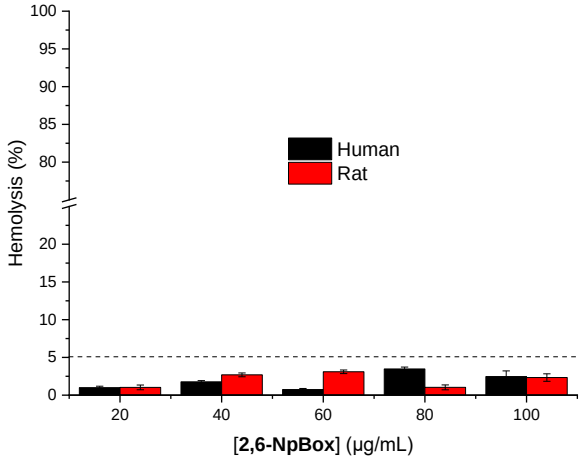

Fig. S61 Hemolysis of human and rat RBCs in the presence of various concentrations of **2,6-NpBox** (545 nm).

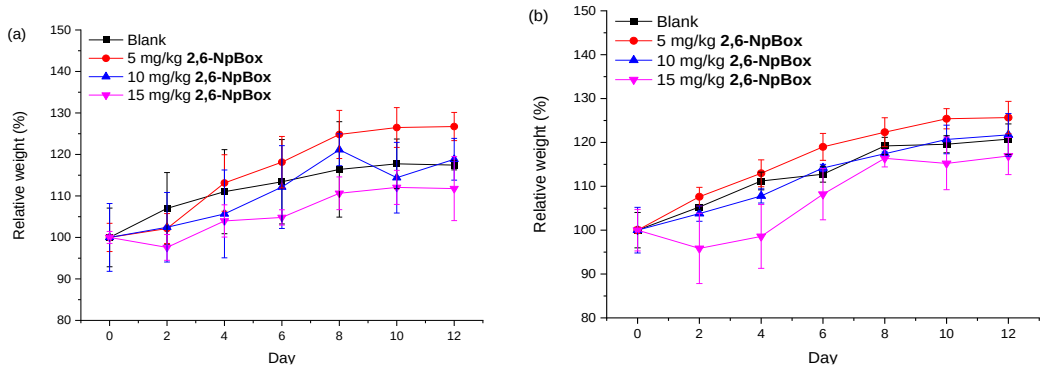

Fig. S62 MTD study performed for **2,6-NpBox**. Male and female Balb/c mice (n = 6 per group: 3 males + 3 females) were dosed via tail vein on day 0 with different

concentrations of **2,6-NpBox** in 5% glucose or **2,6-NpBox** -free 5% glucose (blank). The normalized average weight change per study group is indicated. Error bars represent SEM.

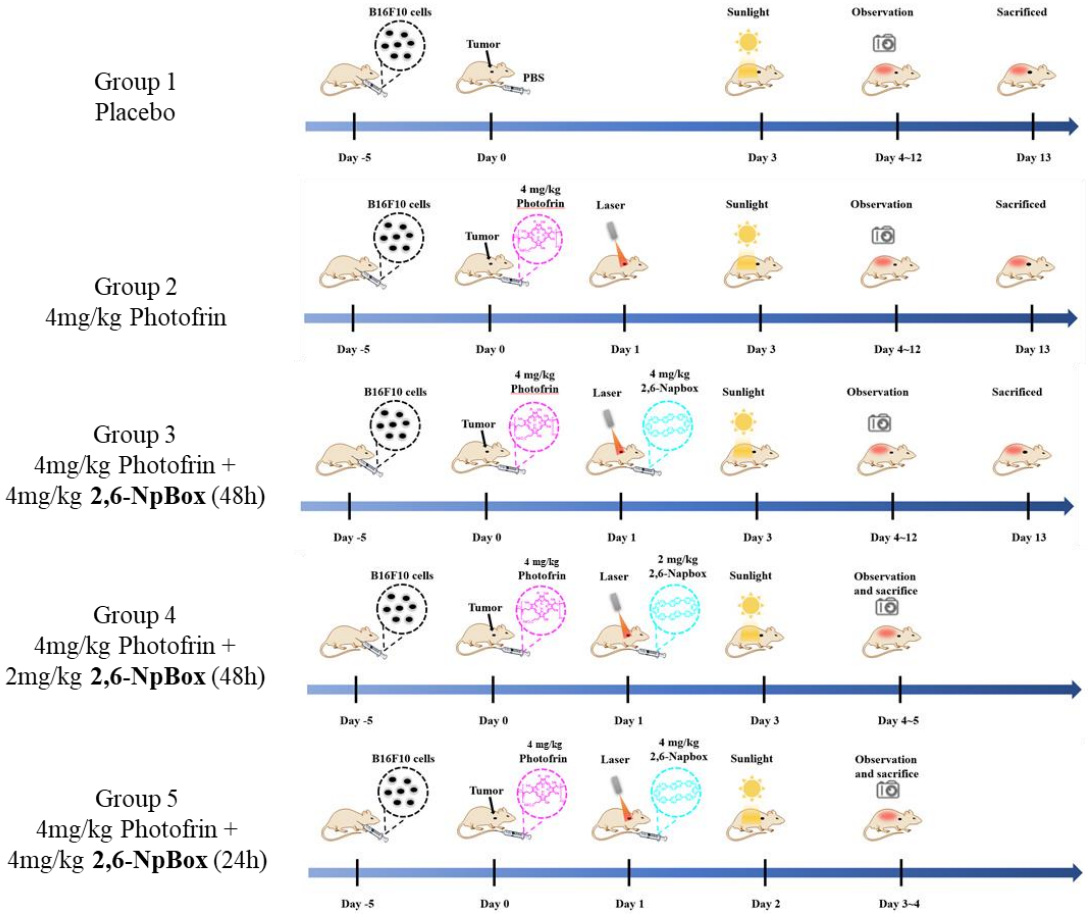

Fig. S63 Time schedule of animal experiment.

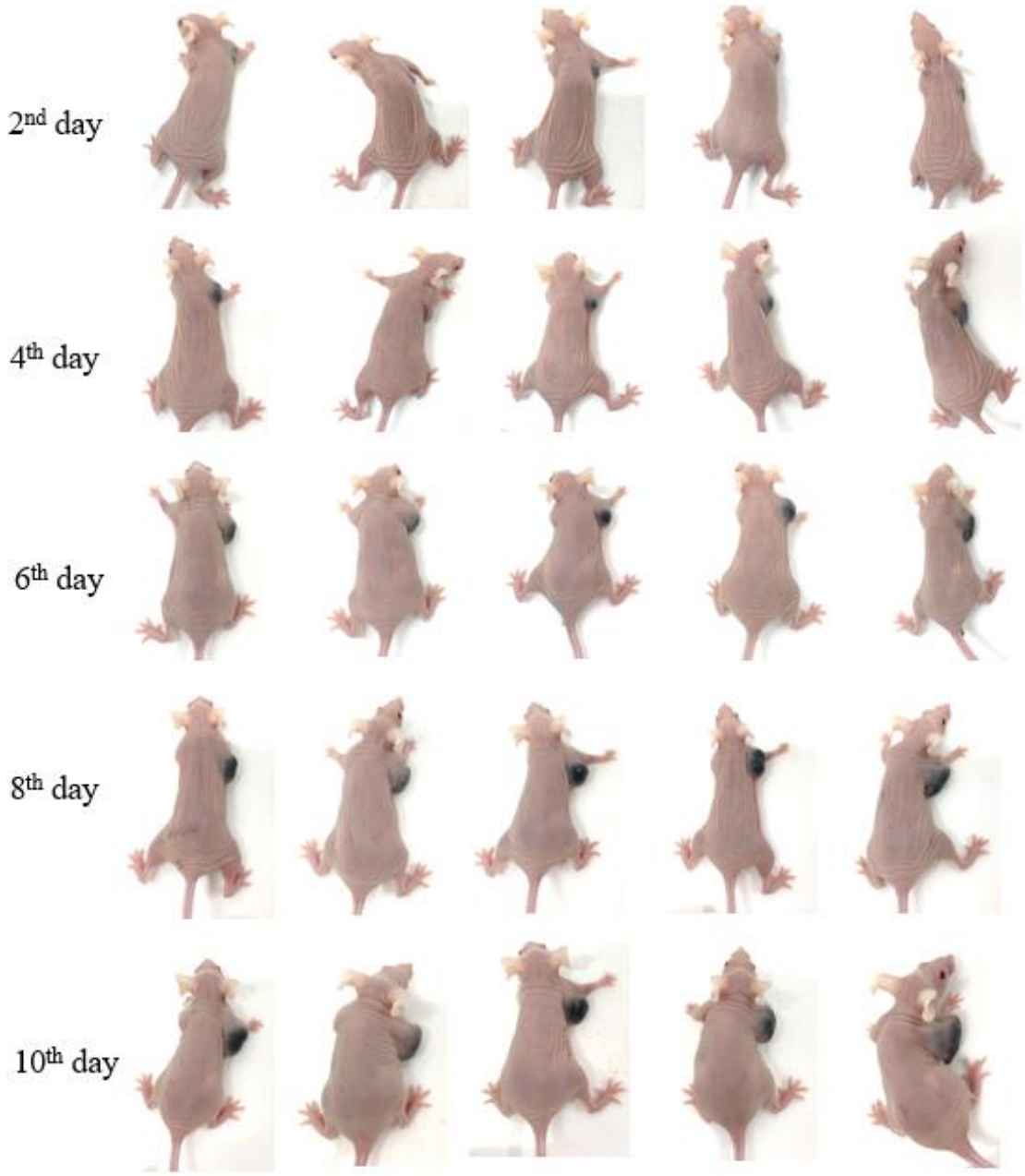

Fig. S64 Skin images of tumor-bearing mice in group 1 as indicated at 2nd day (day 4), 4th day, 6th day, 8th day and 10th day post sunlight (100 mW/cm^2, 30 min) after iv of PBS (n = 5).

Fig. S65 Skin images of tumor-bearing mice in group 2 as indicated at 2nd day (day 4), 4th day, 6th day, 8th day and 10th day post sunlight (100 mW/cm^2, 30 min) after iv of Photofrin (4.0 mg/kg) and PBS (n = 5).

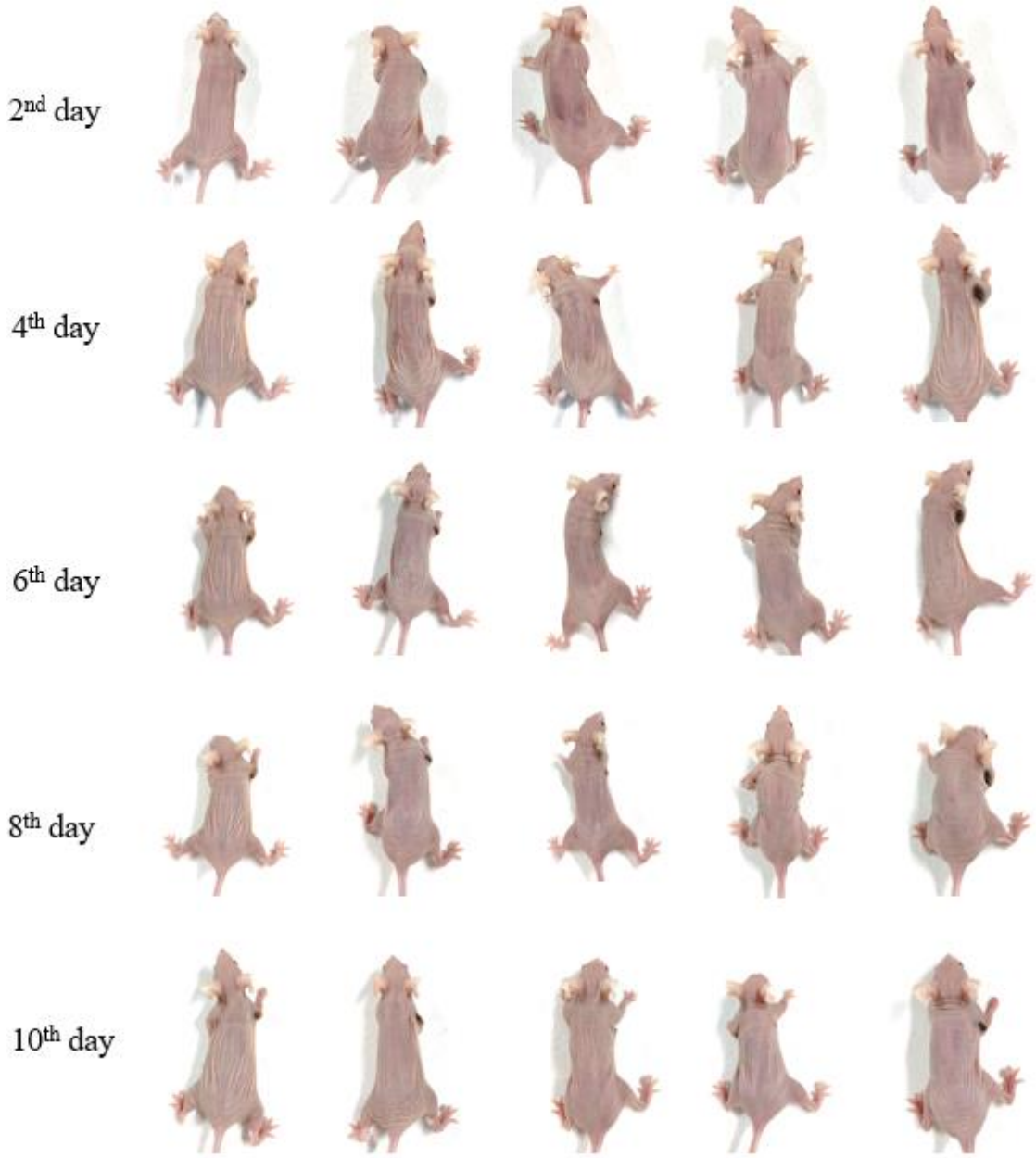

Fig. S66 Skin images of tumor-bearing mice in group 3 as indicated at 2nd day (day 4), 4th day, 6th day, 8th day and 10th day post sunlight (100 mW/cm^2, 30 min) after iv of Photofrin (4.0 mg/kg) and **2,6-NpBox** (4.0 mg/kg) (n = 5).

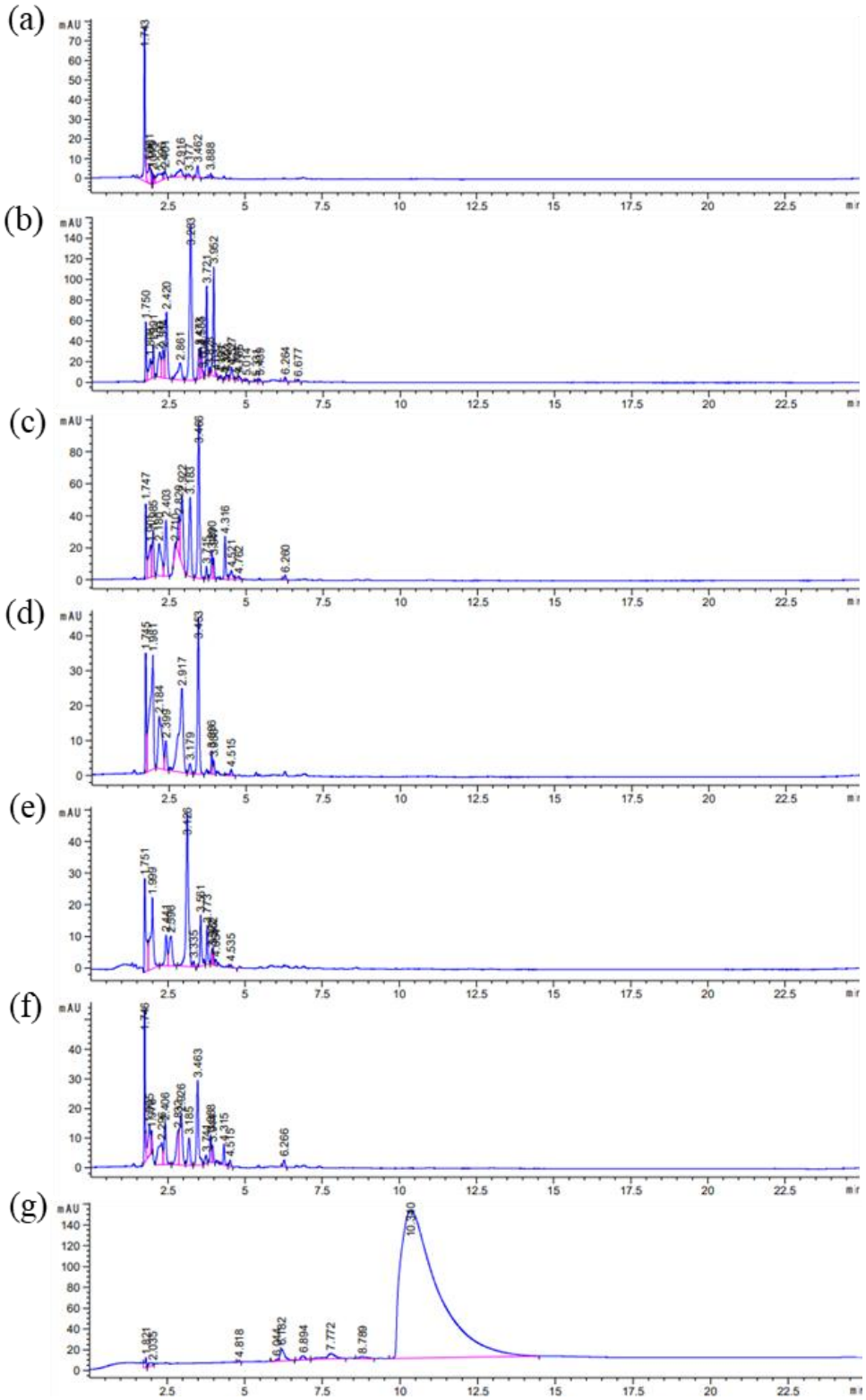

Fig. S67 The group 3 lysates composition analysis of (a) heart, (b) liver, (c) spleen, (d) lung, (e) kidney, (f) skin and the standard sample analysis of (g) **2,6-NpBox** (0.1 mM) by HPLC, all on reverse C18 columns at 254 nm (35 v% MeOH/H_2O with 0.1 v% TFA as additive).

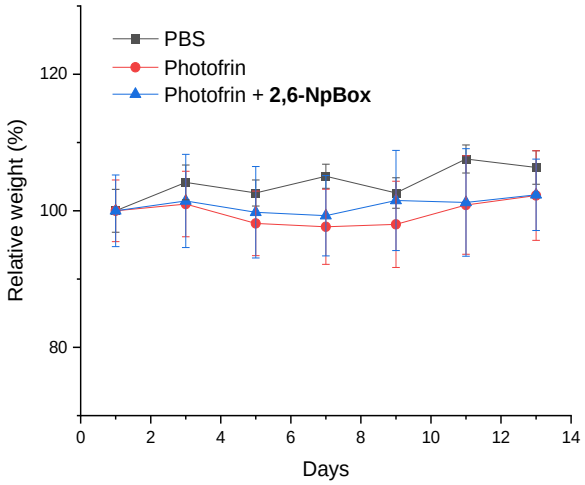

Fig. S68 Weight of tumor-bearing mice as indicated from day 1 to day 13 (n = 5).

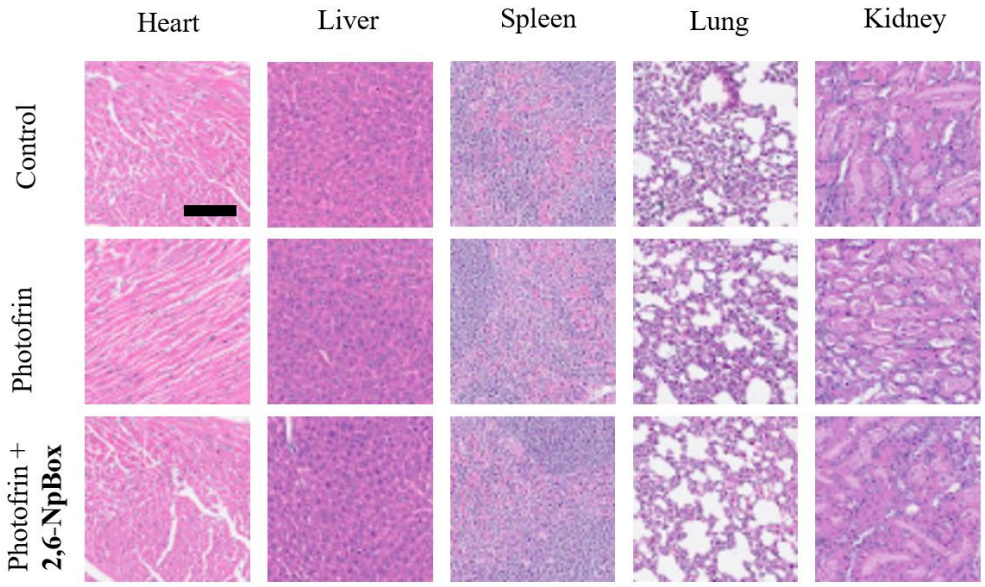

Fig. S69 Slice micrographs of H&E-stained main organs collected from groups 1~3 (scale bar: 100 μm).

Fig. S70 Skin images of tumor-bearing mice in group 4 (upper) and group 5 (down) as indicated at 2nd day post sunlight (100 mW/cm^2, 30 min) after iv of Photofrin (4.0 mg/kg) and **T1** (n = 5).

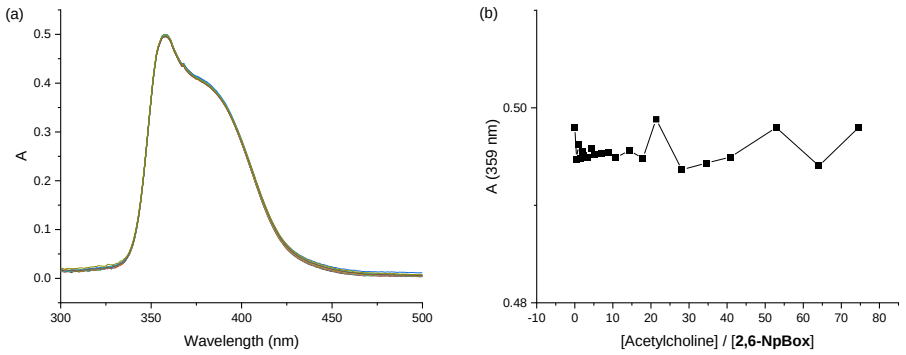

Fig. S71 (a) UV-vis absorption of **2,6-NpBox** (20 μM) with the addition of acetylcholine in 20 mM NaH_2PO_4 buffer (pH 7.4). (b) UV-vis absorption (359 nm) vs [Acetylcholine]/[**2,6-NpBox**].

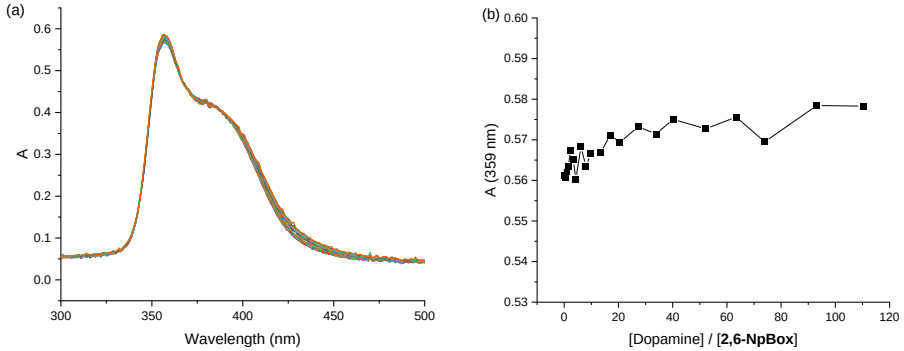

Fig. S72 (a) UV-vis absorption of **2,6-NpBox** (20 μM) with the addition of dopamine in 20 mM NaH_2PO_4 buffer (pH = 7.4). (b) UV-vis absorption (359 nm) vs [Dopamine]/[**2,6-NpBox**].

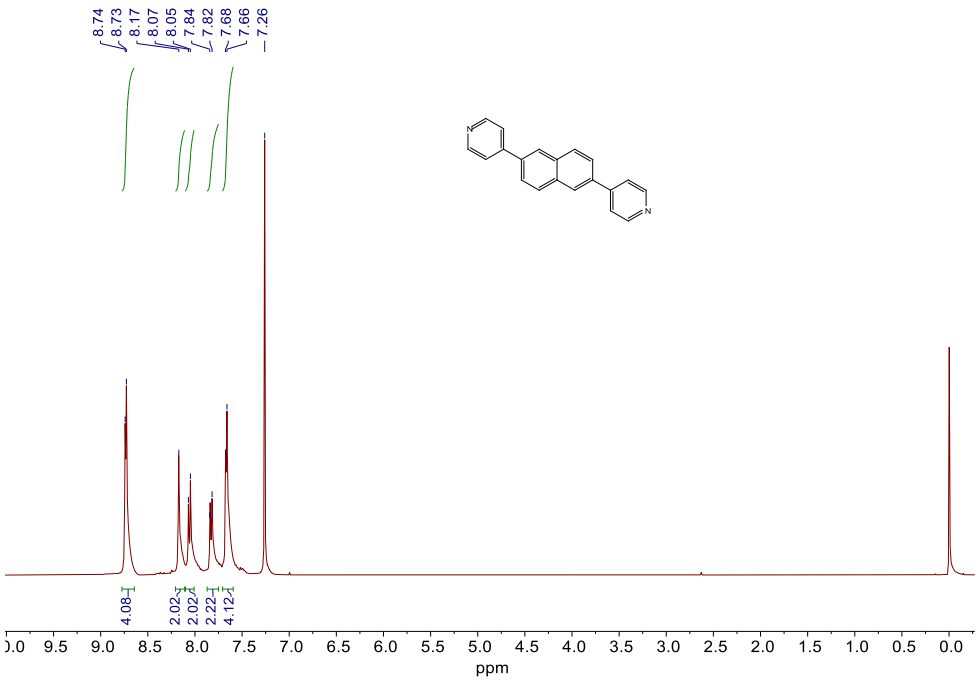

Fig. S73 ^{1}H NMR spectrum (400 MHz) of compound **3a** in $CDCl_3$ at 25 °C.

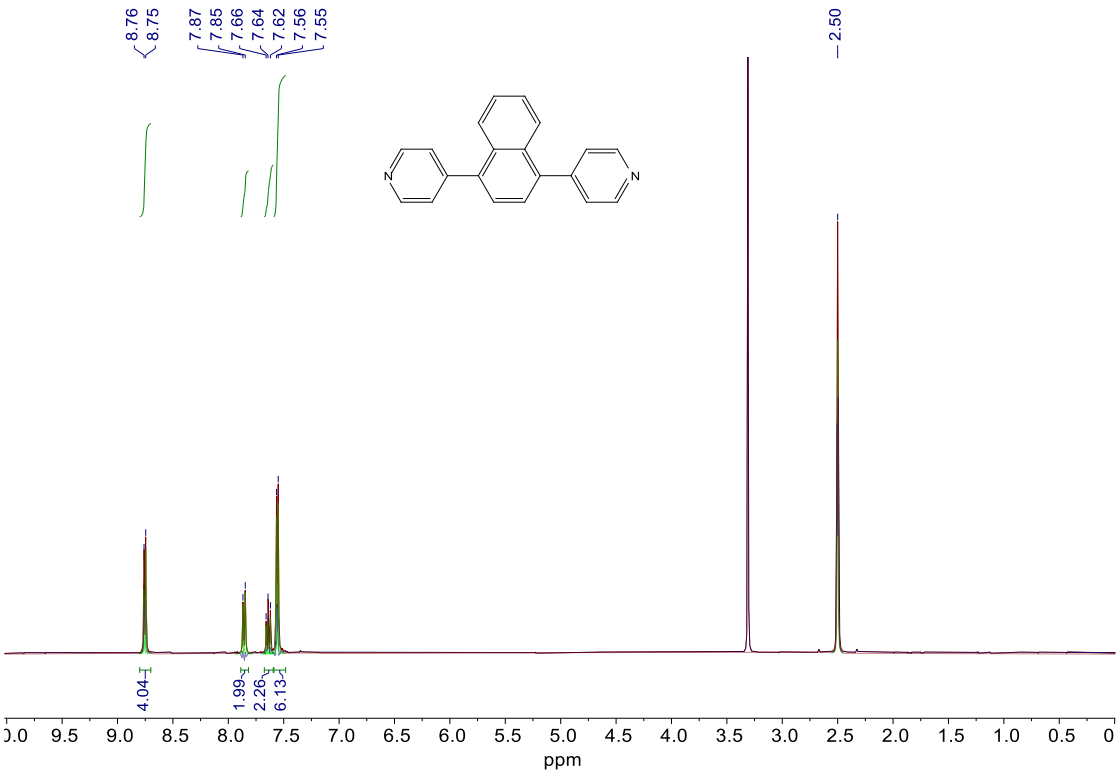

Fig. S74 ^{1}H NMR spectrum (400 MHz) of compound **3b** in DMSO-d_6 at 25 °C.

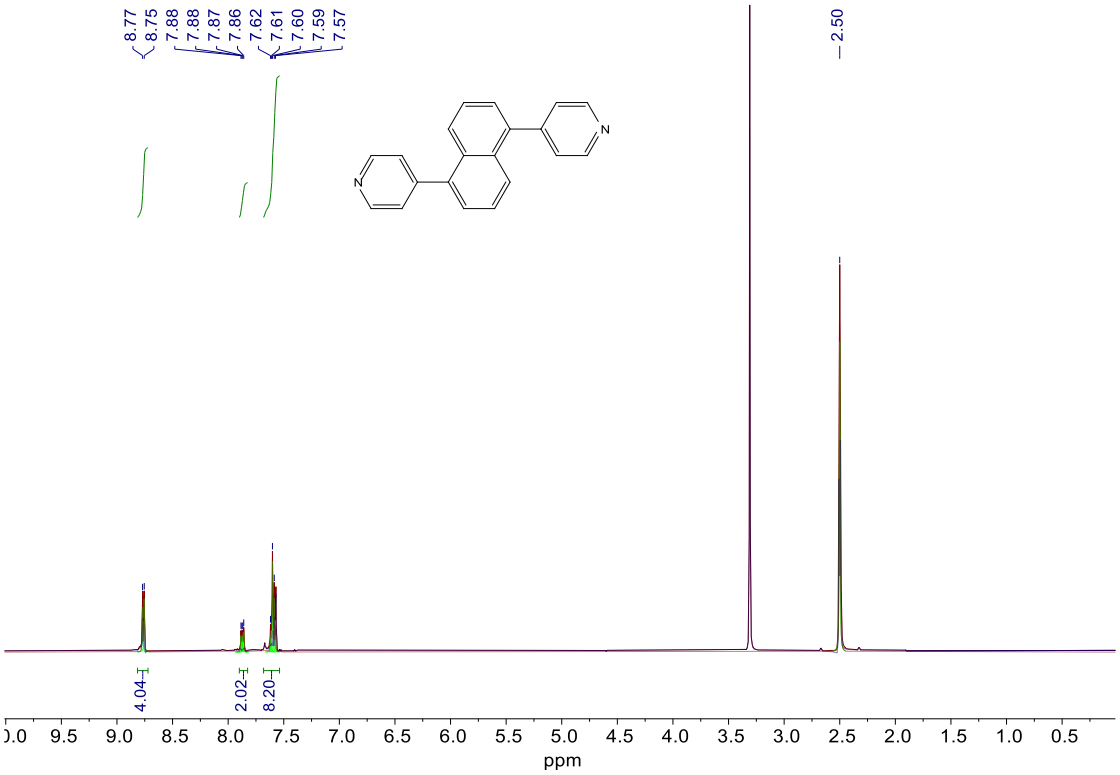

Fig. S75 ^{1}H NMR spectrum (400 MHz) of compound **3c** in DMSO-d_6 at 25 °C.

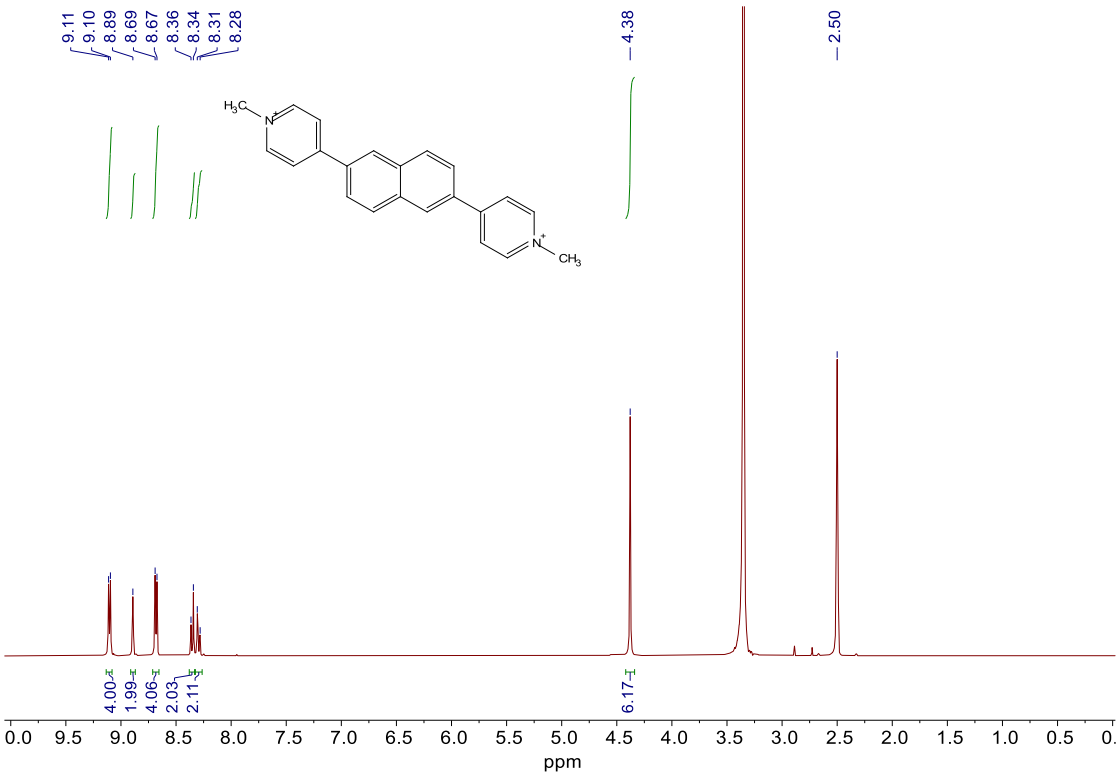

Fig. S76 ^{1}H NMR spectrum (400 MHz) of **2,6-NpBipy** in DMSO-d_6 at 25 °C.

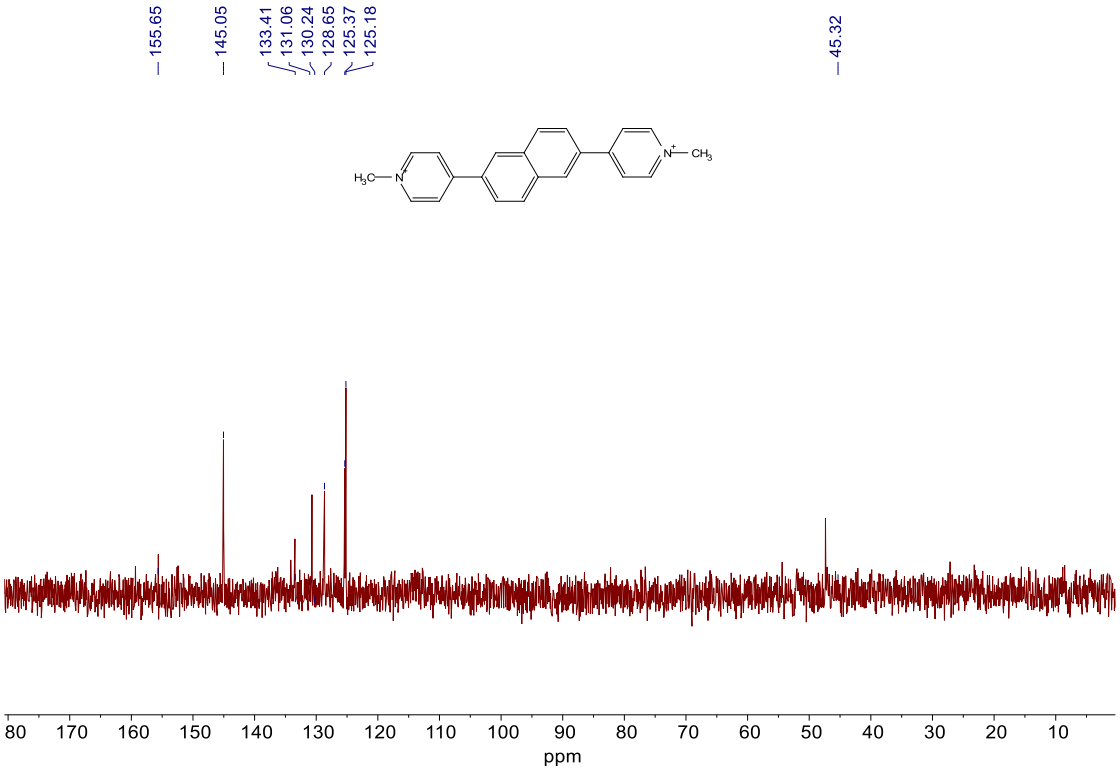

Fig. S77 ^{13}C NMR spectrum (101 MHz) of **2,6-NpBipy** in D_2O at 25 °C.

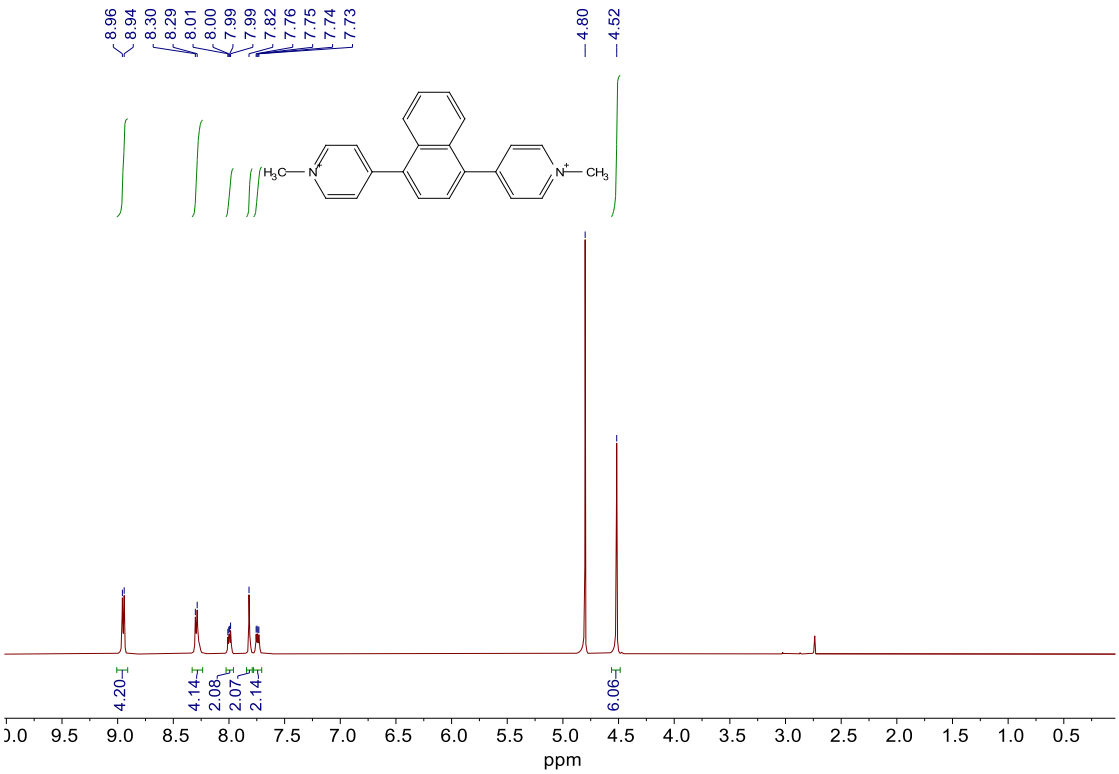

Fig. S78 ^{1}H NMR spectrum (400 MHz) of **1,4-NpBipy** in D_2O at 25 °C.

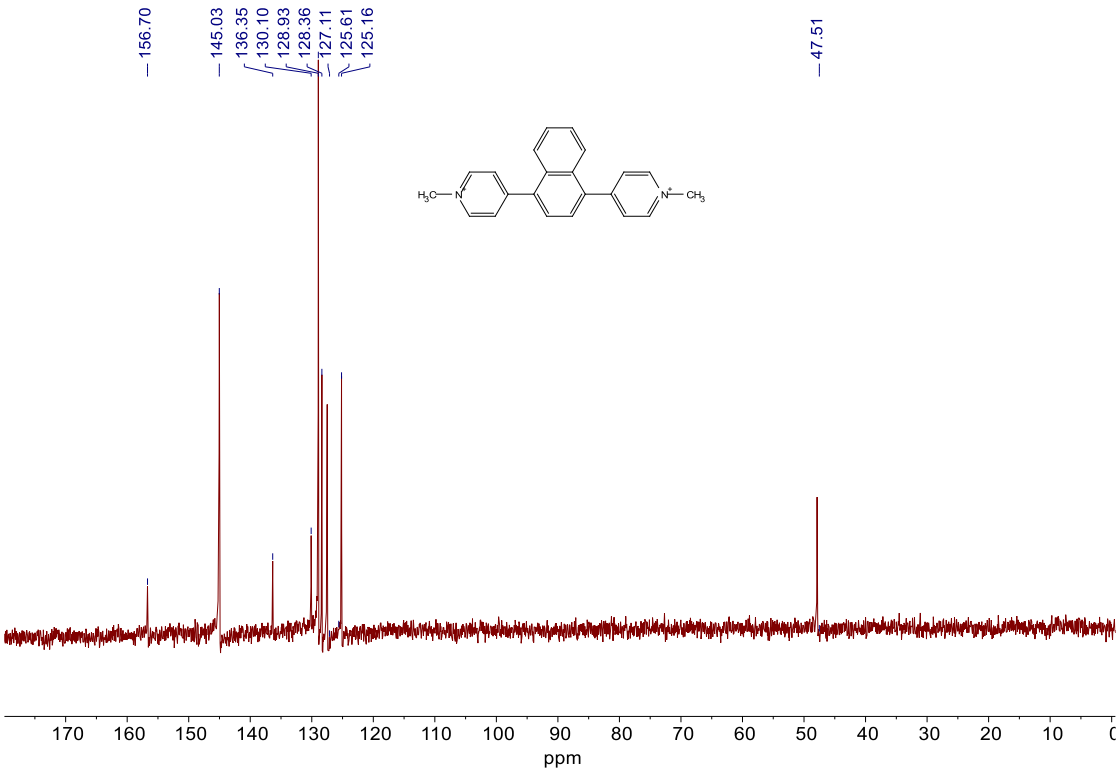

Fig. S79 ^{13}C NMR spectrum (101 MHz) of **1,4-NpBipy** in D_2O at 25 °C.

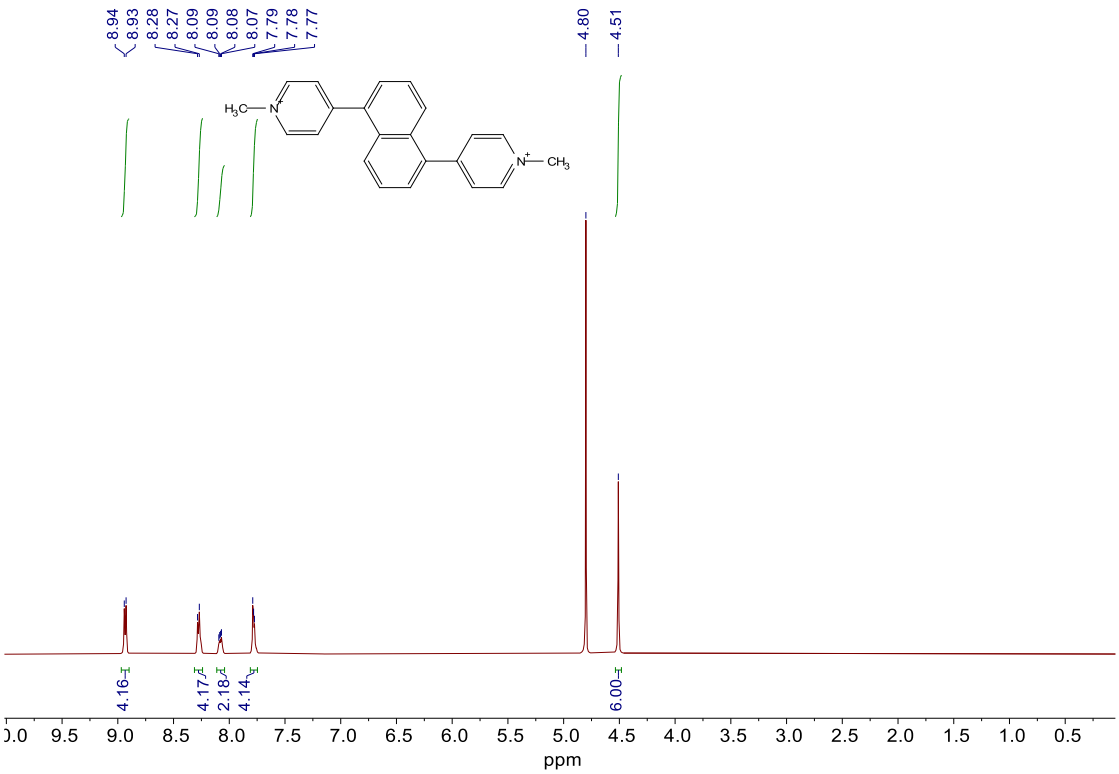

Fig. S80 ^{1}H NMR spectrum (400 MHz) of **1,5-NpBipy** in D_2O at 25 °C.

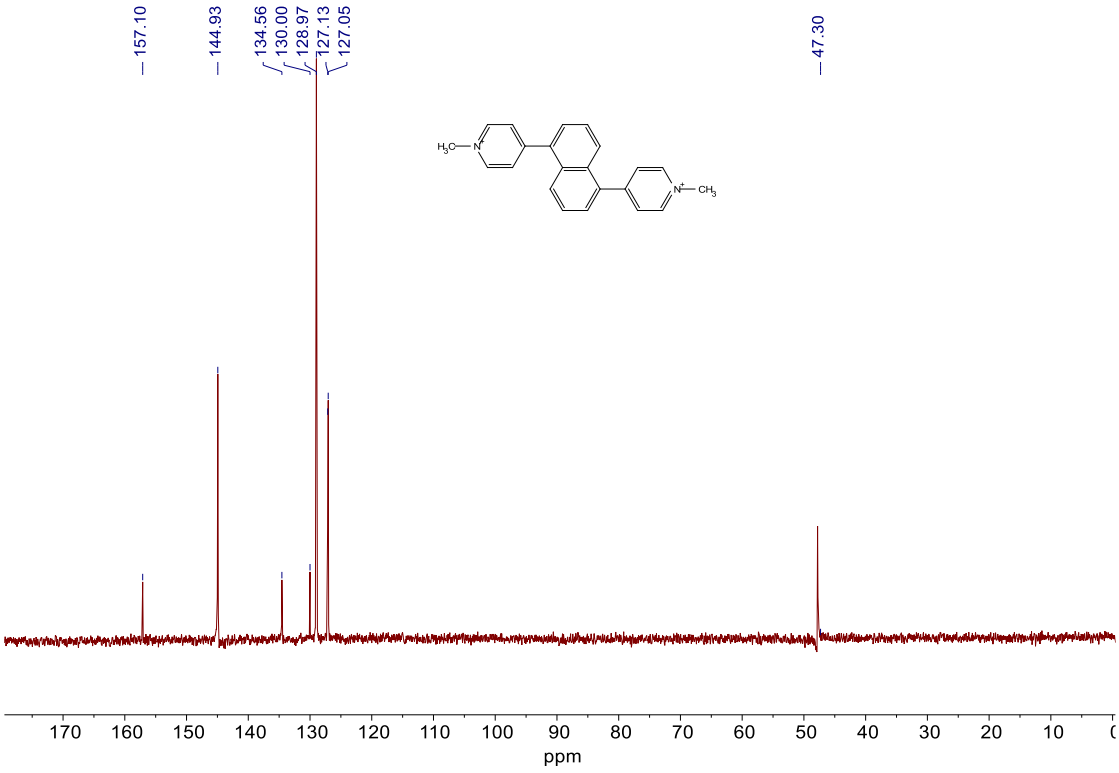

Fig. S81 ^{13}C NMR spectrum (101 MHz) of **1,5-NpBipy** in D_2O at 25 °C.

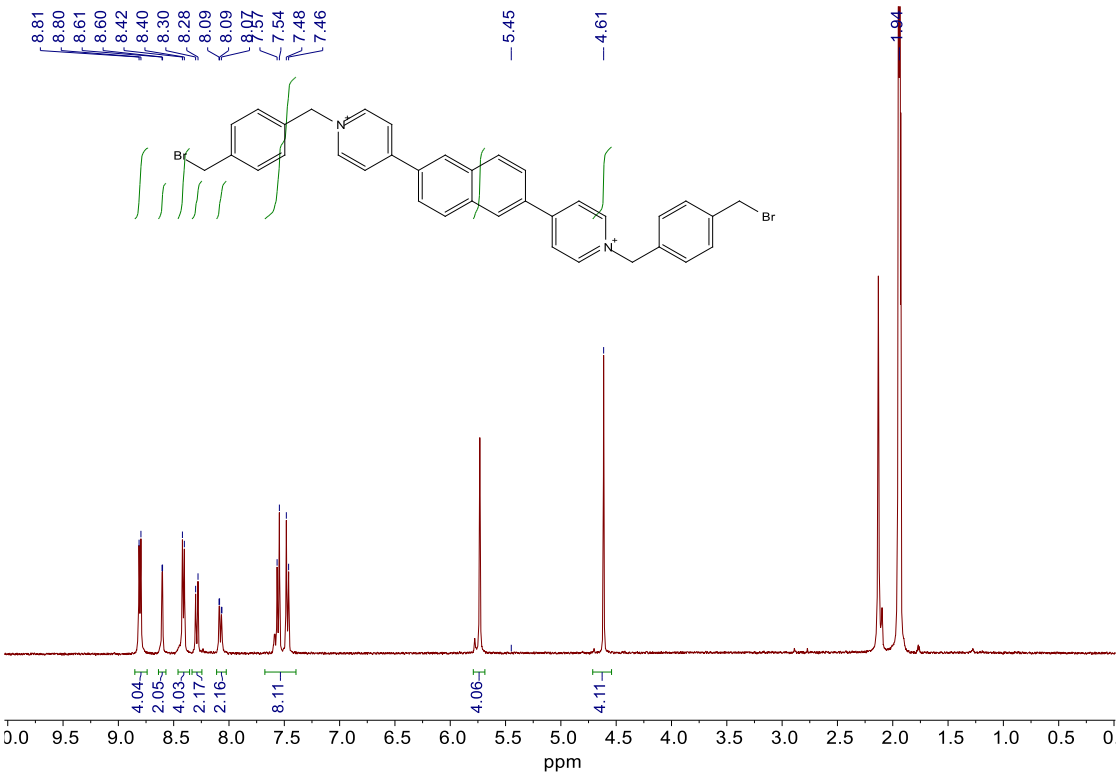

Fig. S82 ^{1}H NMR spectrum (400 MHz) of compound **5a** in CD_3CN at 25 °C.

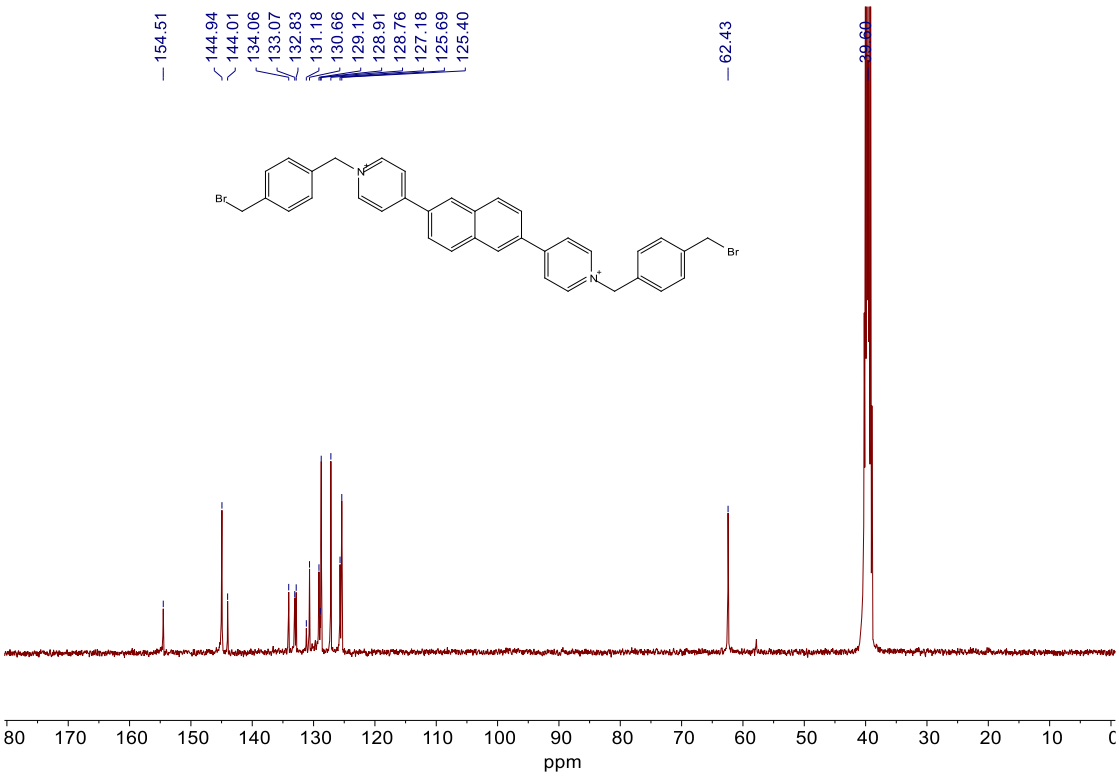

Fig. S83 ^{13}C NMR spectrum (101 MHz) of compound **5a** in DMSO-d_6 at 25 °C.

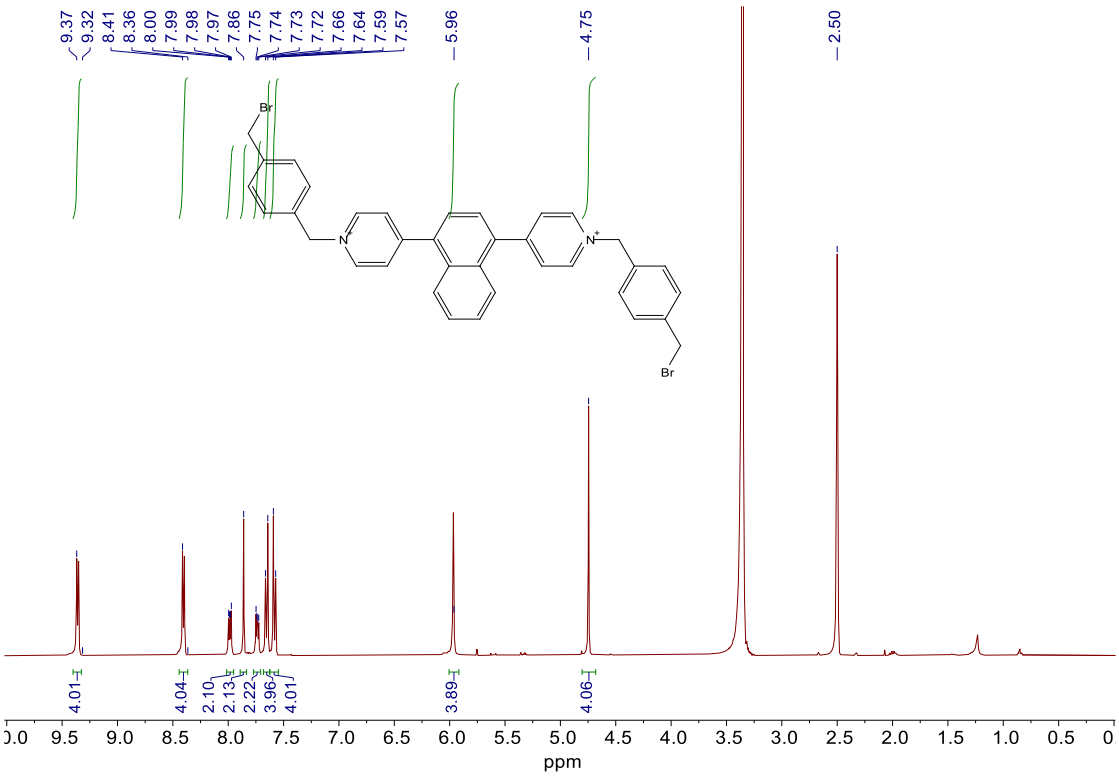

Fig. S84 ^{1}H NMR spectrum (400 MHz) of compound **5b** in DMSO-d_6 at 25 °C.

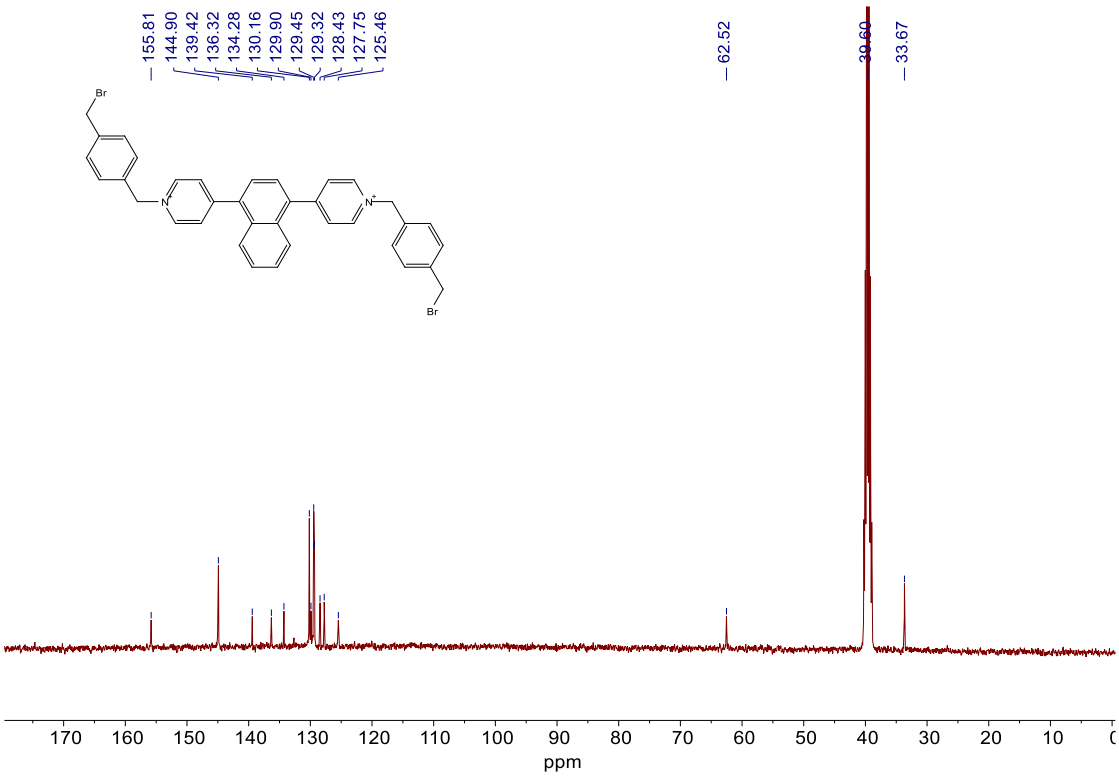

Fig. S85 ^{13}C NMR spectrum (101 MHz) of compound **5b** in DMSO-d_6 at 25 °C.

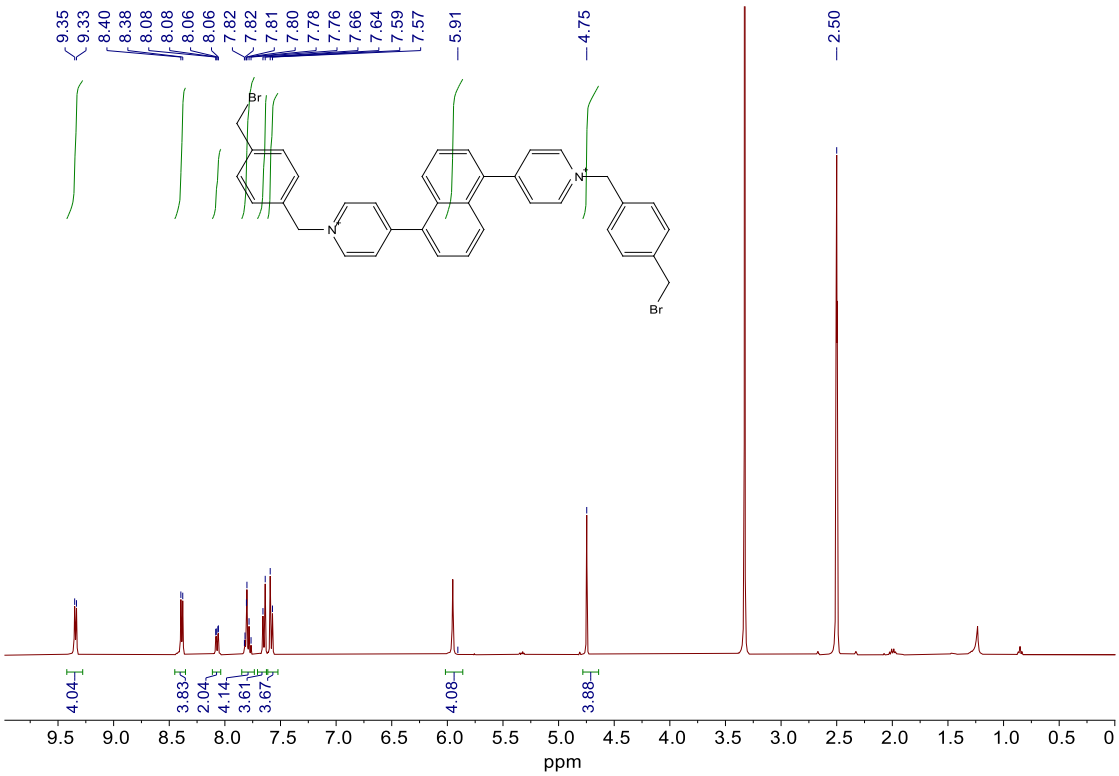

Fig. S86 ^{1}H NMR spectrum (400 MHz) of compound **5c** in DMSO-d_6 at 25 °C.

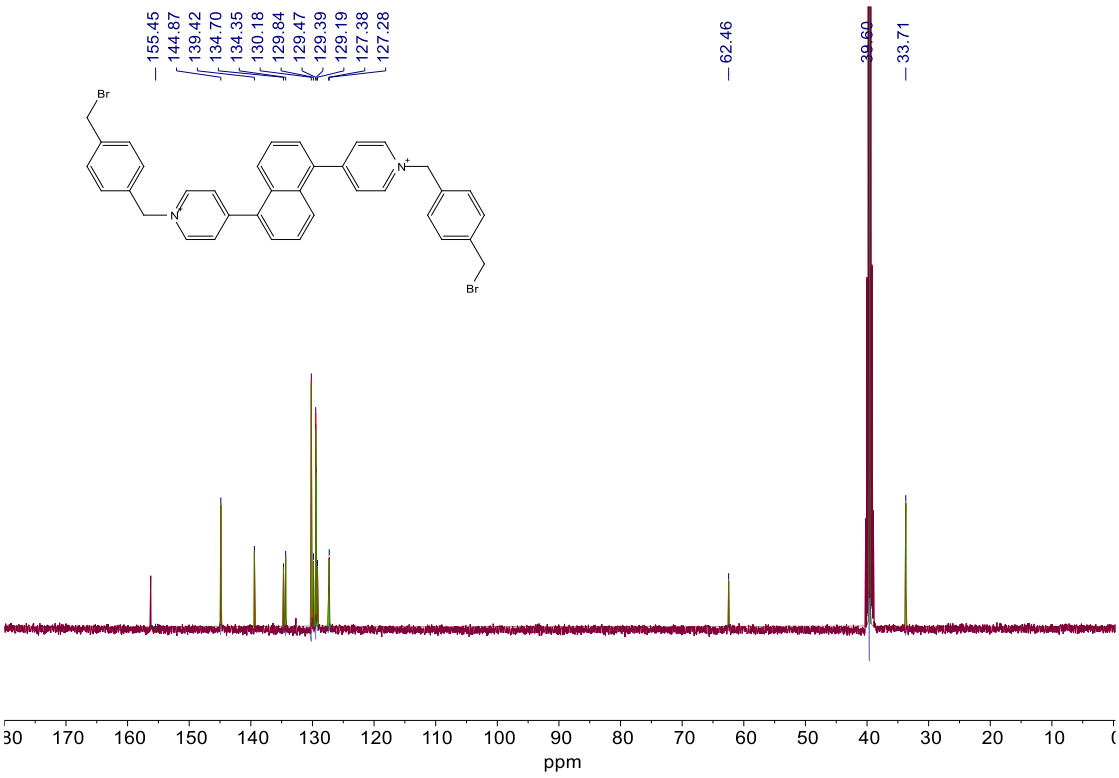

Fig. S87 ^{13}C NMR spectrum (101 MHz) of compound **5c** in DMSO-d_6 at 25 °C.

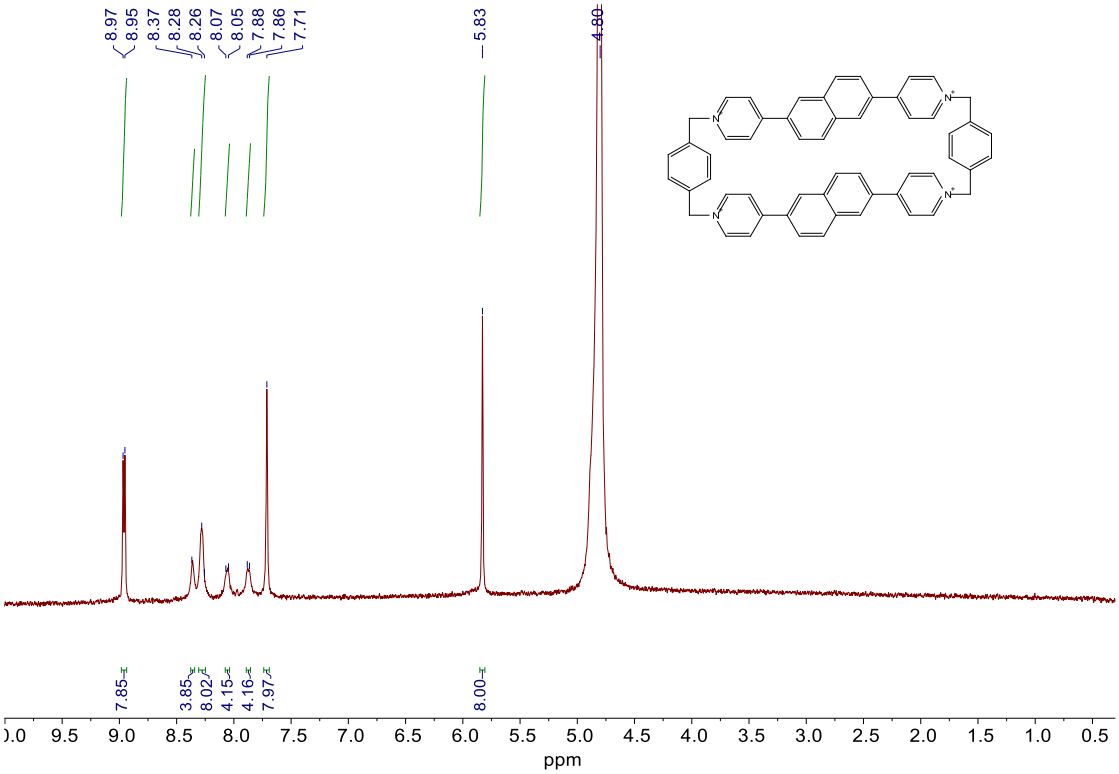

Fig. S88 ^{1}H NMR spectrum (400 MHz) of **2,6-NpBox** in D_2O at 25 °C.

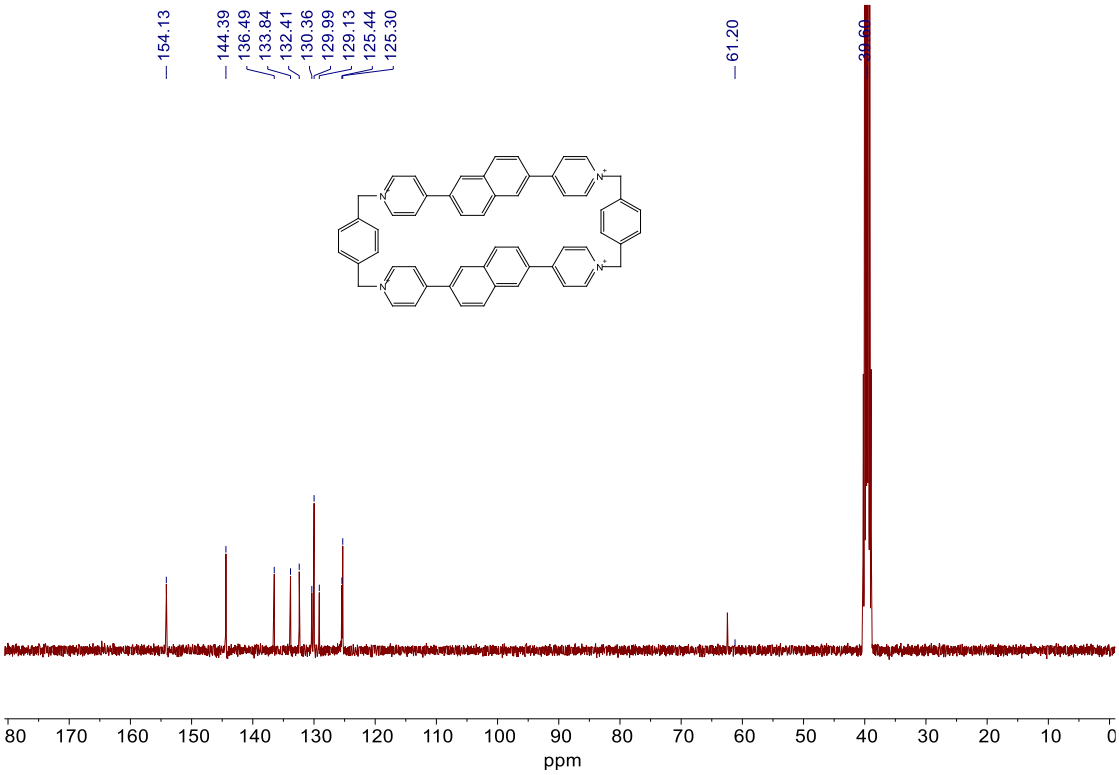

Fig. S89 ^{13}C NMR spectrum (101 MHz) of **2,6-NpBox·4PF$_6$** in DMSO-d_6 at 25 °C.

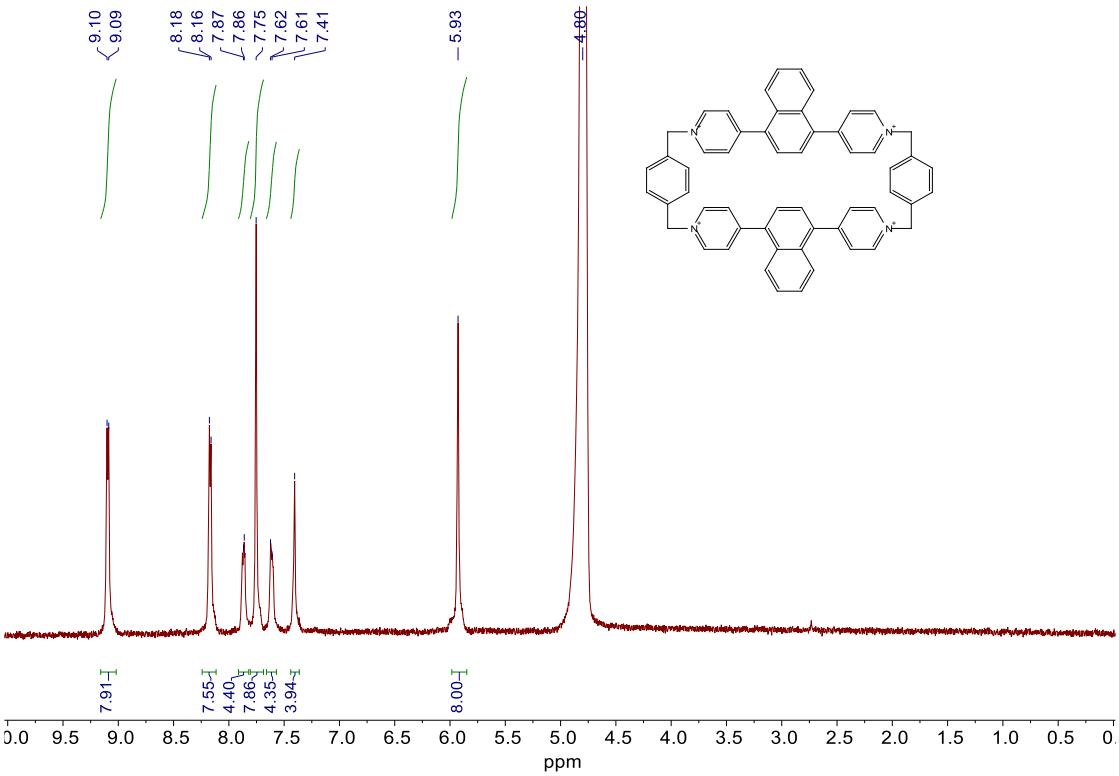

Fig. S90 ^{1}H NMR spectrum (400 MHz) of **1,4-NpBox** in D_2O at 25 °C.

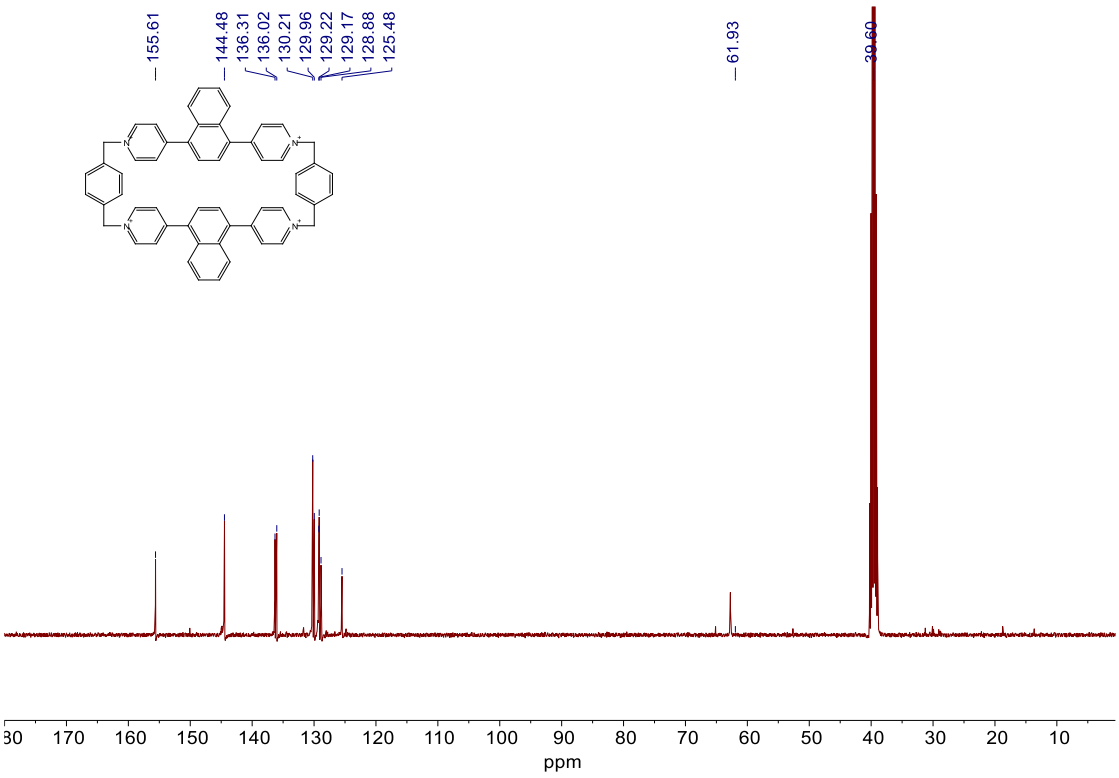

Fig. S91 ^{13}C NMR spectrum (101 MHz) of **1,4-NpBox·4PF$_6$** in DMSO-d_6 at 25 °C.

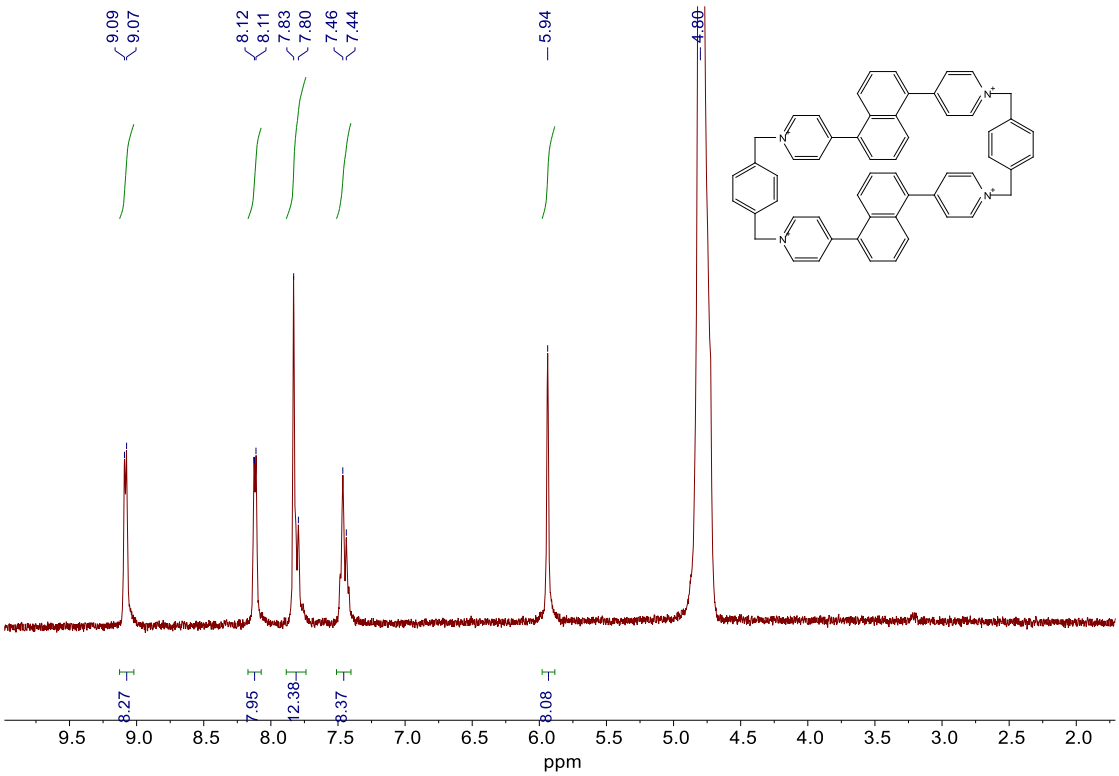

Fig. S92 ^{1}H NMR spectrum (400 MHz) of **1,5-NpBox** in D_2O at 25 °C.

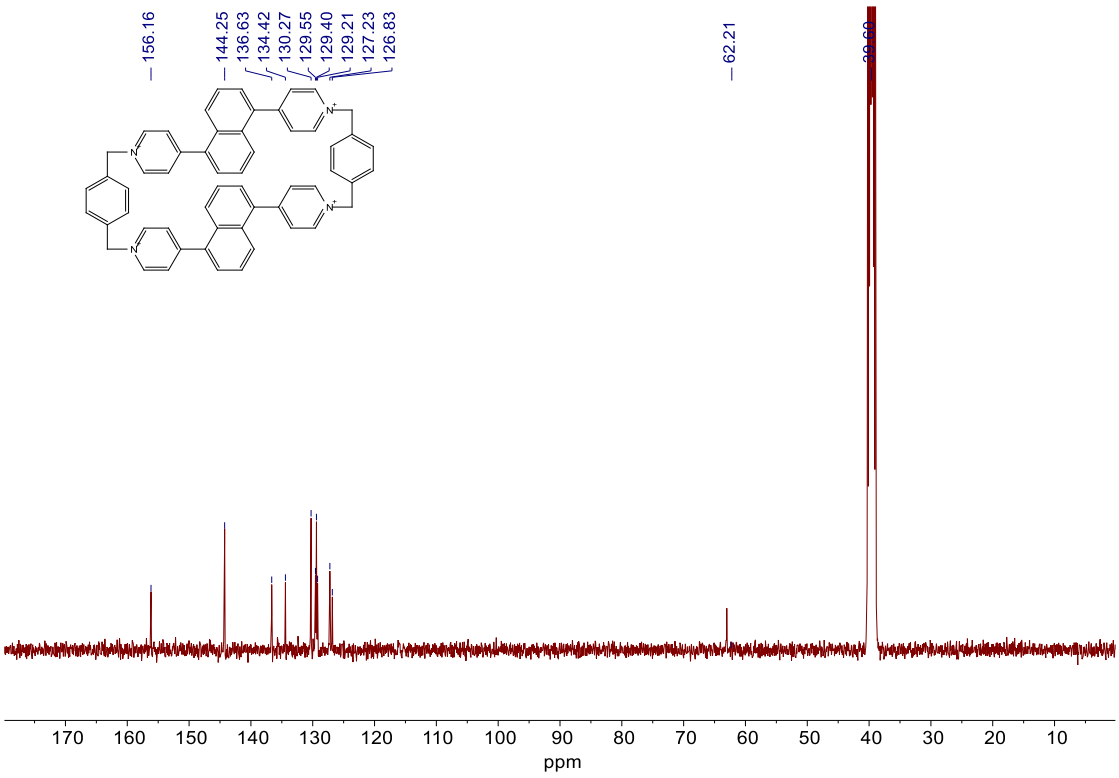

Fig. S93 ^{13}C NMR spectrum (101 MHz) of **1,5-NpBox·4PF$_6$** in DMSO-d_6 at 25 °C.